Imaging Migration and Activation of Lymphocytes: Transgenic Expression of Fluorescent Indicators

Dissertation

zur Erlangung des Doktorgrades der Naturwissenschaften
Fakultät für Biologie
Ludwig-Maximilians-Universität München

Marsilius Mues
München
April 2012

1. Gutachter: Prof. Elisabeth Weiß
Ludwig-Maximilians-Universität, München
Fachbereich Biologie

2. Gutachter: Dr. Josef Mautner
Helmholtz-Zentrum, München
Institut für Klinische Molekularbiologie

Sondergutachter: Prof. Hartmut Wekerle
Max-Planck-Institut für Neurobiologie, Martinsried
Abteilung Neuroimmunologie

Doktorarbeit eingereicht am: 26. April 2012

Tag der mündlichen Prüfung: 17. July 2012

TABLE of CONTENTS

SUMMARY

The timing and progression of cell recruitment, the interplay within the tissue microenvironment, and the differential activation of immune cells are critical factors in shaping the outcome of an inflammatory response. Conventional *in vitro* approaches to study experimental autoimmune encephalomyelitis (EAE), an animal model of multiple sclerosis, are often insufficient to investigate the highly dynamic nature of pathogenic immune cells during trafficking, recruitment, and infiltration of the central nervous system. *In vivo* imaging of immune cells, identification of specific activation processes *in situ*, and precise interference with individual cell subsets will help to better understand the development and course of the disease.

T cells interact with antigen-presenting cells by forming immunological synapses, and productive recognition of an antigen triggers various activation signals within the T cell. These signals include a swift rise of intracellular calcium, that is commonly utilized as a marker for T cell responses. Since synthetic calcium indicators are not applicable to *in vivo* studies due to their short-lived intracellular persistence, the genetically encoded calcium indicator TN-XXL was established as an alternative for calcium imaging in T cells. TN-XXL is composed of two fluorescent proteins with distinct emission wavelengths, linked by the calcium sensitive domain troponin C, and indicates cytosolic calcium levels through Förster resonance energy transfer. After extensive optimization, stable and strong expression of TN-XXL was obtained in primary murine T cells. These cells were successfully used for calcium imaging studies in peripheral immune organs, as well as in the target organ during EAE. Robust responses could be read from T cells upon antigen encounter, however, frequent calcium signals independent of cognate antigen were detectable as well. This approach enables us for the first time to follow the migration and activation patterns of T cells *in vivo* during the course of the disease.

B cells also play crucial roles in the pathogenesis of autoimmune disorders. They produce potentially pathogenic autoantibodies, act as antigen-presenting cells, and secrete cytokines shaping the local inflammatory milieu. To better explore the role of B cells during (auto-)immune responses, a new mouse model dubbed “R&D” was developed during this thesis. These transgenic mice express the red fluorescent protein and the human Diphtheria toxin receptor selectively in B cells, allowing *in situ* imaging of B cells and their selective depletion at any time. This new transgenic mouse strain will be a valuable tool to analyze the role of B cells in different phases of EAE and other autoimmune diseases.

ZUSAMMENFASSUNG

Kritische Parameter im Ablauf einer entzündlichen Reaktion sind die Rekrutierung pathogener Immunzellen, deren Interaktion im betroffenen Gewebe, sowie daraus folgende Aktiverungsmuster. Traditionelle in vitro Methoden zur Untersuchung von experimenteller autoimmuner Enzephalomyelitis (EAE), einem Tiermodell für Multiple Sklerose, sind vielmals unzureichend, um den äußerst dynamischen Immunzellen während ihrer Infiltration in das Zentrale Nervensystem zu folgen. Mikroskopie von Immunzellen in vivo, die Charakterisierung von Aktivierungsprozessen in situ und eine präzise Manipulation spezifischer Zelltypen werden dazu beitragen, die Entwicklung und den Verlauf der Krankheit besser verstehen zu können.

T-Zellen kommunizieren mit antigenpräsentierenden Zellen durch Ausbildung einer immunologischen Synapse. Erfolgreiche Antigenerkennung induziert eine Kaskade von Aktivierungssignalen in der T-Zelle, was einen raschen Anstieg an intrazellulärem Kalzium hervorruft, der oftmals als T-Zell Aktivierungsmarker genutzt wird. Da synthetische Kalziumindikatoren aufgrund ihrer begrenzten intrazellulären Persistenz nicht für in vivo Experimente genutzt werden können, sollte die Mikroskopie mit dem genetisch kodierten Kalziumindikator TN-XXL etabliert werden. TN-XXL besteht aus zwei fluoreszenten Proteinen unterschiedlicher Wellenlänge, verbunden durch die kalziumsensitive Domäne Troponin C, und ermöglicht die Bestimmung intrazellulärer Kalziumkonzentrationen durch Förster-Resonanzenergietransfer. Nach eingehender Optimierung konnten primäre T-Zellen mit stabiler TN-XXL Expression generiert werden, welche erfolgreich zur Kalziummessung in peripheren Immunorganen wie auch während der EAE eingesetzt wurden. Nach Antigenerkennung zeigten sich starke Kalziumsignale in T-Zellen, es konnten jedoch auch zahlreiche antigenunabhängige Kalziumsignale detektiert werden. Dieser Ansatz ermöglich es zum ersten Mal, nicht nur der Migration sondern auch den Aktiverungsmustern von T-Zellen während dem Krankheitsverlauf in vivo zu folgen.

B-Zellen können die Manifestierung von Autoimmunerkrankungen durch die Produktion von pathogenen Autoantikörpern, in ihrer Funktion als antigenpräsentierende Zellen und durch die Sekretion von Zytokinen signifikant beeinflussen. Um ihre Rolle besser verstehen zu können, wurde im Rahmen dieser Doktorarbeit das neuartige Mausmodell „R&D“ entwickelt. In diesen transgenen Mäusen wird rot fluoreszierendes Protein zusammen mit dem humanen Diphtheria-Toxin-Rezeptor selektiv in B-Zellen exprimiert, was sowohl in situ Mikroskopie von B-Zellen als auch deren gezielte Depletion ermöglicht. Damit könnten die „R&D“ Mäuse dazu beitragen, den Einfluss von B-Zellen in verschiedenen Stadien der EAE als auch in anderen Autoimmunerkrankungen genauer zu untersuchen.

INTRODUCTION

1.1 Multiple sclerosis

Multiple sclerosis (MS) is a chronic autoimmune demyelinating disease of the central nervous system (CNS), affecting primarily young people with about 500,000 patients in Europe and 2.5 million worldwide. MS leads to disability at the level of physiological and cognitive functions with symptoms being primarily determined by the particular demyelinated CNS areas and how much neuronal tissue has been damaged. Symptoms can be quite diverse including sensibility disorders, fatigue, dizziness and deterioration of vision, tremors, muscle weakness and spasms, difficulties in balance and coordination, and eventually paralysis. The majority of patients develop MS with a relapsing-remitting (RR) clinical course, with alternating periods of acute disease and recovery. After an initial bout, patients can completely recover and remain free of symptoms until the disease reinitiates. Relapses can last for days or weeks with varying recoveries. Over time, patients with RR MS may develop secondary-progressive MS which can lead to disability. A minority of patients, though, suffer from primary-progressive MS, a rather aggressive form of the disease developing gradually but steadily from the very beginning.

In MS and other autoimmune disorders, such as Type 1 Diabetes or Rheumatoid Arthritis, the immune system reacts with tissue-specific self-antigens by mechanisms that are still poorly understood. The CNS is considered as an immune-privileged organ since it lacks proper lymphatic vessels and is protected by the blood brain barrier (BBB). However, in the case of MS, immune cells attack the myelin sheath, produced by oligodendrocytes and enwrapping the axons of CNS neurons, which presumably leads to axonal damage and, ultimately, to neuronal death (Engelhardt and Coisne, 2011). This assault is mainly driven by autoreactive T lymphocytes. Both, cluster of differentiation (CD)4^+ and $CD8^+$ T cells, targeted against various CNS antigens, are widely prevalent in patients with MS, but also in healthy individuals. However, only after a break of tolerance leading to an inappropriate, excessive response, autoreactive T cells will eventually start to invade the CNS and drive the development of the disease (Kyewski and Klein, 2006).

MS shows a highly complex etiology with both genetic and environmental contributions to the pathogenesis. Striking patterns of genetic predisposition can be found for MS: monozygotic twins show a higher concordance (25%) compared to dizygotic twins (2%) (Dyment *et al.*, 1997). One important genetic risk factor is the major histocompatibility complex (MHC) or human leukocyte antigen (HLA) class II, in particular the HLA-DR15

haplotype in the Caucasian population. Consistent with this, $CD4^+$ T lymphocytes play a critical role in MS pathogenesis as those are activated by antigen-presenting cells (APC) in a HLA class II-dependent manner (Sospedra and Martin, 2005). In addition, genome wide association studies (GWAS) identified the cytokine receptors for interleukin (IL)-2 and IL-7, and the adhesion molecule CD58 as risk factors (Fugger *et al.*, 2009). Most of the risk alleles identified by GWAS are linked to the immune system, stressing the influence of immune cells on the development of the disease.

Environmental influences on MS pathogenesis became evident with geographical differences in MS occurrence, as Northern European and Northern American countries show a higher incidence than regions closer to the equator. This discrepancy might be explained by an insufficient supply of Vitamin D in northern countries due to reduced uptake or sun exposure, leading to a higher probability of developing MS (Smolders *et al.*, 2008). It was also proposed that bacterial or viral infections, like the Epstein-Barr virus, could trigger MS by means of molecular mimicry or through bystander activation of the immune system, but so far none has been definitely proven (Lünemann *et al.*, 2007).

1.2 Experimental autoimmune encephalomyelitis

The studies of MS are limited to magnetic resonance imaging, sampling of peripheral blood and cerebrospinal fluid (CSF), and analysis of post-mortem CNS tissue. Animal models overcome these limitations and offer in-depth analysis of the disease processes. Furthermore, availability of genetically manipulated animals provides the opportunity to study the contributions of different genes to the disease development and progression. Moreover, experimental animals can be treated with various drugs in a highly controlled manner, and lymphoid cells can easily be obtained from donor mice, manipulated *ex vivo*, and transferred to recipient hosts.

Experimental autoimmune encephalomyelitis (EAE) in the mouse is the most commonly studied animal model of MS (Handel *et al.*, 2011). EAE was first described in 1925, when it was shown that immunization with human brain antigen induces paralysis in rabbits (Koritschoner and Schweinburg, 1925). Later, similar results were obtained with a whole range of different experimental animals – rats, mice, sheep, or primates – using whole brain homogenate from various sources or purified CNS antigens (Baxter, 2007). EAE induced in the inbred mouse strain C57BL/6 is associated with a strong inflammation in the spinal cord. It results in a characteristic monophasic disease with ascending paralysis that starts with loss of tail tonus and is followed, from caudal to rostral, by limb weakness and

paralysis. Induction of EAE in the inbred SJL/J mouse strain can lead to similar symptoms, though in a relapsing-remitting fashion and sometimes accompanied by ataxic bouts.

Induced EAE

EAE in mice can be induced by active immunization with subcutaneous injection of myelin protein or peptide emulsified in complete Freund´s adjuvant (CFA) (active EAE) (Olitsky and Yager, 1949; Stromnes and Goverman, 2006a). CFA is composed of mineral oil to allow slow but steady release of the antigen, and heat-inactivated *Mycobacterium tuberculosis* to boost the innate immune response (Freund and McDermott, 1942). In addition, mice receive two consecutive injections of pertussis toxin which is supposed to open the BBB, to influence T lymphocyte migration, and to impair negative regulation of immune cells (Cassan *et al.*, 2006). The most common myelin autoantigens used for active EAE induction are myelin oligodendrocyte glycoprotein (MOG), myelin basic protein (MBP), and proteolipid protein (PLP), with the right combination of mouse strain and antigen determining EAE pathology (Krishnamoorthy and Wekerle, 2009). Unfortunately, the necessity of adjuvant and pertussis toxin for induction of active EAE limits the applicability of this model, especially at the initial stages of autoimmune disease processes. To circumvent these limitations, EAE can also be induced by transfer of pre-activated lymphocytes isolated from immunized donor mice which are reactivated *in vitro* with myelin antigen (Paterson, 1960; Stromnes and Goverman, 2006b). Passive EAE develops faster and more homogeneously than active EAE, it avoids CFA inoculation, allows the manipulation of pathogenic T cells *ex vivo*, and facilitates the analysis of effector functions of transferred T cells (Ben-Nun *et al.*, 1981). Nevertheless, passive EAE is also not suitable to study initial disease triggers.

Spontaneous EAE

All problems inherent to adjuvant-based immunization for active EAE, and bulk transfer of *in vitro* reactivated T cells for passive EAE, can be avoided using mouse models developing spontaneous EAE. With the advent of myelin antigen-specific T cell receptor (TCR) transgenic animals, mice spontaneously developing EAE became available. In the past years two spontaneous EAE models have been established in our group. One model on the C57BL/6 mouse strain background combines 2D2 mice, expressing a MOG_{35-55} peptide-reactive TCR (Bettelli *et al.*, 2003), with IgH^{MOG} mice, expressing a B cell receptor (BCR), derived from a rearranged heavy chain of a MOG-specific antibody (Litzenburger *et al.*, 1998). Double-transgenic offspring from 2D2 x IgH^{MOG} crosses, termed opticospinal EAE (OSE) mice, develop spontaneous EAE at an age of around four weeks with an incidence of about 50%, with close similarities to the MS-related disease Neuromyelitis Optica

(Krishnamoorthy *et al.*, 2006; Bettelli *et al.*, 2006). The other model is a single-TCR transgenic mouse model on the SJL/J strain. These TCR^{1640} mice harbor T cells with a TCR recognizing the MOG_{92-106} peptide. These T cells recruit endogenous MOG-specific B cells and drive EAE at an age older than two months, with an incidence of over 80%. TCR^{1640} mice represent the first spontaneous animal model for the most common form of MS in the Western society, RR MS (Pöllinger *et al.*, 2009). Both spontaneous EAE models described above are dependent on T – B cell co-operation, and offer special advantages over induced EAE models due to the less artificial disease induction and the closer resemblance of the human disease.

1.3 Immune cell infiltration into the CNS

MS features a highly complex pathogenic cascade, which involves the contribution from many immune cells. After activation in the periphery, autoreactive T cells can eventually enter the CNS (Figure 1.1) (Goverman, 2009). This process is a particular challenge to the T cells as the CNS usually is protected from infiltration by the BBB. Tight junctions between the endothelial cells of these barriers limit access to the CNS. However, activated T cells can enter the target organ due to expression of specific adhesion molecules that enable them to surmount these barriers (Ransohoff *et al.*, 2003). Recently, T cells have been proposed to follow unique migratory steps during their entry into the CNS. Initially, T cells start to crawl on the inner vascular surface for some time, before they extravasate and start crawling on the outer surface of the vessel and the underlying leptomeningeal space. Later, these putatively activated T cells invade the CNS parenchyma, which coincides with the onset of first clinical symptoms (Bartholomäus *et al.*, 2009). Intraluminal crawling is mediated by surface expression of $\alpha4\beta1$ integrin on encephalitogenic T cells (Yednock *et al.*, 1992). Blocking of this adhesion molecule interferes with tight attachment and crawling of T cells in the CNS blood vessels. Natalizumab, the therapeutic $\alpha4$ integrin blocking antibody is highly effective in reducing MS relapse rate.

Shortly after extravasation, T cells get reactivated in the CNS. This can be mediated by perivascular macrophages, microglia, dendritic cells (DC), or astrocytes. While the brain-resident microglia and astrocytes are usually poor APCs, they can induce their antigen-processing machinery, and upregulate MHC and co-stimulatory molecule expression after activation. In addition, due to their ubiquitous localization in the CNS, both are a potent source of inflammatory cytokines, influencing local T cell differentiation and global propagation of CNS immune response (Aloisi, 2001). Perivascular macrophages are readily

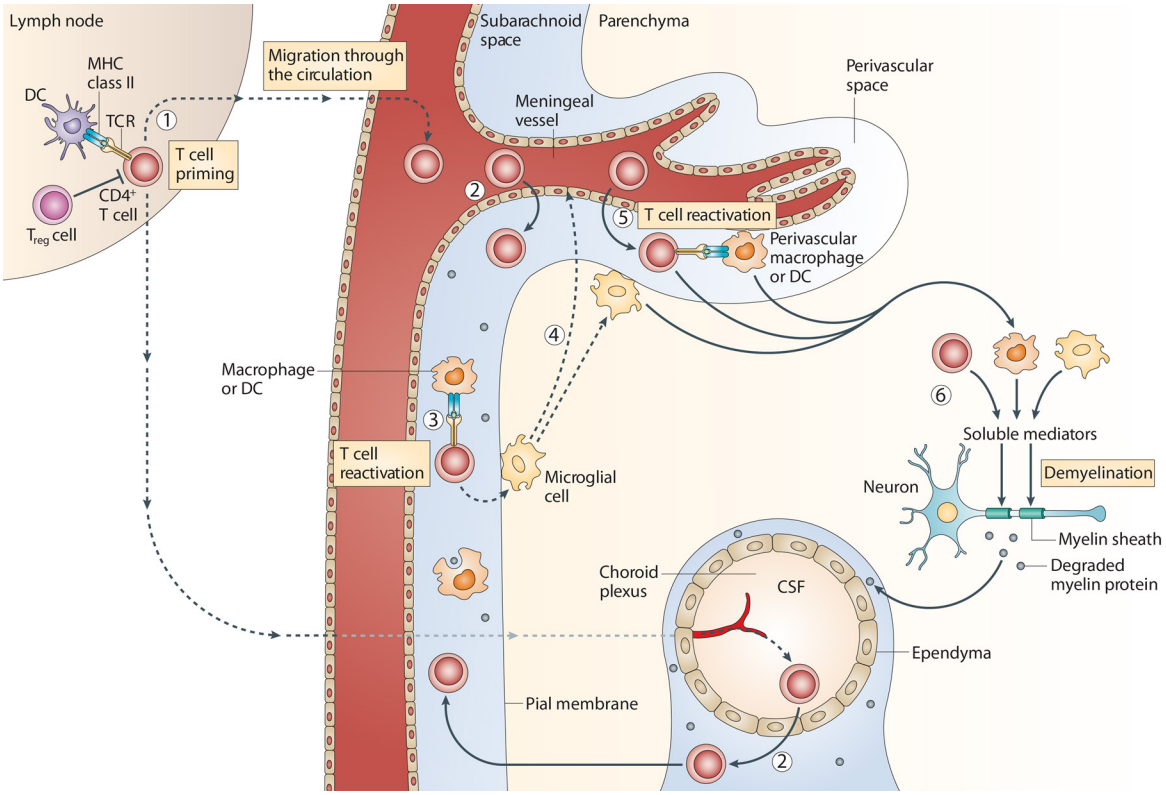

Figure 1.1 T cell infiltration into the CNS. (1) $CD4^+$ T cells are primed in the periphery by DCs presenting myelin (or myelin cross-reactive) epitopes. APCs residing in the CNS can capture myelin antigens *in situ* and migrate to the cervical lymph nodes. Alternatively, soluble myelin antigens can drain from the CNS to lymph nodes to be phagocytosed by local APCs. **(2)** $CD4^+$ T cells enter the subarachnoid space by crossing the blood-CSF barrier either in the choroid plexus or the meningeal venules. **(3)** T cells are re-activated within the subarachnoid space by MHC class II-expressing macrophages and DCs presenting myelin epitopes. **(4)** Reactivated T cells activate microglial cells in the subpial region, triggering activation of distal microglial cells and blood vessels. **(5)** Activated T cells adhere to and cross the activated BBB, enter the perivascular space and are reactivated by perivascular macrophages and DCs. **(6)** T cells enter the parenchyma and, together with activated macrophages and microglial cells, secrete soluble mediators that trigger demyelination (adapted from Goverman, 2009).

found around cerebral blood vessels, thus perfectly situated to interact with extravasating T cells. During MS and EAE, perivascular macrophages highly upregulate MHC class II and co-stimulatory molecules, turning them into professional APCs capable of activating invading T cells (Fabriek *et al.*, 2005). DCs, on the other hand, are recruited from the peripheral lymphoid tissues, mature during their migration to function as professional APCs, and play a key role in reactivating encephalitogenic $CD4^+$ T cells in the CNS. Depending on their subset, DCs can be found in inflammatory foci clustering with $CD4^+$ T cells in perivascular areas, or are dispersed throughout the CNS tissue (Bailey *et al.*, 2006). This reactivation of T cells is also accompanied by an activation of perivascular endothelium, which in turn allows

further recruitment of encephalitogenic T cells into the perivascular space. For subsequent migration of T cells into the parenchyma, tumor necrosis factor α (TNFα) signaling is supposed to play an important role (Gimenez *et al.*, 2006). In addition, it was shown that the strength of T cell reactivation determines the rate of parenchymal infiltration, rather than the capacity of a T cell to infiltrate the perivascular space (Kawakami *et al.*, 2004).

Sustained infiltration of immune cells into the CNS parenchyma will eventually lead to demyelination, axon degeneration, and persistent neuronal damage. Autoreactive $CD8^+$ T cells could directly attack oligodendrocytes or neurons due to their expression of MHC class I (Medana *et al.*, 2001). $CD4^+$ T cells, on the other hand, secrete the pro-inflammatory cytokines interferon γ (IFNγ), IL-17, or TNFα, thus activating macrophages and microglia. Those cells, in turn, produce inflammatory cytokines such as IL-1β or IL-12, and mediators like radical oxygen species (ROS) or nitric oxide (NO), leading to oligodendroglial and neuronal damage (Herz *et al.*, 2010b). Oligodendrocyte destruction, followed by extensive myelin loss, results in increased ion currents in demyelinated axons, severe energy depletion, and axonal decay due to excitotoxicity. In addition, neuronal damage can also happen independently of myelin loss: a reduced oligodendroglial metabolic support of the axonal compartment can cause a pathologically impaired energy balance which leads to reduced axonal transport, swellings, and ultimately, axon degeneration (Nave, 2010).

1.4 T lymphocytes in MS and EAE

The most important cellular mediators of MS pathogenesis are T cells. As described above, in addition to breakdown of self-tolerance, autoreactive $CD4^+$ or $CD8^+$ T cells have to be primed in peripheral lymphoid organs by endogenous antigen released from the CNS, or by molecular mimicry with cross-reactive antigen from exogenous pathogens. In most models of active EAE, myelin-specific $CD4^+$ rather than $CD8^+$ T cells are the central factor of autoimmune pathogenesis, due to the immunization protocol, which favors activation via MHC class II. Similarly, the adoptive transfer of pure encephalitogenic $CD4^+$ T cell lines, but not $CD8^+$ T cells, has been successfully used to induce passive EAE (Wekerle *et al.*, 1994). In contrast, in MS patients, $CD8^+$ T cells usually outnumber $CD4^+$ T cells in CNS lesions, and clonal expansion is detected more frequently among $CD8^+$ than $CD4^+$ T cells (Friese and Fugger, 2005). In addition, specific depletion of only $CD4^+$ T cells in patients did not result in the amelioration of the disease, while treatment with antibodies against CD52, depleting multiple lymphocyte populations, including $CD4^+$ and $CD8^+$ T cells, provided some benefits (Coles *et al.*, 2006). Also, an increased genetic susceptibility has been linked to the MHC

class I molecule HLA-A3. Transgenic mice expressing HLA-A3 along with a myelin-specific autoreactive TCR indeed developed mild $CD8^+$ T cell-driven EAE symptoms, however, progression and manifestation of the disease required additional contributions from $CD4^+$ T cells, suggesting cooperation between these two T cell types (Friese *et al.*, 2008).

Distinct effector T cell subsets have been described to mediate EAE pathogenesis. Naive $CD4^+$ T cells can be differentiated into various subclasses of T helper (T_H) cells depending on the cytokine milieu. IL-12 and IL-18 induce differentiation into T_H1 cells, secreting IFNγ. High concentrations of IL-4, however, yield T_H2 cells, that produce IL-4, IL-5, and IL-13. A third subpopulation of effector T cells are T_H17 cells, secreting IL-17 and IL-22, which can be induced by transforming growth factor β (TGFβ) and IL-6. In a similar cytokine milieu with high concentrations of TGFβ but void of IL-6, naive $CD4^+$ T cells do not differentiate into T_H17 but rather into regulatory T (T_{reg}) cells, that can dampen inflammatory reactions (Leung *et al.*, 2010). This manifold picture of different $CD4^+$ T cell populations gets even more complex, since a certain plasticity between T_H cell subpopulations can be found, too: T_{reg} cells can convert into T_H17 cells (Deknuydt *et al.*, 2009), T_H17 cells into T_H1 cells, or T cells can express both, IFNγ and IL-17 (Lee *et al.*, 2009). In addition, IL-9 secreting T_H9 cells (Veldhoen *et al.*, 2008), and IL-22 secreting T_H22 cells (Eyerich *et al.*, 2009) were reported, however, it is still debatable whether these cell types represent true distinct T cell subsets. In EAE, mainly T_H1 and T_H17 cells are shown to drive inflammation and to contribute to pathogenesis (El-Behi *et al.*, 2010), while T_{reg} cells are essential for peripheral tolerance and are thought to keep T_H1/T_H17 cells in check (Vignali *et al.*, 2008).

1.5 T lymphocyte activation

As discussed above, T cell activation plays a key role during the pathogenesis of MS and EAE. After initial activation in the periphery, which allows myelin-specific T cells to cross the BBB, reactivation of those T cells happens within the CNS. These sequential activation steps are a strict prerequisite for initiation of the disease and ongoing demyelination of the CNS, inevitably leading to clinical symptoms. Therefore it is crucial to decipher T cell activation and to understand the most important molecular events.

The immunological synapse

When migrating through the tissue, T cells scan a large variety of cells, e.g. APCs, endothelium, or stromal cells. At productive recognition of a target antigen, T cells stop migration and form a highly specialized membrane contact, called the immunological

synapse (Figure 1.2). This synapse is characterized by an ordered but still dynamic distribution of a large range of different transmembrane and intracellular molecules, that contribute to the establishment of a stable contact and bidirectional signaling between T cell and APC. Initial events in immune synapse formation after TCR activation are characterized by a rapid reorganization and a marked polarization of the cytoskeleton, followed by clustering of cell surface receptors to form so-called supramolecular activation complexes (SMACs). The region of the central SMAC (cSMAC) is highly enriched in TCR/CD3-MHC/peptide ligand pairs and associated signaling effectors, along with other co-stimulatory molecules like CD28 and CTLA4. In the surrounding peripheral SMAC (pSMAC), cell adhesion interaction partners such as LFA1-ICAM1 prevail and ensure a tight contact between T cell and APC. Further signaling and adhesion molecules, CD44 or CD45, were found in the distal SMAC (dSMAC). After formation of a mature synapse, T cell-APC interaction can last for several hours with ongoing downstream TCR second messenger events, including sustained calcium signaling, before the interacting partners finally break up and T cells undergo proliferation (Dustin and Depoil, 2011).

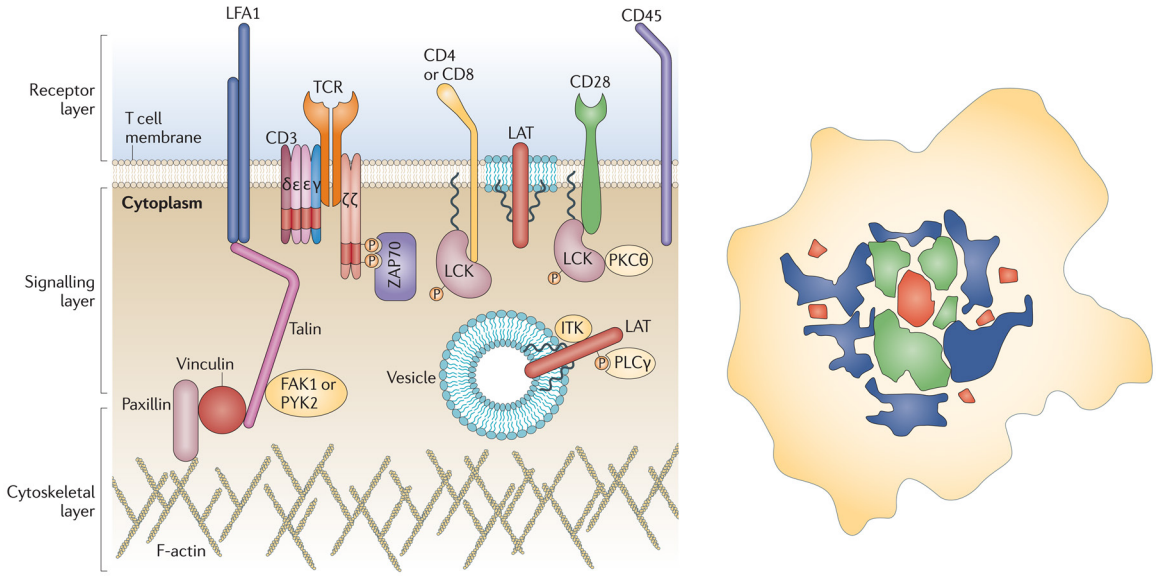

Figure 1.2 The immunological synapse. The three layers on the T cell side of the immunological synapse are depicted on the left. The receptor layer contains the TCR-CD3 complex, CD4 or CD8, CD28, and LFA1. The signaling layer includes LCK, ZAP70, PKCθ, LAT, ITK, and PLCγ. The cytoskeletal layer contains filamentous actin, talin, paxillin, and vinculin. The right figure represents the supramolecular activation complexes (SMAC) of an immunological synapse. The TCR-rich central SMAC core is shown in red, the CD28-rich central SMAC surrounding in green, the LFA1-rich peripheral SMAC in blue, and the distal SMAC in yellow (adapted from Dustin and Depoil, 2011).

Phases of T cell priming

In vivo imaging of T cells interacting with APCs in a lymph node revealed several distinct phases of T cell priming (Figure 1.3). During the initial phase after antigen encounter, which lasts for about 6 hours, T cells form short interactions with APCs. However, already during this stage, T cells are clearly activated as seen by the upregulation of early activation markers, like CD69 or CD44. In phase two, from about 6 to 16 hours, T cells engage in long-lasting interactions with APCs, express the full spectrum of activation markers, and initiate production of cytokines. Thereafter, in the third phase, T cells detach from APCs and again migrate among them performing serial but only short-lived interactions (Mempel *et al.*, 2004).

T cell priming *in vivo*, however, depends on a complex set of parameters. Different APCs feature different T cell stimulatory potentials. B cells, for example, need far more antigen-MHC complexes on their surface for efficient T cell triggering compared to DCs (Delon *et al.*, 1998). Also, depending on the activation status of the APC, antigen presentation and expression of co-stimulatory molecules can vary, and thereby strongly influence the efficiency of T cell activation. In addition, chemokines in the surrounding can enhance or modulate the activation of T cells engaging with APCs as well. Another very important factor is the affinity of the TCR to the MHC-bound antigen. Low levels of a low affinity antigen can induce T cells to make serial encounters with APCs over a certain period of time, integrating minute signals, ultimately leading to full activation. With a high dose of a high affinity antigen, however, T cell activation can be achieved very rapidly (Henrickson and von Andrian, 2007). Indeed, in an *in vivo* experimental setup, a high affinity antigen, loaded in large amounts in DCs, resulted in immediate synapse formation and long-lasting interactions of T cells with DCs (Shakhar *et al.*, 2005).

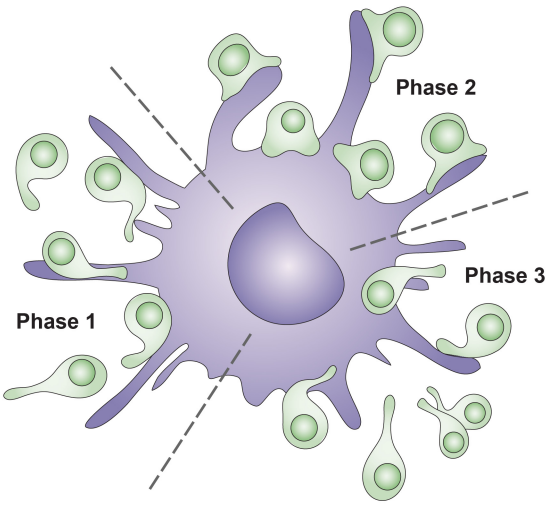

Figure 1.3 Phases of T cell priming. Three phases of T cell priming were shown, using intravital and *ex vivo* microscopy. Phase one, lasting for the first several hours after a T cell has entered a lymph node, is characterized by short interactions between T cells (green) and APCs (blue), with the upregulation of activation markers starting by the end of that phase. Phase two, lasting for the rest of the first day, is characterized by long-term APC-T cell interactions and the initiation of cytokine secretion. Phase three thereafter is characterized by a return to short-term T cell-APC interactions and T cell proliferation. (adapted from Hendrickson and von Andrian, 2007)

1.6 Calcium signaling in T lymphocytes

Resting T cells usually feature cytosolic calcium concentrations of about 100 nM, while much larger concentrations of calcium can be found in intracellular endoplasmatic reticulum (ER) stores (500 µM). Upon activation of T cells via TCR engagement, within few milliseconds a signal transduction cascade leads to depletion of the intracellular calcium stores and a swift rise of cytoplasmic calcium. Subsequently, calcium release activated calcium (CRAC) channels in the plasma membrane open, leading to a sustained influx of calcium from the extracellular milieu (1000 µM) into the cell. This specialized mechanism has been termed as store operated calcium entry (SOCE), and is the main pathway for generating calcium signals in many non-excitable cell types (Feske, 2007). Observations on thymocytes and mature T cells indicate, that an increase in intracellular calcium levels is necessary and sufficient to deliver a migratory STOP signal to T cells. This becomes more evident when intracellular calcium is buffered or sustained calcium influx is blocked, a stable immunological synapse cannot be established (Bhakta *et al.*, 2005). This initial increase of free calcium in the cytoplasm is one of the most critical steps of T cell activation, and a key trigger for all possible downstream events including clonal expansion or effector functions.

After initial activation, T cells show remarkably different calcium signals, ranging from infrequent calcium spikes to sustained oscillations and plateaus. This variety is the result of the interaction of multiple calcium sources and sinks within the cell, and offers the regulation of a highly complex activation machinery. For instance, the translation of various calcium signals allows differential regulation of T cell transcription factors: NFAT and NF-κB seem to favor calcium oscillations over continuously elevated calcium levels for *bona fide* activation. Specifically, NFAT activation needs stronger calcium signals at higher frequencies than activation of NF-κB (Quintana *et al.*, 2005). Many of these calcium-dependent transcriptional responses influence gene expression patterns and shape the long-term outcome of T cell activation, e.g. by changing cytokine expression profiles and inducing differentiation of naïve T cells into various kinds of T helper cells. Effective TCR engagement with strong calcium signaling is supposed to produce a T_H1 bias, whereas weak TCR engagement and lower calcium level changes evoke a T_H2 response. However, calcium signals can induce inhibitory effects, too, as sustained calcium signaling in the absence of any co-stimulatory signal can induce anergy in T cells. This state of unresponsiveness is again characterized by induction of a specific set of anergy-related genes, leading to expression of negative regulators of T cell activation (Feske *et al.*, 2001). Further, these initial calcium signals help to establish primary contacts between T cells and APCs by altering cell motility and inducing cytoskeleton rearrangements. However, only the sum of all varying parameters in amplitude,

course, and duration of the calcium signal over a sustained period of time guarantee an efficient and specific downstream gene activation. This complexity of differential calcium signaling contains a wealth of information that helps lymphocytes to choose between alternate fates in response to antigenic stimulation.

Molecular mechanisms of calcium signal generation

After antigen recognition by the TCR, protein tyrosine kinases such as ZAP70 and LCK get activated, which in turn phosphorylate adapter proteins, like LAT and SLP76. This leads to recruitment of the IL-2 inducible T cell kinase (ITK) and activation of phospholipase C γ (PLCγ). Similarly, binding of G protein-coupled receptors results in activation of PLCβ, both catalyzing the hydrolysis of phosphatidylinositol-4,5-bisphosphate (PtdIns(4,5)P_2) to inositol-1,4,5-trisphosphate (IP_3) and diacylglycerol (DAG). IP_3 binds to its receptor in the ER membrane and induces the release of calcium from the ER, leading to a first rise of calcium levels in the cytosol (Figure 1.4) (Feske, 2007).

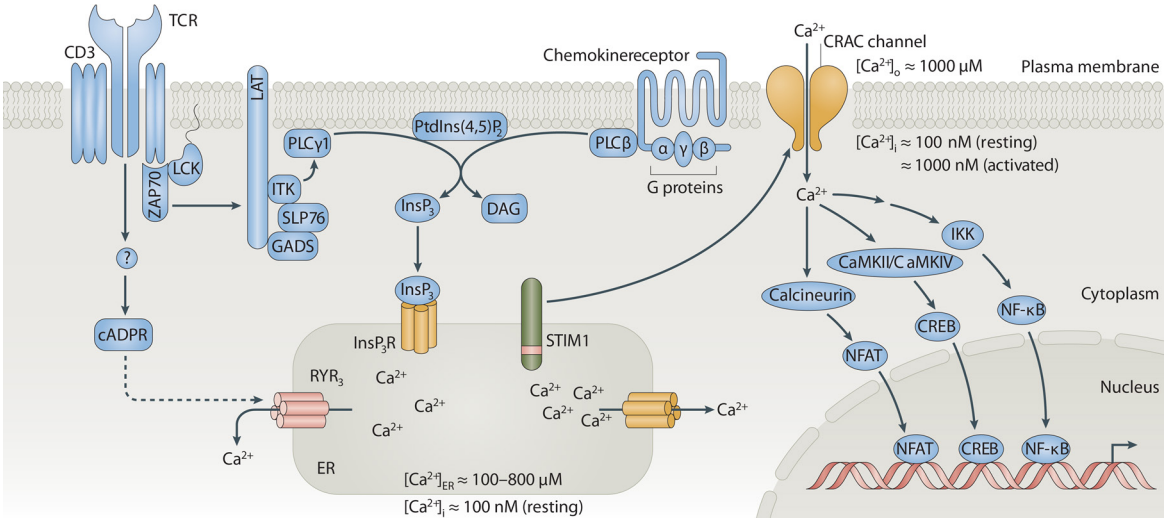

Figure 1.4 T cell activation cascade. In resting T cells, a steep gradient in calcium concentrations exists between the cytoplasm and the extracellular space, as well as between the cytoplasm and the lumen of the ER. The intracellular calcium concentrations in T cells is tightly regulated and kept between ~100 nM in resting cells and ~1000 nM following TCR stimulation. Antigen recognition through the TCR results in the activation of protein tyrosine kinases, such as LCK and ZAP70, which initiate phosphorylation events of adaptor proteins, such as SLP76 and LAT. This leads to the recruitment and activation of ITK and PLCγ. Similarly, binding of G protein-coupled chemokine receptors results in the activation of PLCβ. PLCβ and PLCγ catalyse the hydrolysis of the membrane PtdIns(4,5)P_2 to IP_3 and DAG. IP_3 binds to and opens IP_3 receptors in the membrane of the ER, resulting in the release of calcium from intracellular calcium stores. A decrease in the calcium content of the ER is sensed by STIM1, which in turn activates CRAC channels in the plasma membrane. Calcium influx through CRAC channels and elevated intracellular calcium concentration activate calcium-dependent enzymes, such as calcineurin, and thereby transcription factors, such as NFAT or NF-κB (adapted from Feske, 2007).

The stromal interaction molecule 1 (STIM1), located in the ER membrane, senses the loss of calcium from the ER by its EF-hand motifs facing the ER lumen. After ER depletion, STIM1 molecules cluster via their protein-protein interaction domains SAM (sterile-a-motif) and ERM (ezrin, radixin, and moesin), and form discrete puncta. These STIM1 puncta along with the ER then translocate and directly interact with the pore forming unit ORAI1 of plasma membrane resident CRAC channels. This cellular mechanism has long been speculated about but has only recently been formally shown (Park *et al.*, 2009). In their inactive state, CRAC channels have been proposed to exist predominantly as ORAI1 dimers. After engagement with STIM1 clusters, CRAC channels dimerize to form ORAI1 tetramers, and open to allow localized calcium influx (Hogan *et al.*, 2010). Calcium influx via CRAC channels makes the largest contribution to overall calcium level changes in T cells (Lewis and Cahalan, 1988). Therefore, a major function of calcium release from intracellular stores is to serve as sensitive trigger for controlling a much larger flux of calcium across the plasma membrane. Also, intracellular stores must remain depleted for a sustained calcium influx through CRAC channels. While IP_3 levels are back to base line within 10 minutes, calcium signaling via CRAC channels can last for more than one hour (Guse *et al.*, 1993). It is speculated that this sustained CRAC signaling is mediated by binding of cyclic ADP ribose (cADPR) to ryanodine receptors (RYR_3), which leads to continual depletion of internal calcium stores (Schwarzmann *et al.*, 2002).

Elevated calcium concentrations in the cytosol eventually activate calcium-dependent enzymes such as calcineurin (CN) or calmodulin-dependent kinase (CaMK), which in turn trigger activation of several downstream transcription factors. NFAT, for example, gets rapidly dephosphorylated by CN, which induces a conformational change of the transcription factor, that exposes a nuclear localization signal and results in NFAT translocation to the nucleus. However, as NFAT only weakly binds to DNA, it must cooperate with other transcription factors to efficiently influence gene regulation. This enables integration of various calcium signaling patterns and intensities (Macian, 2005).

In addition to CRAC channel-mediated calcium signaling, other calcium influx and release channels have been described in lymphocytes. ATP-binding P2X receptors or voltage-gated calcium (Ca_V) channels were found to be expressed in T cells as well. Recently it was shown that $Ca_V1.4$ indeed is a critical regulator of TCR signaling and naive T cell homeostasis (Omilusik *et al.*, 2011).

Calcium signaling during disease

Lack of lymphocyte calcium signaling due to a mutation in ORAI1, thus abrogating CRAC channel current activity, can cause severe combined immunodeficiency. T cells from those patients show strong defects in proliferation and cytokine secretion (Ledeist *et al.*,

1995). Similarly, in a mouse model of rheumatoid arthritis, a mutation of the kinase ZAP70 results in strongly reduced TCR signaling and thereby impaired calcium signaling. However, in this model, signaling is not entirely abrogated, but the threshold of T cell selection in the thymus is changed, allowing increased numbers of autoreactive T cells to escape central tolerance (Sakaguchi *et al.*, 2003). With respect to EAE it was shown that sustained calcium signaling is essential, since STIM1$^{-/-}$ mice are protected from active EAE. Disease protection was due to a significantly impaired generation of autoreactive myelin-specific T cell responses *in vivo* (Schuhmann *et al.*, 2010). Further, modulating calcium signaling in encephalitogenic T cells by selective blockade of second messengers reduces clinical symptoms of EAE, opening new possibilities for therapeutic treatments of multiple sclerosis (Cordiglieri *et al.*, 2010).

1.7 Calcium imaging in T lymphocytes

About 30 years ago, with the development of the first organic fluorescent calcium indicators, spatiotemporal investigation of cellular calcium signals became possible (Tsien, 1980). These small molecule indicators are usually available as cell-permeant acetoxymethyl ester derivatives. Once inside the cell, they become hydrolyzed by ubiquitous intracellular esterases, releasing the cell membrane-impermeant ion-sensitive indicator. While Fura-2 is still the most prominent representative of all organic dyes for calcium imaging in cells (Grynkiewicz *et al.*, 1985), the list of synthetic calcium indicators has been growing ever since (Molecular Probes Handbook 2010). Some calcium indicators react to binding of calcium just with an increase in fluorescence intensity. However, most of these indicators are of ratiometric nature and show a shift in their excitation or emission spectrum upon binding of calcium. Measurement of calcium with ratiometric indicators is therefore achieved by using two different fluorescent excitation sources or two detection ranges, respectively. This way of measurement avoids artifacts due to varying probe loading concentrations, indicator bleaching, or changes in focus, and became essential when tracking calcium level changes for extended periods of time in freely moving cells migrating in and out of the focus plane (Dewitt *et al.*, 2003).

The majority of calcium imaging experiments has been performed in neurons, and most calcium indicators have been optimized for neuronal imaging (Rochefort *et al.*, 2008). Nonetheless, there is also a long history of calcium imaging in T cells. Measurement of intracellular calcium levels in lymphocytes is routinely done with synthetic calcium indicators, like Fura-2 or Indo-1, either on a single cell level by microscopy (Grynkiewicz *et al.*, 1985), or

for whole cell populations using fluorescence-activated cell sorting (FACS) analysis (Griffioen *et al.*, 1989). These measurements gave insights into the molecular mechanisms of calcium signaling in lymphocytes, and helped to understand intracellular calcium fluxes at various stages of lymphocyte development, during their maturation, or when in action (Vig and Kinet, 2009).

Unfortunately, however, calcium imaging with synthetic calcium indicators has one major drawback: shortly after loading into the cytoplasm, these indicators can get expulsed from the cell again, a phenomenon attributed to the activity of multidrug resistance (MDR) transporters (Homolya *et al.*, 1993). Many dyes and most ion indicators persist in the cell as free fluorescent anions and get rapidly exported from MDR transporter-expressing cells (Neyfakh, 1988), including T cells (Prechtl *et al.*, 2000). Thus, calcium imaging in T cells with synthetic indicators has to be performed within few hours after labeling the cells, limiting their applicability to *in vitro* or *ex vivo* experiments.

With the advent of genetically encoded calcium indicators (GECI) (Miyawaki *et al.*, 1997), these limitations might be overcome and calcium imaging in T cells could be transferred into true *in vivo* experimental setups. GECIs are transgenically expressed in living cells, and consist of one or two fluorescent proteins (FP) and a calcium sensitive moiety, with no requirement of additional co-factors or chemicals. The calcium responsive element is either derived from the signaling molecule calmodulin (CaM), or from skeletal muscle troponin C (TnC). Both molecules feature calcium-binding EF hands and react with a conformational change upon reversible binding of calcium ions. In single fluorophore GECIs, CaM is inserted into a FP where a conformational change induces ionization of the chromophore, resulting in an increase in fluorescence intensity. These indicators include camgaroos (Baird *et al.*, 1999), pericams (Nagai *et al.*, 2001), and G-CaMPs (Figure 1.5) (Nakai *et al.*, 2001), and have been successfully employed for calcium imaging in neurons. Unfortunately, however, single fluorophore indicators are not of ratiometric nature, and thus cannot be employed in freely migrating T lymphocytes. The other class of GECIs features two FPs of different wavelengths, linked by CaM or TnC. A conformational change of the calcium sensitive moiety within these indicators leads to convergence of the FPs, thus inducing Förster resonance energy transfer (FRET) from the shorter wavelength donor FP to the longer wavelength acceptor FP. Calcium binding therefore yields a ratiometric decrease in donor fluorescence and an increase in acceptor fluorescence, rendering these calcium indicators suitable for freely moving T cells. Ratiometric GECIs include the CaM-based yellow cameleons (YC) (Nagai *et al.*, 2004), and the TnC-based TN-L indicators (Figure 1.5) (Heim and Griesbeck, 2004; McCombs and Palmer, 2008).

Since the first emergence of GECIs, continuous engineering efforts to gain higher calcium affinity, increased signal strength, better pH stability, or faster reaction kinetics, gave

rise to optimized versions of these indicators. Besides those benefits, however, occasional functional interference of transgenically expressed calcium indicators in host cells has been reported. CaM-based yellow cameleon GECIs were essentially inactivated during transgenic expression (Hasan *et al.*, 2004), and constitutive expression of a G-CaMP GECI in the mouse heart induced cardiomegaly (Tallini *et al.*, 2006), a pathologic enhancement of heart size resembling the effect of CaM overexpression in the heart (Gruver *et al.*, 1993). Since CaM is a ubiquitous signaling protein with multiple levels of regulation in the cell, TnC with its highly specific function as regulator of contraction in skeletal muscle seems to be a better choice for constitutive expression at high levels. Therefore, in the present study, the latest version of TnC-based calcium indicators, TN-XXL (Mank *et al.*, 2008), was taken as a starting point to establish *in vivo* calcium imaging in T cells.

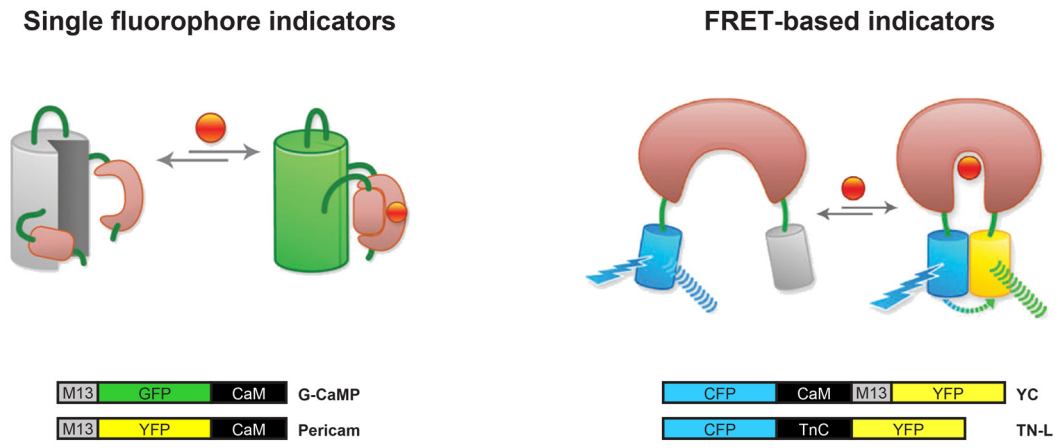

Figure 1.5 Genetically encoded calcium indicators. Single fluorophore indicators employ the calcium-responsive element CaM, and a CaM-binding peptide attached to a fluorescent protein. On binding calcium, CaM executes a conformational change, interacting with the peptide and altering the protonation state of the chromophore, thus changing the fluorescence intensity of the protein (left). FRET-based indicators have a calcium-binding domain located between two flurophorescent proteins. At calcium binding, this domain undergoes a conformational change, bringing the two fluorescent proteins closer together and increasing the efficiency of FRET (right). Below each model are diagrams for the various available families of GECIs (adapted from McCombs and Palmer, 2008).

1.8 B lymphocytes in MS and EAE

B cells and their antibodies play an important role in the pathogenesis of MS and EAE, too, yet their distinctive role remains elusive (Berer *et al.*, 2011a). After antigen-specific activation, B cells can become effector B cells, undergo germinal center reactions, and eventually differentiate into plasma cells, producing large quantities of antibodies. Characteristic oligoclonal immunoglobulin G (IgG) bands can be found in CSF samples from over 90% of all patients, rendering this phenomenon a hallmark of MS diagnosis (Kabat *et al.*, 1942). Clonally expanded brain resident B cells are partially accountable for the emergence of these oligoclonal bands, stressing the importance of B cells for the development or course of the disease (Obermeier *et al.*, 2008). Indeed, ectopic lymphoid follicles were described, enriched with B cells and plasma cells in the meninges of a subset of RR MS patients, potentially providing a suitable microenvironment, where B cells can mature, expand, and locally produce autoantibodies (Serafini *et al.*, 2004).

The role of B cells in EAE

Autoantibodies also play a major role in EAE, as it was shown that transfer of serum from diseased animals could induce subclinical demyelination in recipient animals (Lassmann *et al.*, 1981). Similarly, active EAE was accelerated and showed exacerbated severity in transgenic IgH^{MOG} mice, producing high levels of MOG-specific autoantibodies (Litzenburger *et al.*, 1998). In many EAE models, however, a B cell component is missing, since immunization is mostly performed with a short encephalitogenic peptide. Thus, immunization with whole myelin proteins offers a better understanding of the involvement of B cells in disease development. In one report, B cell deficient µMT mice were susceptible to active EAE induced by immunization with MOG_{35-55} peptide, but not by recombinant MOG, suggesting differential processing and presentation of the encephalitogenic epitope (Lyons *et al.*, 1999). In another report, µMT mice failed to recover from active EAE due to lack of B cell derived IL-10 (Fillatreau *et al.*, 2002). Furthermore, clinical recovery was accounted to B cells interacting with T_{reg} cells through a CD80/CD86 co-stimulatory mechanism (Mann *et al.*, 2007).

Antigen presentation by B cells is of particular importance for the T – B cell crosstalk observed in the spontaneous EAE models mentioned before. IgH^{MOG} B cells in the OSE mouse model can concentrate MOG with their antigen-specific BCR, and efficiently present it to MOG-reactive T cells. This results in mutual activation, proliferation, and differentiation, and B cells of those mice produced high titers of MOG-specific IgGs, while T cells in the CNS secreted more IFNγ and IL-17 than single-transgenic controls. Furthermore, activated B

cells in the OSE model switched isotype to produce MOG-specific IgG1 autoantibodies (Krishnamoorthy *et al.*, 2006; Bettelli *et al.*, 2006). In the TCR^{1640} mouse model, MOG-specific B cells from the endogenous repertoire are recruited by MOG-reactive transgenic T cells and are driven into germinal center reactions, leading to the appearance of spontaneous anti-MOG autoantibodies in the serum of these mice. In addition to T cells, in the TCR^{1640} model B cells infiltrate into the CNS parenchyma, too. Large deposits of antibodies along with some activated complement can be found in demyelinated lesions of diseased TCR^{1640} mice. The recruitment of MOG-specific B cells is strictly dependent on the presence of the target antigen, since TCR^{1640} mice deficient for MOG do not develop RR-EAE nor show any corresponding autoantibodies (Pöllinger *et al.*, 2009). In addition, early infiltration of T and B cells into the CNS of TCR^{1640} mice could already be found at pre-clinical stages at an age of four weeks, and anti-MOG autoantibodies were present in the serum at around five weeks after birth. Germinal centers and autoantibody-secreting B cells were found in cervical lymph nodes of TCR^{1640} mice, however, not in other lymphoid organs. One possible reason could be myelin debris draining from the subclinically inflamed CNS or being transported by phagocytes to cervical lymph nodes. This would induce further activation of MOG-specific T cells which then in turn drive B cells into germinal center reactions. Finally, this could mount a full attack on the target organ by autoreactive T cells along with the emergence of isotype class switched autoantibodies (Berer *et al.*, 2011b).

B cell depletion during EAE

The importance and differential role of B cells on the course of EAE was shown by depletion experiments. Passive transfer of serum containing myelin-specific autoantibodies alone could not induce clinical symptoms of EAE (Lassmann *et al.*, 1981), and early depletion of B cells by anti-IgM rendered animals immunized with MBP resistant to EAE (Willenborg and Prowse, 1983). Nonetheless, when combining both treatments – serum transfer into B cell depleted recipients – severity of active EAE could be restored (Willenborg *et al.*, 1986). B cells can also be efficiently depleted by antibodies targeting the B cell-specific surface marker CD20. While anti-CD20-mediated B cell depletion before the induction of active EAE exacerbated disease symptoms, depletion of B cells during disease progression profoundly suppressed symptoms. The increased severity of EAE with early B cell depletion resulted from an increased influx of encephalitogenic T cells into the CNS, due to the depletion of the rare IL-10-secreting $CD1d^{hi}/CD5^{+}$ regulatory B cell subset. During late depletion, B cells were removed from the system otherwise essential for continuous production of autoantigen-specific $CD4^{+}$ T cells and sustained entry of encephalitogenic T cells into the CNS (Matsushita *et al.*, 2008). Thus, B cells can have dual functions: either in driving autoimmunity as APCs, by producing autoantibodies, or by secreting inflammatory

cytokines, as IFNγ and IL-12; or in suppressing autoimmunity as IL-10-producing regulatory B cells, dampening the inflammatory potential of effector T cells or influencing the activity of other surrounding APCs (Figure 1.6) (Lund and Randall, 2010).

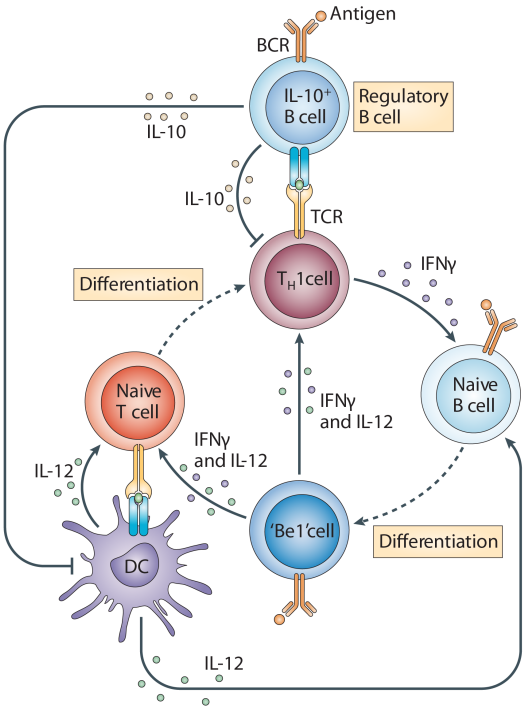

Figure 1.6 T – B cell interactions. Effector and regulatory B cells can present antigen to $CD4^+$ T cells and provide co-stimulation and cytokines. Effector B cells ('Be1' cells) can secrete cytokines, such as IFNγ and IL-12, that reinforce and stabilize the cytokine profile of T_H1 effector cells. In addition, the effector B cells can recruit additional naive T cells into the inflammatory response. By contrast, the regulatory B cells produce IL-10 which suppresses the inflammatory potential of effector T cells, alters the activity of antigen-presenting DCs, and promotes regulatory T cell development and expansion (adapted from Lund and Randall 2010).

OBJECTIVES

Activation of T cells is a crucial step in disease initiation. Since sustained intracellular calcium signaling is a prerequisite for effective activation of T cells, this process needs to be studied in detail for in-depth understanding of T cell function *in situ*. Unfortunately, so far calcium imaging in T cells was restricted to *in vitro* experiments, due to the limited intracellular persistence of synthetic calcium indicators. Therefore, sustained measurement of intracellular calcium level changes in T cells *in vivo* needs to be established by the use of a genetically encoded calcium indicator, like TN-XXL. T cells with stable transgenic expression of TN-XXL are to be obtained, and must be tested *in vitro* and *in vivo* with respect to functionality of the calcium indicator and potential interference with the expressing cell. This approach then allows imaging of T cell activation in peripheral immune organs as well as in the central nervous system, thus transferring calcium imaging from an artificial *in vitro* to a real *in vivo* setting.

B cells play a critical role in the development and persistence of EAE and MS, too. Therefore, in addition to calcium imaging in T cells, a novel mouse model for better analysis of B cells was to be established. Transgenic B cells in this mouse model should be fluorescently labeled for sustained imaging and tracking. This allows to follow the fate of B cells during their development, in steady-state conditions, or during an inflammatory response. Furthermore, B cells should be susceptible to toxin-mediated cytotoxicity to allow specific and efficient depletion of B cells at any time. Thereby, basic concepts of B cell biology as turnover rates or homeostasis as well as the specific role of B cells during disease could be studied.

MATERIAL and METHODS

2.1 MATERIAL

2.1.1 Bacteria

E. coli DH5α (Clontech, Heidelberg), F^- deoR endA1 hsdR17 (r_k^- m_k^-) supE44 thi-1 recA1 gyrA96 relA1 Δ(argFV196-lacZYA) ϕ80 lacZΔM15

E. coli GM2163 dam^-/dcm^- (NEB, Frankfurt), ara-14 leuB6 fhuA31 lacY1 tsx78 glnV44 galK2 galT22 mcrA dcm-6 hisG4 rfbD1 R(zgb210::Tn10) Tet^S endA1 rspL136 (Str^R) dam13::Tn9 (Cam^R) xylA-5 mtl-1 thi-1 mcrB1 hsdR2

LB (Luria Bertani) medium
10 g tryptone, 5 g yeast extract, 5 g NaCl, *ad* 1 l H_2O. 100 µg/ml ampicillin or 30 µg/ml kanamycin was added for selection. For agar plates 15 g agar was added to 1 l LB medium.

2.1.2 Oligonucleotides

Cloning primers

Name	Sequence 5´→3´	Gene	Purpose
mb1 delATG mut sens	CCGACTCACTGGCAGACGCTGCCAGGGGG	mb1	ΔATG exon I (SDM)
mb1 delATG mut antis	CCCCCTGGCAGCGTCTGCCAGTGAGTCGG	mb1	ΔATG exon I (SDM)
DTR mutUAG XbaI re	CGACCTCTAGATCCTAGTGGGAATTAGTCATGC	DTR	Recovers stopcodon
DTR mutUAG XhoI for	CAATACTCGAGTTCGCCACCATGAAGC	DTR	Recovers stopcodon
mb1 exonII mut sense	CACAGGTCGCGGCCGCCCGGGCCTGCGGGTAG	mb1	ΔATG exon II (SDM)
mb1 exonII mut antis	TACCCGCAGGCCCGGGCGGCCGCGACCTGTGG	mb1	ΔATG exon II (SDM)
pBKS MluI mut sense	CCCGGGCTGCACGCGTTCGATATCAAGC	$pBKS^-$	MluI-site (SDM)
pBKS MluI mut antis	GCTTGATATCGAACGCGTGCAGCCCGGG	$pBKS^-$	MluI-site (SDM)
IRES2-ECMV EcoRI f	TTAAAGAATTCCGCCCCTCTCCCTCCC	IRES2	Amplifies IRES2
IRES2-ECMV XhoI re	CTTGCTCTCGAGGGTTGTGGCCATATTATC	IRES2	Amplifies IRES2
WPRE EcoRI for	GGAATTCAATCAACCTCTGGATTACAAAATTTGTG	WPRE	Takes out WPRE
WPRE XhoI rev	TATCTCGAGCAGGCGGGGAGGCGG	WPRE	Takes out WPRE
NF-L link-1 SphI for	TATATAGCATGCTGTCTGAGCCTTCCC	NFL	Amplifies $NF\text{-}L_{130\text{-}275}$
NF-L link-2 SacII rev	TATTATGAGCTCCTGCATGTTCTTGGCG	NFL	Amplifies $NF\text{-}L_{130\text{-}275}$
YFP SacII Kozak for	GGATCCCGCGGCCGCCACCATGGGCGGCGTGC	YFP	Amplifies YFP
YFP EcoRI pRSETB r	GTTAGCAGCCGGATCAAGCTTCG	YFP	Amplifies YFP
TropC SacII Kozak fo	GGATCCCGCGGCCGCCACCATGCTGAGCG	ckTnC	Amplifies TnC
mTagBFP SacII for	ATATACCGCGGCCGCCACCATGAGCG	tBFP	Amplifies mTagBFP
mTagBFP SphI rev	GCTGAGCATGCTATTAAGCTTGTGCCCC	tBFP	Amplifies mTagBFP

(SDM, site-directed mutagenesis)

Genotyping primers

Name	Sequence 5´→3´	Gene	Mouse line
mb1-intronI end down	CGCTGCATCTAAGGTTCTGCCC	mb1 intron	mb1-R&D
tdRFP N-term up	CCTCGATCTCGAACTCGTGGC	tdRFP	mb1-R&D
sVA-TNXXL N-term for	AGGCACGTGGTTAAGCTCTCGG	hCD2 intron	hCD2-TN-XXL
sVA-TNXXL N-term re	TCGTGCTGCTTCATGTGGTCGG	CFP	hCD2-TN-XXL
CFP/YFP N-term for	AAGCTGACCCTGAAGTTCATCTGCACC	CFP or YFP	CAG(W)-TN-XXL
CFP/YFP C-term rev	TGTTGCCGTCCTCCTTGAAGTCGATGC	CFP or YFP	CAG(W)-TN-XXL

Quantitative PCR primers

Name	Sequence 5´→3´	Gene	Detection
CMV-prom 5´ seq for	TCCGCGTTACATAACTTACGG	CMV promoter	SYBR green
CMV-prom mid seq rev	TGATACACTTGATGTACTGCC	CMV promoter	SYBR green
CFP_Chr_for	CTGACCTGGGGCGTGCAGTGCTTC	CFP	SYBR green
CFP/YFP C-term rev	TGTTGCCGTCCTCCTTGAAGTCGATGC	CFP or YFP	SYBR green
Fabpi-200 for	TGGACAGGACTGGACCTCTGC	Fabpi	SYBR green
Fabpi-200 rev	GCTTTGCCACATCACAGGTCATTCAG	Fabpi	SYBR green
pCAGGS seq for	CTCTGCTAACCATGTTCATGCC	CAG intron	SYBR green
CAG prom 3´e for	CTGACTGACCGCGTTACTCC	CAG promoter	SYBR green
CFP/YFP N-term rev	ACTTGTGGCCGTTTACGTCG	CFP/YFP	SYBR green
GAPDH sense SYBR	GTGTCCGTCGTGGATCTGA	GAPDH	SYBR green
GAPDH AS SYBR	CCTGCTTCACCACCTTCTTG	GAPDH	SYBR green
IFNγ sense	TCAAGTGGCATAGATGTGGAAGAA	IFNg	FAM-TAMRA
IFNγ AS	TGGCTCTGCAGGATTTTCATG	IFNg	FAM-TAMRA
IFNγ probe	TCACCATCCTTTTGCCAGTTCCTCCAG	IFNg	FAM-TAMRA
IL-17 sense	AACTCCCTTGGCGCAAAAGT	IL-17a	FAM-TAMRA
IL-17 AS	GGCACTGAGCTTCCCAGATC	IL-17a	FAM-TAMRA
IL-17 probe	CCACGTCACCCTGGACTCTCCACC	IL-17a	FAM-TAMRA
IL-5 sense	CCGCTCACCGAGCTCTGTT	IL-5	FAM-TAMRA
IL-5 AS	AGATTTCTCCAATGCATAGCTGG	IL-5	FAM-TAMRA
IL-5 probe	CAGGAAGCCTCATCGTCTCATTGCTTGT	IL-5	FAM-TAMRA
IL-10 sense	CAGAGAAGCATGGCCCAGAA	IL-10	FAM-TAMRA
IL-10 AS	TGCTCCACTGCCTTGCTCTT	IL-10	FAM-TAMRA
IL-10 probe	TGAGGCGCTTGTCATCGATTTCTCCC	IL-10	FAM-TAMRA
mFoxP3 sense	AGGAGAAGCTGGGAGCTATGC	FoxP3	FAM-TAMRA
mFoxP3 AS	TGGCTACGATGCAGCAAGAG	FoxP3	FAM-TAMRA
mFoxP3 Probe	AAGGCTCCATCTGTGGCCTCAATGGA	FoxP3	FAM-TAMRA
mTNFα sense	CATCTTCTCAAAATTCGAGTGACAA	TNFa	FAM-TAMRA
mTNFα AS	TGGGAGTAGACAAGGTACAACCC	TNFa	FAM-TAMRA
mTNFα probe	CACGTCGTAGCAAACCACCAAGTGGA	TNFa	FAM-TAMRA
GAPDH sense	TCACCACCATGGAGAAGGC	GAPDH	FAM-TAMRA
GAPDH AS	GCTAAGCAGTTGGTGGTGCA	GAPDH	FAM-TAMRA
GAPDH probe	ATGCCCCCATGTTTGTGATGGGTGT	GAPDH	FAM-TAMRA

All DNA oligonucleotides used in this thesis were synthesized by Metabion (Martinsried).

2.1.3 Plasmids

Vector backbones

pBluescript II SK- (pBSK)	Bacterial cloning vector	Stratagene, Heidelberg
pCAG	Composite actin promoter	(Niwa *et al.*, 1991)
pcDNA3	Expression vector	Invitrogen, Karlsruhe
pEGFP-C1	EGFP fusion vector	Clontech, Heidelberg
pIRES2-eGFP	Coexpression vector	Clontech, Heidelberg
pmb1	B cell-specific promoter	(Hobeika *et al.*, 2006)
pMSCVneo	Retroviral vector	Clontech, Heidelberg
pRSET-B	Expression vector	Invitrogen, Karlsruhe
psVAhCD2MI232	T cell-specific promoter	(Zhumabekov *et al.*, 1995)
pUC13	Expression vector	(Messing, 1983)

Subcloned plasmids

Name	Backbone	Insert	Sel.
pHL-FB	pEGFP-C1	tdRFP	Kan
pIRES2-EGFP	expression vector	none	Kan
pEGFP-N1-DTR	pGEFP-N1	DTR	Kan
pCMV-tdRFP-IRES2-DTR	pEGFP-C1	tdRFP-IRES2-DTR	Kan
pBKS(-)mutMluI	mut cloning vector	none	Amp
pBKS-mutMluINruI	pBKS	none	Amp
pBKS-mMN-tdRFP	pBKS	tdRFP	Amp
pBKS-RFP/DTR	pBKS	tdRFP-IRES2-DTR	Amp
pUC13-mb1-6.4E	pUC13	mb1	Amp
pUC13-mb1-delATGexonI	pUC13	mb1	Amp
pUC13-mb1-delATGexonI+II	pUC13	mb1	Amp
pmb1-RFP/DTR	pUC13-mb1-delATGs	tdRFP-IRES2-DTR	Amp
pcDNA3-TNXXL	pcDNA3	TNXXL	Amp
sVAhCD2MI232	pBSK(-)	sVAhCD2	Amp
sVAhCD2-TNXXL	sVAhCD2MI232	TNXXL	Amp
pcDNA3-TNXXL-WPRE	pcDNA3	SFLTNXXL-WPRE	Amp
pCAGGS-MCS	pCAGGS	none	Amp
pCAGGS-SFLTNXXL	pCAGGS	SFLTNXXL	Amp
pCAGGS-SFLTNXXL-WPRE	pCAGGS	SFLTNXXL-WPRE	Amp
pCL-Eco	pCK	gag/pol/env	Amp
pMSCVneo-dsRed2	pMSCV	dsRed2	Amp
pMSCVneo-YFP	pMSCVneo	YFP only	Amp
pMSCVneo-TNXXL	pMSCVneo	TNXXL fulllength	Amp
pMSCVneo-TNXXL-TropC-NFL	pMSCVneo	TNXXL-TropC-NFL	Amp
pMSCVneo-TNXXL-delTropC	pMSCVneo	TNXXL-delTropC	Amp
pMSCVneo-TagBFP-link-Citcp174	pMSCVneo	TagBFP-link-Citcp174	Amp
pMSCVneo-TNXXL-CFP/Venuscp174CD	pMSCVneo	TNXXL-CFP/Venuscp174CD	Amp
pMSCVdelneo-TNXXL-CFP/Venuscp174CD	pMSCVneo	TNXXL-CFP/Venuscp174CD	Amp
pMSCVdelneo-TN3XL-CFP/Venuscp174CD	pMSCVneo	TN3XL-CFP/Venuscp174CD	Amp

2.1.4 DNA analysis buffers

TAE running buffer
40 mM Tris-HCl, 40 mM acetic acid, pH 8.0, 1 mM EDTA

DNA loading dye 10x
50 mM Tris-HCl, pH 7.6, 60% glycerol, 0.05% bromophenol blue, 0.05% xylen cyanol FF

Low salt / high salt buffer
0.2 M / 2.0 M NaCl, 20 mM Tris-HCl, 1 mM EDTA, pH 7.4

Microinjection buffer
10 mM Tris-HCl, 0.2 mM EDTA, pH 7.5

2.1.5 Cell culture

EL4 – Lymphoma induced in a C57BL/6 mouse by 9,10-dimethyl-1,2-benzanthracene treatment (suspension cells) (Gorer, 1950) (ATCC: TIB-39).

Phoenix – Retrovirus producer line based on HEK293 cells for the generation of helper free ecotropic retroviruses (semi-adherent cells) (Pear *et al.*, 1993).

RPMI 1640 and DMEM (complemented)
Media RPMI 1640 and DMEM (both Sigma-Aldrich, Taufkirchen) were complemented with 100 µM MEM non-essential amino acids, 1 mM sodium pyruvate, 50,000 units penicillin, 50 mg streptomycin, 2 mM L-glutamine (all Gibco, Karlsruhe), and 10% fetal calf serum (FCS) (Biochrome, Berlin). RPMI 1640 medium was further complemented with 200 µM 2-ME. Prior to use FCS was inactivated for 1 h at 56°C. Media were sterilized by filtration (pore size 0.2 µm). All quantities refer to 500 ml of medium.

2.1.6 Western blot analysis

RIPA buffer
50 mM Tris-HCl, pH 7.5, 150 mM NaCl, 1 mM EDTA, 1% Triton-X 100, 0.5% sodium deoxycholate, 0.1% SDS

Lämmli running buffer 10x
250 mM Tris-base, pH 8.8, 1% SDS, 1.92 M glycine

Lämmli loading buffer 2x
200 mM Tris-HCl, pH 6.8, 10% SDS, 10% glycerol, 10% β-ME, bromophenol blue to taste

Anode buffer I
300 mM Tris, pH 10.4, 20% methanol

Anode buffer II
25 mM Tris, pH 10.4, 20% methanol

Cathode buffer
25 mM Tris, pH 9.4, 40 mM 6-aminohexanic acid, 20% methanol

Primary antibodies
anti-GFP rabbit monoclonal, 1:5000 (Research Diagnostics Inc., Flanders, NJ, USA)
anti-GAPDH mouse monoclonal, 1:30000 (Sigma-Aldrich, Taufkirchen)

HRP-coupled secondary antibodies
anti-rabbit IgG goat polyclonal and anti-mouse IgG horse polyclonal, both 1:2000
(Cell Signaling Technology, Boston, MA, USA)

2.1.7 Frequently used buffers and solutions

Phosphate buffered saline (PBS)
10 mM Na_2HPO_4, 1.8 mM KH_2PO_4, pH 7.4, 140 mM NaCl, 2.7 mM KCl

Mammalian saline buffer
140 mM NaCl, 5 mM KCl, 1 mM $CaCl_2$, 1 mM $MgCl_2$ and 10 mM Hepes, pH 7.4

Mouse tail digestion buffer
100 mM Tris-HCl, pH 8.5, 200 mM NaCl, 5 mM EDTA, 1% Tween-20, 1 mg/ml Proteinase K

ACK buffer
150 mM NH_4Cl, 10 mM $KHCO_3$, 0.1 mM EDTA

Cell lysis buffer (native)
150 mM NaCl, 20 mM Tris-HCl, 1% Triton-X 100

2x BES (pH 6.95)
50 mM N,N-bis(2-hydroxyethyl)-2-aminoethanesulfonic acid, 280 mM NaCl, 1.5 mM Na_2HPO_4

2.1.8 Flow cytometry

FACS staining buffer

1% BSA, 0.1% sodium azide, in PBS

FACS markers

Specificity	Clone	Antibody class	Company
CD3ε	145-2C11	Ar Ham IgG1, κ	BD
CD4	RM4-5	Rat IgG2a, κ	eBioscience
CD5	53-7.3	Rat IgG2a, κ	BD
CD8α	53-6.7	Rat IgG2a, κ	eBioscience
CD11b	M1/70	Rat IgG2b, κ	BD
CD11b	M1/70	Rat IgG2b, κ	BD
CD19	1D3	Rat IgG2a, κ	BD
CD21	7G6	Rat IgG2b, κ	BD
CD23	B3B4	Rat IgG2a, κ	BD
CD24	M1/69	Rat IgG2b, κ	BD
CD25	3C7	Rat IgG2b, κ	eBioscience
CD44	IM7	Rat IgG2b, κ	BD
CD62L	MEL-14	Rat IgG2a, κ	eBioscience
CD69	H1.2F3	Ar Ham IgG1, λ3	BD
CD117	2B8	Rat IgG2b, κ	eBioscience
B220	RA3-6B2	Rat IgG2a, κ	eBioscience
IgM	R6-60.2	Rat IgG2a, κ	BD
F4/80	CI:A3-1	Rat IgG2b, κ	AdB Serotec
Gr-1	RB6-8C5	Rat IgG2b, κ	eBioscience
NKp46	29A1.4	Rat IgG2a, κ	eBioscience
Ly6C	AL-21	Rat IgM, κ	BD
Va3.2	RR3-16	Rat IgG2b, κ	BD
Va8.3	KT50	Rat IgG2a, κ	BD
Va2	B20.1	Rat IgG2a, l	BD
Streptavidin	-	-	eBioscience
AnnexinV	-	-	BD
TO-PRO-3	-	-	Invitrogen

FACS markers were directly fluorescently labeled with FITC, PE, PerCP, or APC, or were biotinylated and used in conjunction with Streptavidin-coupled fluorescent labels. All markers were purchased from BD (Heidelberg), eBioscience (Frankfurt), AdB Serotec (Düsseldorf), or Invitrogen (Karlsruhe).

2.2 METHODS

2.2.1 DNA techniques

In silico DNA analysis. Plasmid maps were drawn with Vector NTI 11 (Invitrogen, Karlsruhe); restriction enzyme digestions were designed using NEBcutter 2.0 (NEB, Frankfurt) and Webcutter 2.0 (Yale, New Haven, CT, USA); oligonucleotide primers were designed using IDT SciTools software (Integrated DNA Technologies, Coralville, IA, USA); DNA sequencing results were analyzed by BioEdit (Ibis Therapeutics, Carlsbad, CA, USA); sequence alignment was done by ClustalW (EMBL-EBI, Cambridge, UK); and DNA translation by ExPASy (SIB, Lausanne, Switzerland).

DNA modification. DNA was modified with enzymes using standard protocols provided by the manufacturers (NEB, Frankfurt; MBI Fermentas, St. Leon-Rot).

Plasmid precipitation. DNA precipitation was done by addition of 0.1 vol of 3 M sodium acetate and 1 vol of isopropanol, followed by centrifugation at 20,000 rcf for 20 min at 4°C. The DNA pellet was washed with 70% ethanol, dried in a Savant Speed Vac Concentrator (Thermo Fisher Scientific, Schwerte), and dissolved in H_2O.

DNA amplification by PCR. DNA was amplified by polymerase chain reaction using either Taq (Invitrogen, Karlsruhe), Easy-A High-Fidelity (Stratagene, Amsterdam, Netherlands), or Expand High Fidelity^{PLUS} (Roche, Mannheim) polymerase, according to the instructions of the manufacturers, run on a PTC-200 DNAEngine (MJ Research, Bio-Rad, München) cycler.

DNA purification. PCR products or DNA fragments were purified by the QIAquick PCR Purification Kit (Qiagen, Hilden) following the manufacturer´s instructions.

Agarose gel electrophoresis. DNA fragments were separated in agarose gels (1% agarose in TAE buffer, 1 µg/ml ethidiumbromide) using approx. 1 V/cm^2. DNA bands in analytical gels were visualized in the Geldoc XR system (Bio-Rad, München). For excision of DNA bands from preparative gels, long wavelength UV light (312 nm) on a IL 200 M transilluminator (Bachofer, Reutlingen) was used.

DNA extraction from agarose gels. DNA fragments were excised from agarose gels and DNA was isolated using the Wizard SV Gel Clean-Up System (Promega, Mannheim) following the instructions supplied by the manufacturer.

Ligation of DNA fragments. Following estimation of DNA concentration by Nanodrop ND-100 (PeqLab, Erlangen) measurement, vector backbone and insert were mixed in molar ratios of 1:2 to 1:5. The fragments were ligated in a total volume of 20 µl T4 DNA ligase buffer using 400 units T4 DNA ligase (NEB, Frankfurt) for 1 hour at RT.

Oligonucleotide duplex insertion. To introduce a new or modified multiple cloning site (MCS) into plasmids, sense and antisense oligonucleotides were designed to contain required restriction sites and to feature appropriate restriction site overhangs after dimerization for ligation into the target vector. For duplex formation, oligonucleotides were diluted to 10 µM each, mixed 1:1, denatured for 7 min at 95°C, and annealed for 5 min on ice. Thereafter, duplex was diluted to 500 nM final concentration and ligated with open target vector at 2.5 nM concentration in a 20 µl ligation reaction.

Preparation of electrocompetent E. coli. 15 ml LB medium were inoculated with *E. coli* DH5α and incubated at 37°C o/n on a Multitron 2 bacterial shaker (Infors HT, Bottmingen, Switzerland). From this culture, 6 ml were transferred to 500 ml LB medium, and grown to an OD_{600} of 0.6. Bacteria were chilled for 30 min on ice, harvested by centrifugation at 4,000 rcf for 15 min at 4°C, and washed twice, first in 500 ml, then in 250 ml of chilled sterile 10% glycerol. Thereafter, the bacteria were washed again in 10 ml and finally resuspended in 1 ml of sterile 10% glycerol, of which 50 µl aliquots were shock-frozen on dry ice.

Electroporation of E. coli. Electrocompetent *E. coli* were thawed on ice, and 50 µl of cell suspension were mixed with 1 µl DNA, transferred to a chilled electroporation cuvette, and transfected using the GenePulser (Bio-Rad, München) at 25 µF, 1.7 kV, and 200 Ω. After electroporation the bacteria were immediately transferred to 500 µl LB medium and agitated for 30 to 45 min at 37°C. 200 µl of cell suspension were plated onto LB agar plates containing antibiotic selection and incubated at 37°C o/n.

Long-term stocks of E. coli. For storage of transformed bacteria, 600 µl of an overnight culture was mixed with 400 µl of glycerol and stored in cryotubes at -80°C.

Isolation of plasmid DNA from E. coli. Small amounts of DNA for analytical digests were extracted from 3 ml of an overnight culture using a standard alkaline lysis protocol (Sambrook and Russel, 2001). Higher quantities of plasmid DNA were isolated with the HiSpeed Plasmid Midi Kit (Qiagen, Hilden) according to the instructions of the manufacturer; DNA was eluted in H_2O. The quantity of nucleic acids in solution was determined by Nanodrop ND-100 (PeqLab, Erlangen) measurement.

DNA purification for pronuclear injection. 25 µg of DNA were digested with restriction enzymes to release the transgene from the bacterial vector backbone, and the fragments were separated on a 0.8% agarose gel. The transgene fragment was excised under low intensity UV light (312 nm) and transferred into a dialysis tubing filled with TAE buffer. The dialysis bag was then fixed in the gel chamber across the electric field, and electrophoresis was continued for 1 hr at 80 V to allow the transgene DNA to migrate out of the gel. To force DNA back from the dialysis wall into solution, polarity was changed several times for 30 sec, before recovering the DNA-containing buffer from the tubing. The DNA was isolated using Elutip-d Purification Minicolumns (Schleicher & Schüll, Dassel) following the instructions of the manufacturer, EtOH precipitated, dried, and dissolved in 50 µl microinjection buffer. The

transgene concentration, purity and integrity was estimated by Nanodrop ND-100 (PeqLab, Erlangen) and gel electrophoresis, before the DNA concentration was adjusted to 100 ng/µl and submitted to the institute´s pronuclear microinjection service unit.

Codon diversification and gene synthesis. To optimize the calcium indicator TN-XXL for retroviral transduction, the original TN-XXL DNA sequence was codon diversified without changing the amino acid sequence and synthesized (Sloning Biotech, Puchheim).

Isolation of genomic DNA. Total genomic DNA was isolated from organs using the QIAamp DNA Mini Kit (Qiagen, Hilden) using the protocol provided by the manufacturer.

2.2.2 RNA techniques

RNA extraction. Total RNA was isolated from purified cells or whole tissue by TRI Reagent (Sigma-Aldrich, Taufkirchen) following the instructions provided by the manufacturer.

Reverse transcription. cDNA was generated from RNA using SuperScript II Reverse Transcriptase (Invitrogen, Karlsruhe) or the Verso cDNA Kit (Thermo Fisher Scientific, Schwerte), according to the manufacturer´s instructions.

Quantitative PCR. Real-time qPCR was performed using the ABsolute QPCR Mixes (Thermo Fisher Scientific, Schwerte) according to the instructions of the manufacturer, and samples were run on a 7900HT Fast Real-Time PCR System and analyzed by SDS 2.3 software (both Applied Biosystems, Darmstadt).

2.2.3 Cell culture

Cultivation of cell lines. Cell lines or primary cells were cultivated in fully complemented RPMI or DMEM medium in standard cell culture-treated plastic dishes (BD, Heidelberg; Nunc, Roskilde, Denmark; Corning, Kaiserslautern) in a humidified incubator (Heraeus, Langenselbold) at 37°C and 5% or 10% CO_2, respectively. Cells growing in suspension were harvested by resuspending the culture; semi-adherent cells were flushed off the culture dish surface; and adherent cells were first briefly rinsed with PBS and then trypsinized with Trypsin-EDTA (PAA Laboratories, Pasching, Austria) for 3 to 5 minutes at 37°C. Cell densities were regularly determined using a Neubauer hemocytometer (Neubauer, Marienfeld). Cultures were kept subconfluent by regular dilution with fresh medium at ratios from 1:2 to 1:10. Cells were pelleted by centrifugation at 250 rcf for 10 min at 4°C.

Freezing and thawing of stocks. For preparation of long-term stocks, 5 x 10^6 cells were harvested and resuspended in 500 µl 10% DMSO in FCS. Stocks were frozen in a Cryo 1°C Freezing Container (Thermo Fisher Scientific, Schwerte) at -80°C and subsequently stored

in liquid nitrogen. For thawing, stocks were transferred to 37°C and washed once with 10 ml fresh medium to remove DMSO, before resuspension in 10 ml warm medium.

Electroporation of cell lines. EL4 cells (7 x 10^6 per transfection) were centrifuged at 250 rcf for 10 min at 4°C and washed twice with RPMI medium. Cells were suspended in 800 µl RPMI and kept for 10 min on ice, before 30 µg of linearized DNA in 50 µl RPMI were mixed in. After another 10 min incubation time on ice, cells were electroporated in a GenePulser (Bio-Rad, München) with 280 V and 960 µF. Cells were allowed to rest for 10 min on ice before being transferred into 10 ml complemented RPMI and incubated at 37°C.

Calcium phosphate transfection of Phoenix cells. 2 x 10^6 Phoenix cells were seeded per 10 cm culture dish in 10 ml medium and incubated o/n. Prior to transfection 25 µM chloroquine (Sigma-Aldrich, Taufkirchen) was added to the medium. The transfection complex was generated by diluting 12 µg DNA in 438 µl H_2O, mixing in 62 µl 2 M $CaCl_2$, and adding 500 µl 2x BES dropwise while vortexing. After 20 min incubation at 37°C the calcium phosphate-DNA co-precipitate was transferred dropwise onto the Phoenix cells. After o/n incubation culture medium was replaced to detoxify from calcium phosphate and chloroquine.

Retroviral transduction of primary T cells. $CD4^+$ T cells were purified from WT mouse spleens using the MagCellect negative isolation kit, and 2 x 10^6 cells per well were stimulated in 6-well plates pre-coated with 0.5 µg/ml anti-CD3 and anti-CD28 antibodies (both BD, Heidelberg). Alternatively, transgenic splenocytes from 2D2 x IgH^{MOG}, TCR^{1640} x IgH^{MOG}, or OT-II mice were used without any previous purification step, and stimulated by adding 20 µg/ml recombinant MOG or 10 µg/ml OVA peptide, respectively. Cells were incubated for 2 days prior to retroviral transduction to ensure robust proliferation. To obtain virus for transduction, Phoenix packaging cells were calcium phosphate transfected with pMSCV vectors featuring inserts of interest. Two days after transfection Phoenix supernatant was collected and centrifuged at 6,000 rcf for 18 hrs at 4°C in Corex II glass centrifugation tubes (Corning, Amsterdam, The Netherlands) to concentrate the virus. Virus pellets were resuspended in fresh Phoenix supernatant collected from the same transfectant, supplemented with 8 µg/ml polybrene, and used for spin-infection of stimulated primary T cells at 500 rcf for 90 min at RT in RetroNectin-coated (Takara, Ōtsu, Japan) culture dishes. 48 hrs after transduction transgene expression was estimated by FACS analysis.

Cell labeling with tracking dyes. 2 x 10^7 cells were suspended in 5 ml RPMI, 1% FCS, mixed with 2 µM CFSE (Invitrogen, Karlsruhe), 5 µM eFluor 670 (eBioscience, Frankfurt), or 5 µM SNARF-1 (Invitrogen, Karlsruhe), and incubated for 10 min at 37°C with occasional shaking. To stop labeling process, 45 ml cold PBS was added and cells were centrifuged at 250 rcf for 10 min at 4°C. After another washing step with cold PBS, cells were resuspended in growth medium for culturing or PBS for direct intravenous injection.

Cell labeling with calcium dye Fura Red. 6 x 10^6 cells were resuspended in 1 ml 1x Hank´s balanced salt solution containing 1% FCS, 1x Powerload, and 10 µM Fura Red (all Invitrogen, Karlsruhe). After incubation for 30 min at 37°C cells were washed twice with PBS.

Proliferation assay. 2 x 10^5 lymphocytes per well were seeded in 96-well round-bottom plates in a total volume of 200 µl growth medium in triplicates. After a culture period of 48 hours, 1 µCi ^{3}H-labeled thymidine (PerkinElmer, Rodgau) was added per well. Samples were harvested 16 hours later and tritium incorporation was measured on a Matrix 9600 Direct Beta Counter (Packard, Meriden, CT, USA).

Cell lysate preparation (native). Lysates were prepared by resuspending cells in 500 µl cell lysis buffer, followed by incubation for 30 min at 4°C with constant rotation. Cell fragments were spun down by centrifugation at 20,000 rcf for 1 hour, before supernatant was recovered and analyzed. Fluorescent proteins were measured on a Cary Eclipse fluorescent spectrophotometer (Varian, Darmstadt).

2.2.4 Mouse routine

Mouse license. All animals used in this study were bred in the animal facilities of the Max Planck Institutes of Biochemistry and Neurobiology. The animal procedures were in accordance with guidelines of the committee on animals of the Max Planck Institute for Neurobiology, and with the license of the Regierung von Oberbayern.

Generation of transgenic mice. Purified transgene constructs were submitted to the pronuclear injection service unit (MPI of Biochemistry, Martinsried). Up to 300 C57BL/6 fertilized oocytes from superovulated female mice were harvested and microinjected into the pronucleus. Groups of 30 embryos were reimplanted into the oviduct of pseudopregnant female recipients. Offspring were analyzed for transgene presence, positive mice then crossed to C57BL/6 mice, and F1 offspring were reanalyzed for transgene transmittance.

Mouse genotyping. Transgenic mice were genotyped either by tail biopsy digested o/n in tail digestion buffer followed by PCR analysis with transgene-specific primers on phenol-chloroform (Roth, Karlsruhe) extracted DNA; by FACS analysis of PBMCs for expression of fluorophores or presence of certain surface markers; or by whole mount illumination to test for ubiquitous fluorophore expression in the skin in a custom build illumination chamber.

Leukocyte isolation from peripheral blood. 2 to 5 droplets of blood were collected from anesthetized mice by retro-orbital bleeding into 100 µl 200 U/ml heparin (Sigma-Aldrich, Taufkirchen) in PBS. Erythrocytes were lysed by incubation in 1 ml ACK buffer, and leukocytes were spun down at 500 rcf for 5 min, washed with 1 ml ACK buffer, and finally resuspended in 200 µl FACS buffer.

Lymphocyte preparation from isolated organs. Mice were sacrificed and lymphoid organs were removed by dissection. Single cell suspensions were obtained by dissociating tissues through 40 µm cell strainers (BD, Heidelberg). Cells were centrifuged at 250 rcf for 10 min at 4°C and resuspended in complemented RPMI for culturing or further downstream analysis.

For spleen or bone marrow preparations, an additional erythrocyte lysis step was performed by incubating the cell suspension in 0.83% NH_4Cl for 3 min at RT and washing with RPMI.

Cell transfer for lymph node imaging. One day after retroviral transduction, 5-15 x 10^6 OT-II T cells were adoptively transferred by i.v. injection into the tail vein of mildly irradiated (20 Gy) C57BL/6 recipients. Mice were allowed to recover for one week before adoptive transfer of APCs. For imaging of T cell – DC interactions, BMDCs were obtained from C57BL/6 mice femurs and cultured in the presence of GM-CSF producing hybridoma-conditioned medium, with repeated medium exchange to deplete non-adherent cells. After 8 days in culture, BMDCs were trypsinized and activated o/n in fresh medium supplemented with 1 µg/ml LPS. Activated BMDCs were labeled with SNARF-1 (Invitrogen), and 2 x 10^6 BMDCs were injected subcutaneously into the lower leg. Imaging of the draining popliteal lymph node was performed on the next day. For imaging of T – B cell interactions, B cells were obtained from IgH^{MOG} mice mouse spleens using the MagCellect B cell isolation kit (R&D) and cultured in the presence of 1 µg/ml LPS. Two days later, B cells were pulsed o/n with 20 µg/ml recombinant MOG, labeled with SNARF-1, and 15 x 10^6 B cells were injected i.v. into the tail vein. Popliteal lymph node imaging was performed 2 hours (early), 8 hours (intermediate), or 24 hours (late) after B cell transfer.

OT-II T cell transfer during active EAE. C57BL/6 mice were subcutaneously immunized at the base of the tail with 200 µg recombinant MOG emulsified in complete Freund´s adjuvant (Difco, Franklin Lakes, NJ, USA). 400 ng pertussis toxin (List Biological Laboratories, Campbell, CA, USA) was injected i.p. on days 0 and 2. One week after immunization 10 x 10^6 transduced OT-II T cells were adoptively transferred by i.v. injection into the tail vein, and 4-5 days later spinal cord imaging was performed.

Passive EAE. For induction of adoptive transfer EAE, T cells from *in vitro* cultures were centrifuged at 250 rcf for 10 min at 4°C, washed once with cold PBS, and resuspended in cold PBS. Recipient mice were fastened in a restrainer and 250 µl cells were injected i.v. into the tail vein. In addition 400 ng of pertussis toxin (List Biological Laboratories, Campbell, CA, USA) were injected intraperitoneally. Clinical symptoms were evaluated by classical EAE scores: score 0 – no disease; score 0.5 – reduced tail tonus; score 1: limp tail; score 1.5 – limp tail and ataxia; score 2 – limp tail and hind limb weakness; score 2.5 – at least one hind limb paralyzed/weakness; score 3 – both hind limbs paralyzed/weakness; score 3.5 – complete paralysis of hind limbs; score 4 – paralysis until hip; score 5 – moribund or dead.

Diphtheria toxin treatment. For depletion of B cells in R&D mice, Diphtheria toxin (DTx) (Sigma-Aldrich, Taufkirchen) was injected intraperitoneally at concentrations and time points as mentioned at the respective experiment.

Intracardiac perfusion. In anesthetized mice the thoracic cavity was opened and a butterfly needle was inserted into the left ventricle. After incising the right atrium, mice were slowly perfused with 30 ml PBS 4% PFA in PBS for later dissection and histological analysis.

2.2.5 Western blotting

Preparation of protein lysates. Tissue was cut in small pieces, frozen in liquid nitrogen, and pestled. Fragments were suspended in RIPA buffer and homogenized in a Polytron PT 3000 (Kinematica, Luzern, Switzerland) on ice. Cell fragments were pelleted by centrifugation for 10 min at 20,000 rcf before supernatants were recovered and stored at -20°C.

BCA assay. Protein concentration was estimated using the BCA protein assay following the manufacturer´s instructions (Thermo Scientific Pierce, Rockford, IL, USA).

SDS-PAGE. Separation of proteins was achieved by denaturing, discontinuous, one-dimensional SDS polyacrylamide gel electrophoresis (Lämmli, 1970), using pre-cast Novex 4-12% tris-glycine gels (Invitrogen, Karlsruhe). 2x Lämmli buffer was added to 10 µl cell lysate, boiled for 5 min at 100°C, and loaded to each lane. Electrophoresis was performed in Lämmli running buffer at 100 V for stacking, and at 130 V for resolving of proteins in a Mighty Small gel chamber (Hoefer, San Francisco, CA, USA). To verify appropriate sample loading, gels were stained with Coomassie Brilliant Blue G-250 (Bio-Rad, München).

Western transfer. Proteins were electrophoretically transferred from polyacrylamide gels to Immobilion-FL PVDF membranes (Millipore, Schwalbach) using the semi-dry blot technique. Configuration of the Western blot was: 6 layers Whatman paper wetted in anode buffer I, 3 layers Whatman paper pre-wetted in anode buffer II, PVDF membrane (pre-equilibrated in methanol), polyacrylamide gel, 6 layers Whatman paper wetted in cathode buffer. The transfer was carried out at a current of 0.8 mA/cm^2 for one hour at RT.

Immunodetection of proteins. All incubations were done on a rocking table. After transfer of proteins, the membrane was blocked by incubation in PBS 5% milk powder o/n in the cold room. The primary antibody was diluted in PBS 0.1% Tween-20 1% milk powder. Primary antibody incubation was done for 1 hour at RT. After four washings with PBS 0.2% Tween-20 for 5 min, the membrane was incubated with HRP-coupled secondary antibody in PBS 0.1% Tween-20 1% milk powder for 1 hour at RT in the dark. The membrane was washed four times for 5 min; final washing was done in PBS without Tween-20. Bands were detected using ECL Western Blotting Substrate (Thermo Scientific Pierce, Rockford, IL, USA) on Amersham Hyperfilm ECL (GE Healthcare, München).

2.2.6 Flow cytometry (FACS)

FACS staining. Cells to be analyzed were transferred into 96-well V-bottom plates and centrifuged at 250 rcf for 10 min at 4°C. Cells were washed in 200 µl FACS buffer twice, resuspended in 50 µl FACS buffer containing directly labeled surface marker-binding antibodies at appropriate dilutions, and incubated for 20 min at 4°C. After washing and

resuspension in 100 µl FACS buffer, samples were acquired on a FACS Calibur or FACS Canto (all FACS machines from BD, Heidelberg), and analyzed using FlowJo 7.6 software (TreeStar, Ashland, OR, USA).

FACS sorting. Antibody stained splenocytes or transgenic cell lines expressing fluorescent proteins were resuspended in RPMI and sorted on a FACS Vantage SE or a FACS Aria II.

In situ calcium calibration. FACS-based intracellular calcium calibrations were obtained as described previously (June and Moore, 2004). Briefly, cells were resuspended in 10 mM MOPS buffer containing defined amounts of 10 mM CaEGTA and K_2EGTA. To force cells to equilibrate with extracellular calcium levels, MOPS buffer was poisoned with 4 µM ionomycin, 10 µM carbonyl cyanide m-chlorophenyl hydrazone, 40 mM 2-deoxyglucose, and 60 mM sodium azide. Cells were incubated for 90 minutes at 37°C to allow for clamping and calcium equilibration before acquisition on a FACS Canto.

2.2.7 Fluorescence microscopy

Tissue sections. Organs from PFA perfused mice were fixed in 4% PFA in PBS for 1 hr, and immerged in 30% sucrose o/n. Tissues were embedded in Tissue-Tek O.C.T. Compound (Sakura, Staufen), and 10 µm sections were cut on a CM3050 S Cryocutter (Leica, Wetzlar).

Fluorescence immunohistochemistry. (Note: between every change of reagent, samples were washed 3 times with PBS at RT.) Tissue sections were thawed, fixed in cold acetone for 10 min, and blocked with 5% BSA in PBS for 2 hrs at RT. Incubation with anti-CD4 antibody (rat monoclonal, 1:500, BD, Heidelberg) was done in 5% BSA in PBS o/n at 4°C. Incubation with Alexa Fluor 488-labeled secondary antibody (anti-rat IgG goat polyclonal, 1:2000, Invitrogen, Karlsruhe) was done in 5% BSA in PBS for 2 hrs at RT. Cell nuclei were stained with DAPI (Invitrogen, Karlsruhe) in PBS for 5 min at RT, before sections were eventually rinsed with H_2O and embedded in anti-fading mounting medium (Sigma-Aldrich, Taufkirchen). Images were acquired on an inverted SP2 confocal microscope (Leica, Wetzlar) or an inverted AxioVert 200M microscope (Carl Zeiss, München). Individual images were assembled for overviews of whole organs using the Photomerge function of Photoshop CS5 software (Adobe Systems, Unterschleißheim).

In vitro widefield time-lapse microscopy. EL4 thymoma or primary T and B cells were suspended in saline buffer supplemented with 10 mM glucose. Cells were seeded on a glass bottom culture dish (MatTek, Ashland, MA, USA) coated with type I collagen (Invitrogen, Karlsruhe). Time-lapse images were acquired on a Axiovert 200M microscope (Carl Zeiss, München) equipped with a 37°C incubation chamber. TN-XXL was excited with a 436/20 nm band-pass filter, and CFP and FRET emission was detected with a 480/40 nm and a 535/30 nm band-pass filter, respectively (Semrock, Rochester, NY, USA). Microscopy data was processed using MetaMorph (Molecular Devices) and ImageJ (NIH) software.

In vivo two-photon microscopy. Time-lapse two-photon laser-scanning microscopy was performed using a SP2 confocal microscope (Leica, Wetzlar) equipped with a 10 W Millenia/Tsunami laser (Newport Spectra Physics, Darmstadt). Excitation wavelength was tuned to 835 nm and routed through a Leica x25 water immersion objective (NA 0.95). Typically areas of 240 x 240 µm size were scanned, and 25-30 µm z-stacks were acquired with 3-4 µm z-step. Acquisition rate was 16-20 s interval time, with images averaged twice. Fluorescent signals were detected using non-descanned photomultiplier tube detectors (Hamamatsu, Herrsching) equipped with 475/50 nm, 537/26 nm, 630/69 nm, and 685/40 nm band-pass filters (Semrock, Rochester, NY, USA). Mice were anaesthetized by intra-muscular injection of fentanyl/midazolam/medetomidine (50 µg/kg, 5 mg/kg, and 500 µg/kg bodyweight, respectively), orotracheally intubated, and ventilated with 1.5% isoflurane. Popliteal lymph nodes were exposed by cutting the skin at the hollow of the knee and careful dissection of the adductor musculature. For spinal cord imaging a spinal cord window was prepared at level Th12/L1. After midline skin incision, the paravertebral musculature was detached from the spine and laminectomy on one spine disc was performed. Animals were stabilized in a custom-made microscope stage and body temperature was regulated by a heated pad (37.5°C). Electrocardiograms were recorded and physiological parameters were constantly monitored during imaging. Blood vessels were visualized by intravenous infusion of Texas Red-conjugated dextran (50 µg; 70 kDa; Invitrogen, Karlsruhe).

Image analysis. Time-lapse images were acquired using Leica LCS software (Leica, Wetzlar), and subsequently processed and analyzed by ImageJ (NIH, Bethesda, MD, USA). To obtain two-dimensional movies, a Gaussian blur filter was applied and maximum intensity z-projections were made. Ratiometric pseudocolor pictures were generated by dividing the FRET by the CFP channel and applying a fire lookup table. For analysis, cell shape at each time point was manually outlined in the maximum projection picture, and average signal intensities of all pixels within this area were calculated. Motility parameters and cell trajectories were calculated from the obtained position coordinates using Excel (Microsoft, Unterschleißheim). The linearity index is defined as the sum of total displacement divided by the path length of a T cell, the circularity index is defined as $4\pi(\text{area}/\text{perimeter}^2)$. Cell trajectories were calculated from the obtained coordinates and aligned for starting position.

Calcium data transformation. Calcium indicator specificities are determined by the dissociation constant K_d (indicating the binding affinity for calcium) and the Hill coefficient h (specifying the slope of the calcium binding curve). For ratiometric calcium indicators, ratio changes are calculated by relating the fluorescence intensities at the respective wavelength maximum of the calcium-bound to the calcium-free state. Values then get normalized to display the fractional ratio change $\Delta R/R$ in percent, with $\Delta R/R = (R-R_0)/R_0$ (R = actual ratio, R_0 = ratio at zero calcium) (Gunter and Gunter, 2001).

RESULTS

3.1 THE R&D MOUSE

3.1.1 Cloning of R&D constructs

The aim of the R&D project was to obtain another valuable tool to study B cell functions in EAE by engineering B cells to simultaneously express red fluorescence protein (RFP) to allow *in vivo* tracking, and the human Diphtheria toxin receptor (DTR) to deplete them at any given time by injection of Diphtheria toxin (DTx) (Saito *et al.*, 2001). Since quite a number of various RFPs is available (Shaner *et al.*, 2004), a variant, tandem dimer RFP (tdRFP), was chosen that is suitable for sustained and high expression in murine lymphocytes (Luche *et al.*, 2006). tdRFP consists of two monomeric RFPs interlinked by a flexible linker (Campbell *et al.*, 2002). This duplication yields two advantages: (1) increased fluorescence intensity due to the presence of two identical fluorophores; (2) reduced risk of intermolecular protein aggregation (which RFP tends to) by promoting intramolecular dimerization. For simultaneous expression of tdRFP and DTR (termed R&D), both genes were placed in succession, separated by an internal ribosomal entry site (IRES), and subcloned into the cytomegalovirus (CMV) promoter-driven expression vector pCMV to obtain pCMV-R&D (cloning scheme in Figure 3.1.1).

3.1.2 Functional characterization of the R&D construct in EL4 cells *in vitro*

The approach to specifically deplete murine cells by DTx utilizes a distinct difference between mice and men: rodents in general are resistant to DTx due to lack of binding of the toxin to the low affinity endogenous murine heparin-binding epidermal growth factor (HB-EGF) receptor. However, transgenic expression of the high affinity human HB-EGF receptor renders a murine cell susceptible to DTx-mediated depletion, which blocks translation and thereby drives apoptosis pathways (Figure 3.1.2A) (Palmiter, 2001).

Initial verification of the R&D construct was done *in vitro* in EL4 murine lymphoma cells. EL4 cells were transfected with linearized pCMV-R&D, and cell clones stably expressing the R&D construct were obtained by FACS sorting and limiting dilution. The clone with the highest RFP expression was chosen for further analysis. Both, FACS analysis and microscopy analysis confirmed strong expression of RFP in EL4 cells (Figure 3.1.2B).

To test the efficiency of DTx-mediated killing, R&D-expressing EL4 cells were treated with increasing concentrations of DTx. After overnight incubation, transgenic cells showed a

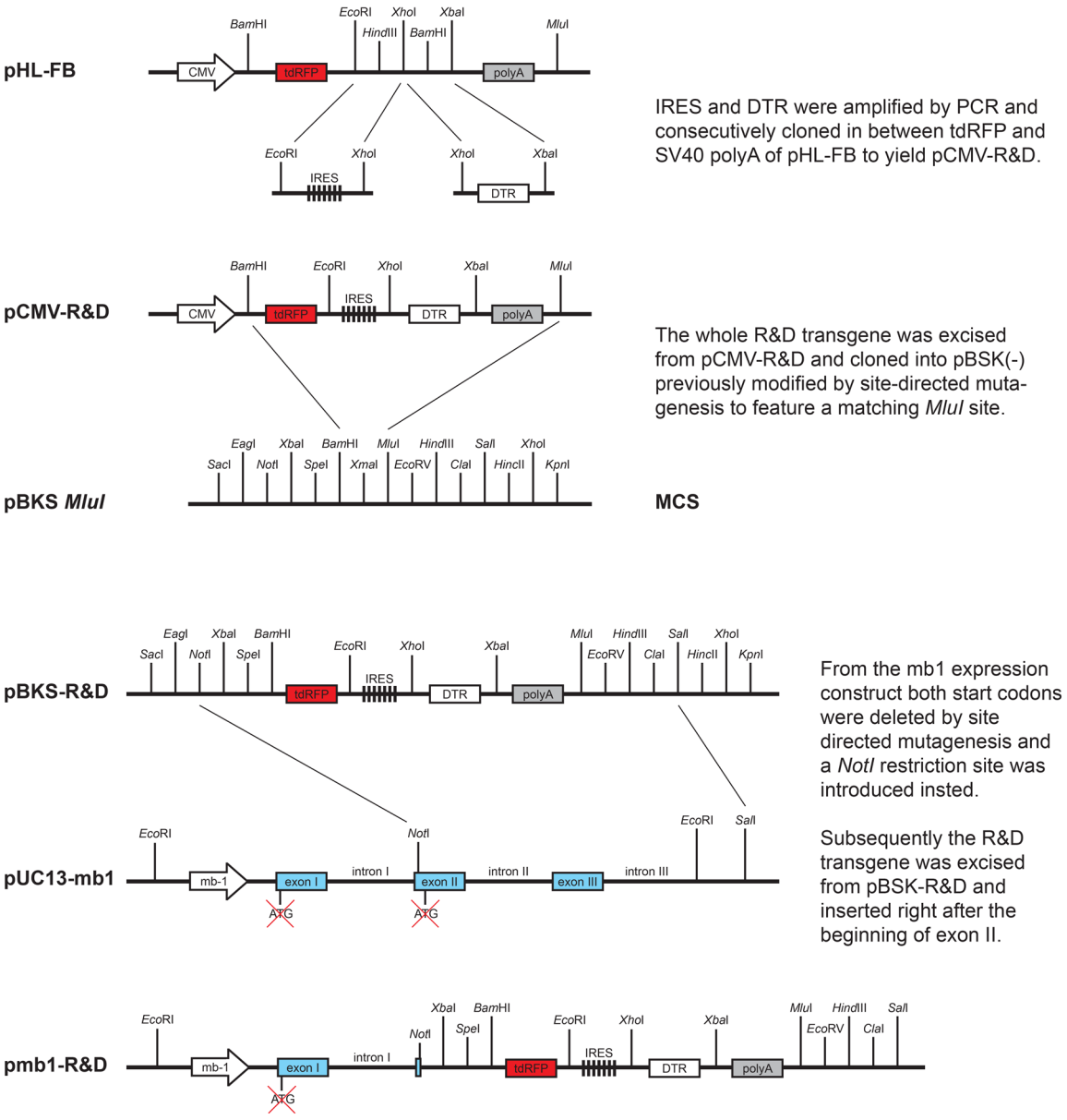

Figure 3.1.1 Generation of the construct for transgenic mb1-R&D mice. Schematic representation of the cloning strategy for the expression construct, pmb1-R&D, used for generation of R&D transgenic mice. The tandem-dimer red fluorescent protein (tdRFP) and the human Diphtheria toxin receptor (DTR), separated by an internal ribosomal entry site (IRES), are driven by the B cell-specific *mb-1* promoter.

10^5 higher sensitivity to DTx over wild-type (WT) EL4 cells, which were killed only at the highest DTx concentration (Figure 3.1.2C). To follow the actual time course of DTx-mediated cytotoxicity, a concentration of 50 ng/ml was applied to R&D-expressing EL4 cells. Apoptotic cells as detected by AnnexinV staining first emerged after 12 hours, followed by dead cells positive for the cell death marker TO-PRO-3 after 15 hours. At 24 hours all cells incubated with 50 ng/ml DTx were dead (Figure 3.1.2D).

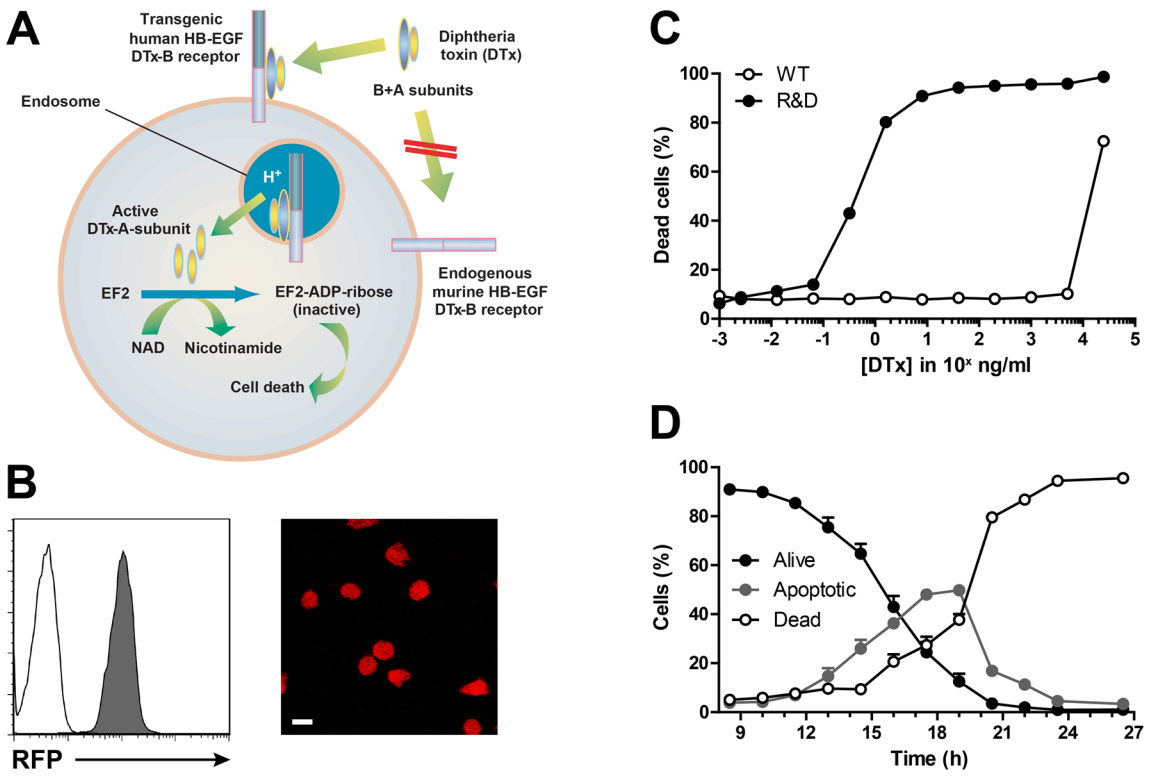

Figure 3.1.2 Transgenic expression of the R&D construct in EL4 cells. (A) Schematic depiction of Diphtheria toxin-mediated killing of a mouse cell: DTx cannot bind to the endogenous murine HB-EGF receptor, but efficiently binds to a transgenically expressed human HB-EGF receptor. After endocytosis and endosome release, the active DTx subunit induces a translation block which causes cell death (modified from Palmiter, 2001). **(B)** FACS histogram and microscopic image of RFP fluorescence in EL4 cells. Scale bar 10 µm. **(C, D)** *In vitro* killing assay of R&D-expressing EL4 lymphoma cells, **(C)** using increasing DTx concentrations and measurement after 24 hrs, or **(D)** over time using 50 ng/ml DTx. Apoptotic cells were determined by AnnexinV staining, dead cells by TO-PRO-3 staining.

3.1.3 Generation and characterization of R&D transgenic mice

Having successfully tested the R&D construct *in vitro* in EL4 cells, the construct was excised from the pCMV-R&D construct and further subcloned into a vector containing the B cell-specific *mb-1* promoter to generate transgenic mice expressing R&D in B lymphocytes (cloning scheme in Figure 3.1.1). The *mb-1* gene encodes the small Ig-α signaling subunit of the B cell receptor which is expressed from the early pro-B cell developmental stage on (Hobeika *et al.*, 2006). After sequence verification, the final pmb1-R&D transgene was linearized with EcoRI and PvuI, separated from the bacterial backbone, and microinjected into fertilized C57BL/6 oocytes. Out of five transgenic founder lines obtained, three transmitted the R&D transgene to the next generation. Analysis of red fluorescence in B cells of peripheral blood showed bright fluorescence specifically in B cells of the F1 progeny from one transgenic mouse line. This mouse line with the strongest RFP expression, termed R&D mice, was chosen for further analysis.

RFP expression in B cells of R&D mice was well detectable at the population level, with a high degree of selectivity for B cells as analyzed by FACS (Figure 3.1.3A). RFP-expressing B cells were easily distinguishable from other cell types by live microscopy as well as in fixed lymph node slices (Figure 3.1.3A). The tdRFP fluorophore used for generation of the R&D mouse is superior for two-photon microscopy (Drobizhev *et al.*, 2011). Nonetheless, higher wavelength light is necessary for efficient excitation of red fluorescent proteins. By using 920 nm or shorter wavelengths (as usually taken for excitation of GFP), almost no red fluorescence was detectable; only with wavelengths above 1000 nm, red fluorescence was well visible by two-photon microscopy in R&D B cells (Figure 3.1.3B).

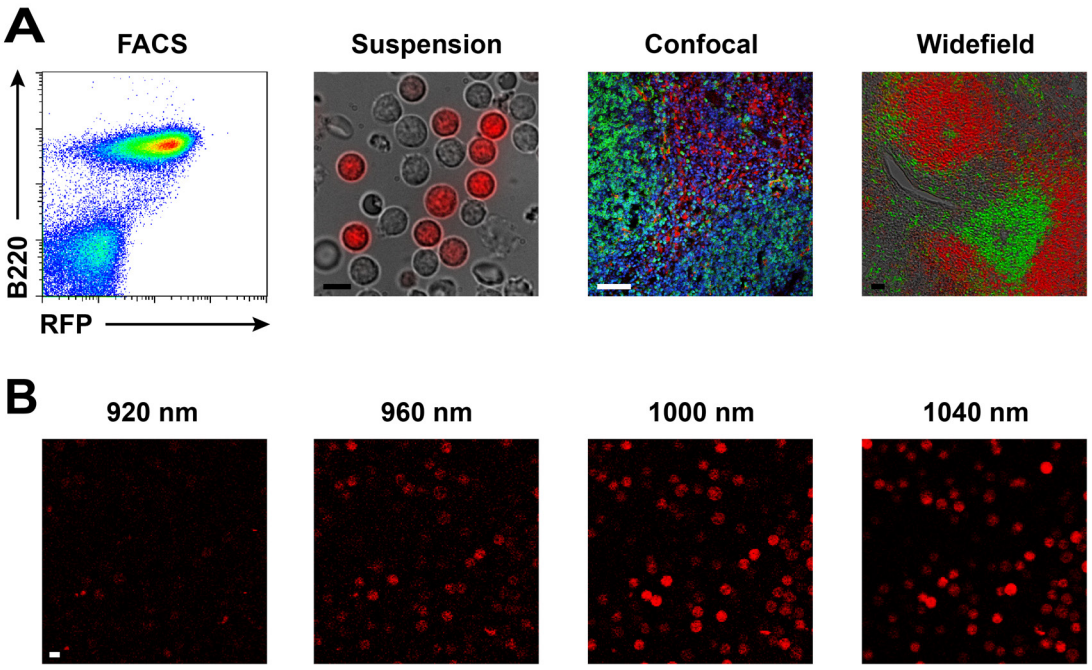

Figure 3.1.3 Transgenic expression of RFP in murine B cells from R&D mice. (A) Analysis of RFP expression in B220 positive B cells by FACS analysis of peripheral blood lymphocytes. Microscopic analysis of splenocyte suspension cells by widefield microscopy, and by confocal microscopy (DAPI nuclear stain in blue) as well as widefield composite microscopy of fixed spleen sections, costained with anti-CD4 (green) for T cell staining. **(B)** Two-photon microscopic acquisition of R&D B cells in suspension at various excitation wavelengths. Scale bars for suspension cells 10 µm, for sections 100 µm.

To estimate changes in RFP expression levels in B cells during their maturation, bone marrow from R&D mice was stained with specific developmental surface markers (Figure 3.1.4A). Grouping B cells into different developmental subsets (Hardy fractions A-F (Li *et al.*, 1993)) and analyzing corresponding fluorescence levels showed a constant increase of RFP expression paralleling B cell maturation (Figure 3.1.4A).

Another interesting feature of the R&D mouse appeared when analyzing transgenic females: only about 50% of all B cells showed expression of RFP, suggesting an X-linked inheritance of the transgene. This proofed to be true when interbreeding R&D mice did eventually yield homozygous females with 100% of all B cells showing red fluorescence (Figure 3.1.4B). X-linked expression of the R&D construct did not influence transgene properties but allowed straightforward screening for homozygous females and establishing a homozygous breeding scheme with hemizygous males.

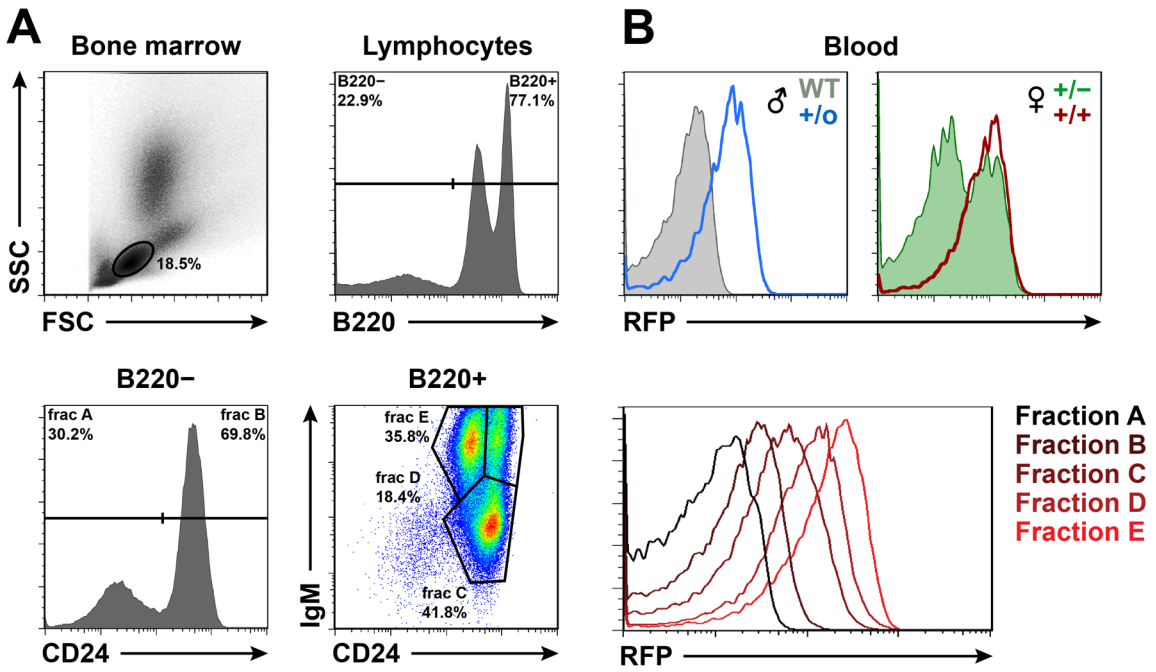

Figure 3.1.4 RFP expression during B cell maturation. (A) FACS analysis of bone marrow cells stained by specific markers for B cell development allows grouping in consecutive maturation stages (Hardy fractions): **A** $B220^{-}/CD24^{-}$, **B** $B220^{-}/CD24^{+}$, **C** $B220^{+}/CD24^{+}/IgM^{lo}$, **D** $B220^{+}/CD24^{+}/IgM^{hi}$, **E** $B220^{+}/CD24^{hi}/IgM^{hi}$. R&D B cells showed increasing levels of RFP expression in later stages of B cell development. Frac, Hardy fraction. **(B)** X-linked expression of R&D transgene as shown by random X-inactivation in heterozygous females: Hemizygous male mice showed red fluorescence in all B cells (left). Heterozygous female mice in contrast showed R&D transgene expression in only about 50% of all B cells, while homozygous female mice again showed red fluorescence in all B cells (right).

To exclude a possible deleterious effect of R&D transgene expression on the constitution of the murine immune system, distinct sets of immune cells from blood, spleen, bone marrow, lymph node, and peritoneum of R&D and WT mice were quantified using FACS analysis. In all immune compartments tested, no obvious difference could be detected between transgenic and WT mice, neither in developing B cells nor for mature B or T cells (Figure 3.1.5).

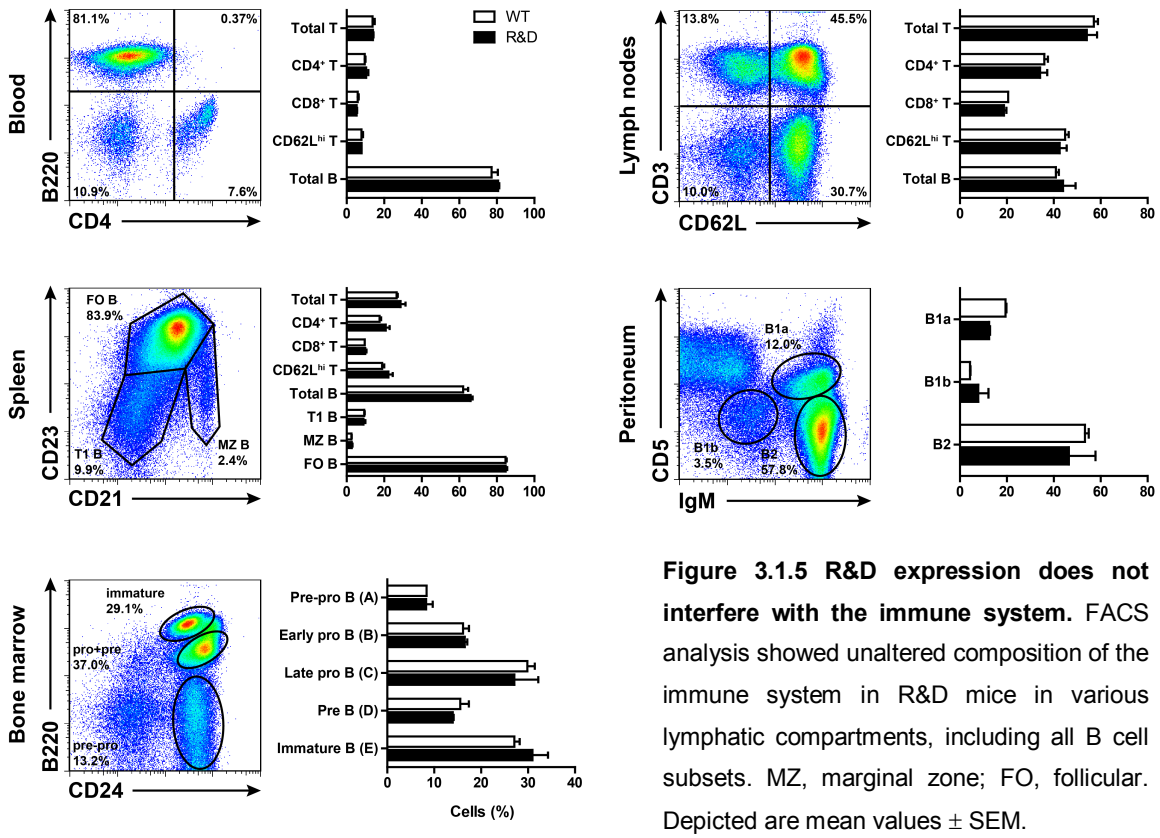

Figure 3.1.5 R&D expression does not interfere with the immune system. FACS analysis showed unaltered composition of the immune system in R&D mice in various lymphatic compartments, including all B cell subsets. MZ, marginal zone; FO, follicular. Depicted are mean values ± SEM.

3.1.4 Live cell microscopy of *in vitro* cultivated R&D B cells

In order to verify the usability of RFP-labeling for long-term tracking during *in vitro* live cell microscopy, splenocytes from R&D x IgH^{MOG} mice harboring MOG-specific B cells, and 2D2 x $Rag2^{-/-}$ (Hao and Rajewsky, 2001) splenocytes containing MOG-specific T cells were mixed at a 1:1 ratio together with 20 µg/ml recombinant MOG (rMOG). The interactions

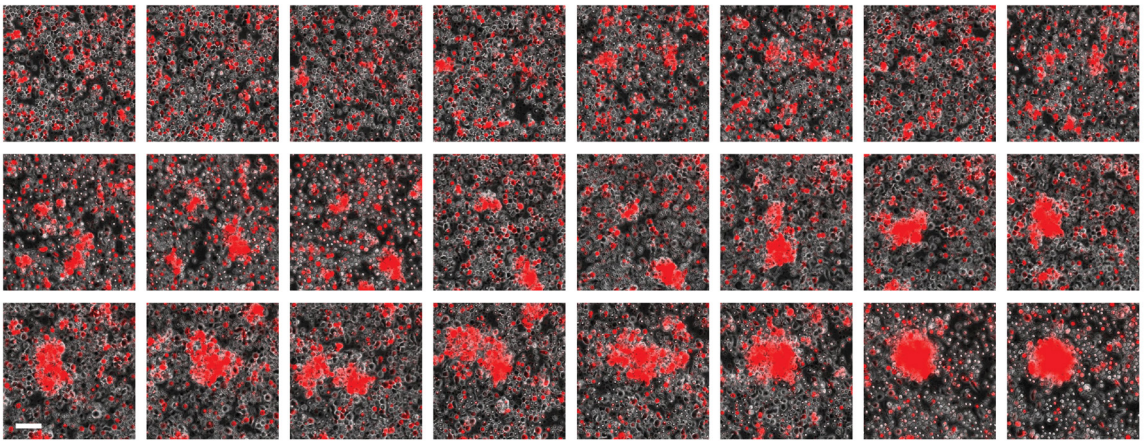

Figure 3.1.6 R&D B cells show highly photostable RFP fluorescence. Long-term widefield live microscopy of cells during coculture of red fluorescent MOG-specific R&D B with unlabeled 2D2 T cells, in the presence of 20 µg/ml rMOG. 40 hours total imaging time, 100 min interval depicted, scale bar 100 µm.

between T cells and B cells were followed using a live cell imaging setup. Image acquisition for transmitted light and red fluorescence was performed every 5 min, continuously for over 40 hours, providing a detailed view of progressing cell interactions (Movie 1). R&D transgenic B cells exhibited stable RFP fluorescence throughout the whole imaging period, allowing efficient tracking of cells forming dense activation clusters (Figure 3.1.6).

3.1.5 B cell depletion in R&D mice

To analyze the efficiency of B cell depletion in R&D mice, DTx at 10 ng/g body weight was injected i.p. into R&D and WT mice. Peripheral blood B cell frequencies were monitored at regular intervals to estimate the efficiency of toxin-mediated B cell depletion. Injection of six consecutive doses of DTx induced a rapid and near complete depletion of B cells in R&D mice, while B cells in WT mice remained unaffected (Figure 3.1.7A). After stopping the toxin application, B cell levels started to recover, reaching normal levels about 40 days later (Figure 3.1.7A). B cell repopulation was characterized by an initial rapid increase of immature B220^{+}/CD23^{+} B cells, reaching a plateau at one week after the final DTx injection, before giving way to fully matured B220^{+}/CD23^{-} B cells (Figure 3.1.7B). In addition, the body weight of experimental animals was monitored constantly and did not show any significant changes between R&D and WT mice, suggesting no side-effects by DTx injection or complications evoked by strong and sustained changes in B cell numbers (Figure 3.1.7C).

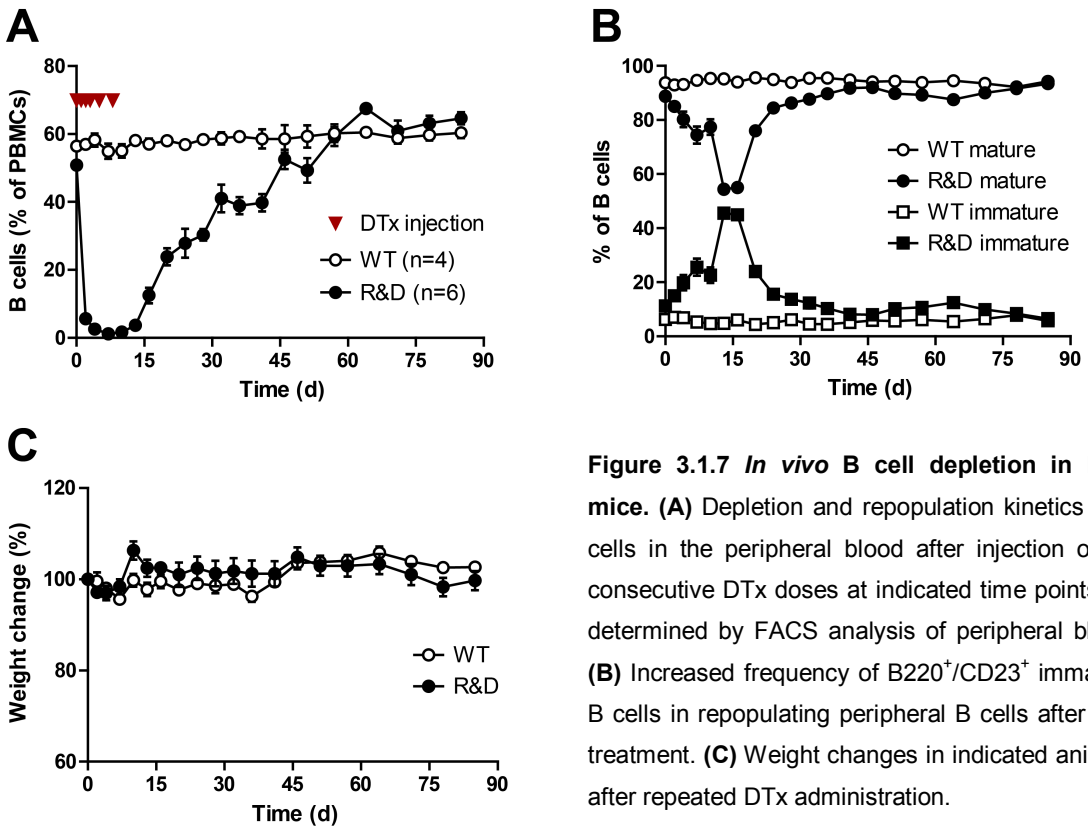

Figure 3.1.7 ***In vivo*** **B cell depletion in R&D mice. (A)** Depletion and repopulation kinetics of B cells in the peripheral blood after injection of six consecutive DTx doses at indicated time points, as determined by FACS analysis of peripheral blood. **(B)** Increased frequency of B220^{+}/CD23^{+} immature B cells in repopulating peripheral B cells after DTx treatment. **(C)** Weight changes in indicated animals after repeated DTx administration.

3.1.6 Comparison of B cell depletion by anti-CD20 or DTx

At present, anti-CD20 antibody treatment is the gold standard for efficient B cell depletion (Reff *et al.*, 1994). To compare efficiencies of B cell depletion by anti-CD20 with the new toxin-mediated method presented in this study, R&D mice immunized with keyhole limpet hemocyanin (KLH) were injected i.p. with either 250 µg IgG2a control antibody, 250 µg anti-CD20 antibody, or 1 µg DTx. Two days later B cell populations from different lymphoid organs were analyzed by FACS and compared between the three groups (Figure 3.1.8). While depletion of B cells in the blood was comparable between anti-CD20 and DTx, major differences were seen in other lymphoid organs. The depletion of total B cells in the spleen was slightly more efficient in DTx than in anti-CD20 treated animals. Notably, DTx efficiently depleted CD21^{hi}/CD23^{+} marginal zone B cells in the spleen, which are known to be resistant to anti-CD20 antibodies (Bekar *et al.*, 2010). Furthermore, DTx treatment almost completely depleted B cells in the bone marrow of R&D mice, whereas anti-CD20 antibodies only partially depleted mature B cells. Similarly, while B cells are not efficiently targeted by anti-CD20 in the peritoneal cavity due to insufficient numbers of macrophages (Hamaguchi *et al.*, 2006), DTx killed most of the B cells present in the peritoneum (Figure 3.1.8).

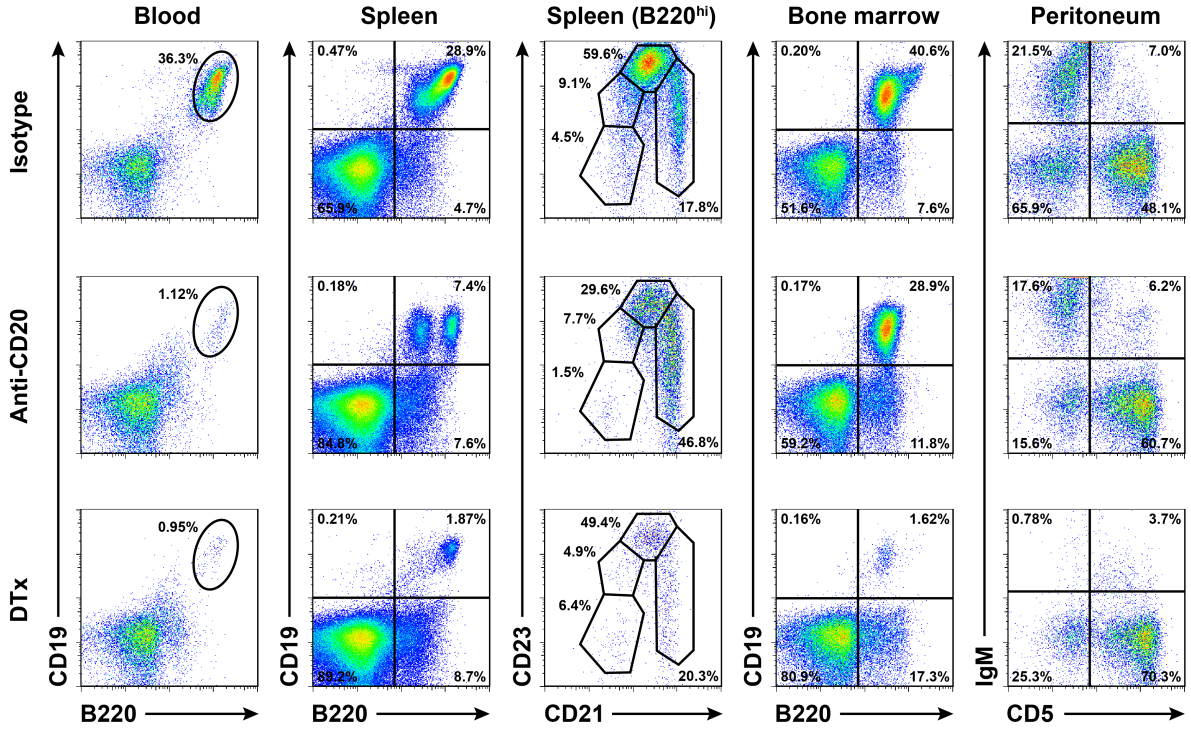

Figure 3.1.8 Comparison of anti-CD20 and DTx-mediated B cell depletion. FACS analysis of lymphocyte populations two days after B cell depletion by 250 µg IgG2a control antibody, 250 µg anti-CD20, or 1 µg DTx i.p., in KLH-immunized R&D mice.

Microscopic analysis of lymph node sections from R&D mice treated with anti-CD20 or DTx as described above also revealed drastic architectural changes after B cell depletion. While confined T and B cell zones were clearly visible in control mice, B cell depletion lead to distorted compartmentalization, noted by a spreading of T cells throughout the lymph node. This effect was detectable with anti-CD20 treatment, but was even stronger after depletion of B cells by DTx (Figure 3.1.9).

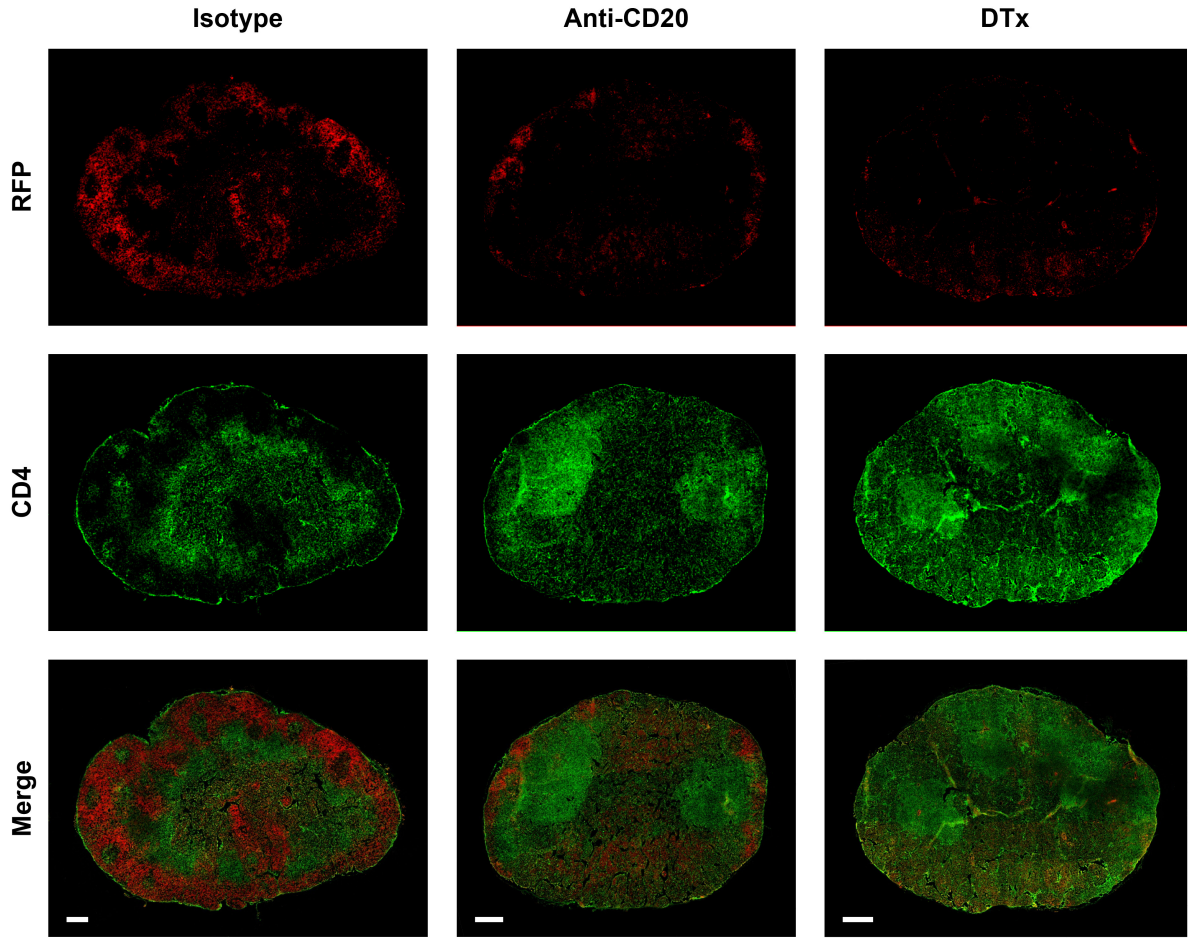

Figure 3.1.9 Depletion efficiency of anti-CD20 and DTx in lymph nodes. Composite widefield microscopic images of lymph node sections from KLH-immunized R&D mice, two days after treatment with 250 µg IgG2a control antibody, 250 µg anti-CD20, or 1 µg DTx. RFP fluorescence is shown in red, anti-CD4 staining for T cells in green. Scale bars 100 µm.

3.2 TN-XXL TRANSGENIC MICE

3.2.1 Synthetic calcium indicators are not suitable for *in vivo* calcium imaging

To monitor T cell activation events *in vivo*, synthetic calcium dyes were tested which have been successfully used for *in vitro* studies to document antigen recognition by T cells (Irvine *et al.*, 2002). Murine primary T cells were loaded *in vitro* with the visible light-excited calcium dye Fura Red, and its intracellular persistence was followed by flow cytometry over time. In agreement with published reports (Homolya *et al.*, 1993), a dramatic loss of Fura Red was observed within few hours that approached complete expulsion from cells after overnight incubation (Figure 3.2.1A). Quantification of the label intensity showed that after 28 hours in culture just barely detectable levels (approximately 10x higher Fura Red fluorescence intensity over unlabeled control cells) were present (Figure 3.2.1B). Further, to test the use of calcium dyes in immune cells *in vivo*, murine splenocytes, double-labeled with the calcium indicator Fura Red along with the cell tracking dye eFluor 670 which is irreversibly coupled to cellular proteins, were transferred into WT host animals. After 24 hours, total splenocytes isolated from recipient animals were analyzed, and a substantial loss of Fura Red in all cell tracker-tagged cells was found (Figure 3.2.1C). Collectively, these data confirmed the limited use of synthetic calcium dyes for *in vivo* calcium imaging of T lymphocytes.

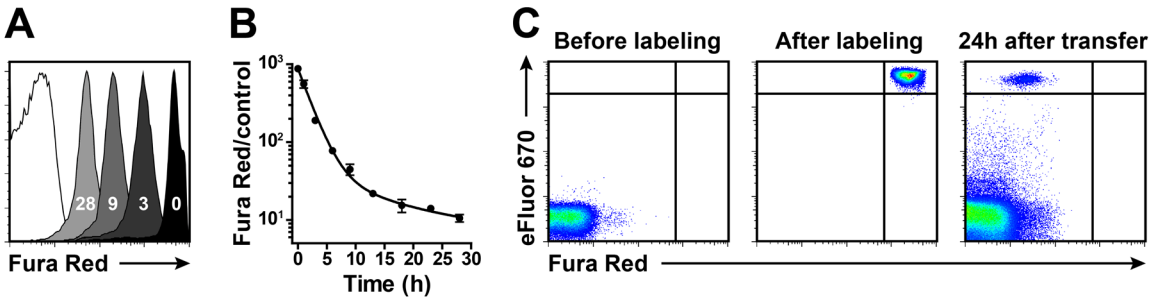

Figure 3.2.1 Synthetic calcium indicators are not stable in T cells. (A) Loss of synthetic calcium dye Fura Red from T cells within hours: Overlay of Fura Red-labeled T cells, analyzed by FACS after 0, 3, 9, and 28 hours, along with unstained control cells. **(B)** Quantification of Fura Red label intensity in relation to unlabeled control cells. **(C)** Selective loss of synthetic calcium dye fluorescence from labeled splenocytes *in vivo* after adoptive transfer: Fura Red fluorescence vanishes while the cell tracking dye eFluor 670 remains stable.

3.2.2 Evaluation of TN-XXL in immortalized T cells

As a promising alternative to synthetic calcium dyes, the genetically encoded, FRET-based calcium indicator TN-XXL (Mank *et al.*, 2008) was examined for calcium imaging in lymphocytes *in vivo*. TN-XXL is composed of two fluorescent proteins, cyan fluorescent protein (CFP) as FRET donor and yellow fluorescent protein (YFP) as FRET acceptor, linked by the calcium sensitive moiety of troponin C (TnC) from chicken skeletal muscle. Upon binding free calcium, TnC undergoes a reversible conformational change, leading to energy transfer from CFP to YFP (Figure 3.2.2A), thus changing the ratio of YFP to CFP fluorescence. This ratiometric change can be used as direct measure of calcium level changes in the cytoplasm at a given time. Since accurate calcium calibration in a real *in vivo*

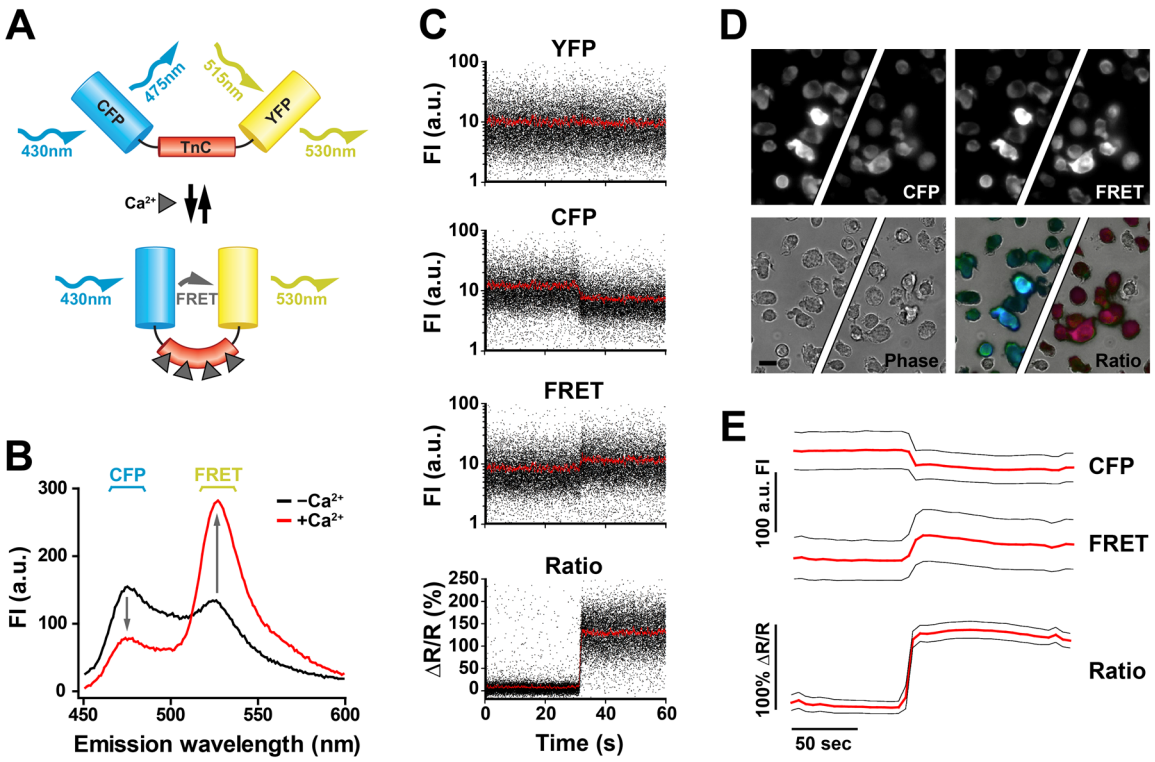

Figure 3.2.2 Genetically encoded calcium indicators are suitable for calcium imaging in T cells. (A) Schematic depiction of the calcium indicator TN-XXL, with donor fluorophore CFP, acceptor YFP, and the calcium sensitive domain Troponin C, before and after binding of calcium. **(B)** Spectrophotometric analysis of cell lysate from TN-XXL-expressing EL4 cells, before (black) and after (red) addition of 1 mM calcium. FI, fluorescence intensity; a.u., arbitrary units. **(C)** FACS-based measurement of calcium influx into TN-XXL-expressing EL4 cells after stimulation with 4 µM ionomycin: CFP fluorescence intensity drops and FRET intensity rises, yielding a robust ratio change. YFP fluorescence alone remains unchanged. Fluorescence intensities (FI) and fractional fluorescence change of the FRET/CFP ratio (ΔR/R) are plotted as function of time. **(D)** Epifluorescence and phase contrast images of TN-XXL-expressing EL4 cells, before (left) and after (right) addition of 4 µM ionomycin. Overlay showing pseudocolor image of FRET/CFP ratio. Scale bar 10 µm. **(E)** Average fluorescence intensities of CFP and YFP, and average response of the ratiometric signal after induction of calcium influx into TN-XXL-expressing EL4 cells by addition of 4 µM ionomycin.

setting is rather error-prone, all calcium level changes shown in this report will be plotted as fractional change in emission ratio, expressed as $\Delta R/R = (R-R_0)/R0$ (R, actual ratio measured; R_0, ratio at zero calcium), and are not translated into definite intracellular calcium concentrations.

To assess the suitability of TN-XXL for calcium imaging in lymphoid cells, EL4 lymphoma cells were stably transfected with a plasmid encoding TN-XXL driven by the CMV promoter. Spectrophotometric measurement of cell lysates from TN-XXL-expressing EL4 cells showed a maximal fluorescence ratio change ($R_{max} \approx 290\%$) upon addition of 1 mM calcium (Figure 3.2.2B), comparable to values previously estimated for purified recombinant TN-XXL protein (Mank *et al.*, 2008). FACS analysis of TN-XXL-expressing EL4 cells showed a high fluorescence ratio change upon addition of the calcium ionophore ionomycin, indicating a sharp rise of intracellular calcium (Figure 3.2.2C). These results were confirmed by widefield fluorescence microscopy (Figure 3.2.2D and 3.2.2E, and Movie 2). Taken together, the results obtained with EL4 cells supported the possible applicability of TN-XXL for calcium imaging in T lymphocytes *in vivo*.

3.2.3 T cell-specific TN-XXL transgenic mice (hCD2-TN-XXL)

To obtain T cell-specific expression in transgenic mice, TN-XXL was cloned in between the human CD2 (hCD2) promoter and the hCD2 locus control region (LCR) (Figure 3.2.3A). The hCD2 promoter (Zhumabekov *et al.*, 1995) was chosen since it has been successfully used to generate transgenic mice with strong and T cell-specific expression of

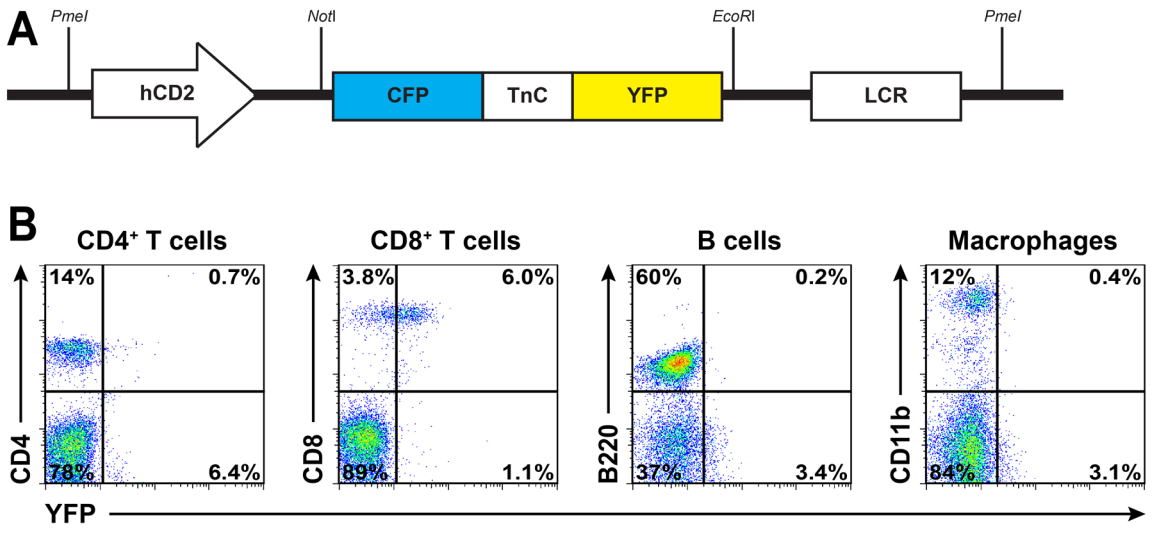

Figure 3.2.3 TN-XXL expression under control of the hCD2 promoter. (A) Schematic representation of the transgene construct used for the generation of hCD2-TN-XXL transgenic mice. **(B)** FACS analysis of splenocytes from hCD2-TN-XXL transgenic mice.

GFP (De Boer *et al.*, 2003). After sequence verification, hCD2-TN-XXL was linearized with PmeI, separated from the bacterial backbone, and microinjected into fertilized C57BL/6 oocytes. Out of nine transgenic founder lines, six transmitted the hCD2-TN-XXL transgene to the next generation. Unexpectedly, only one transgenic founder-derived F1 mouse line showed slight TN-XXL expression (as seen by YFP fluorescence) in peripheral blood lymphocytes. TN-XXL expression was largely restricted to the $CD8^+$ T cell lineage, and none of the $CD4^+$ T cells, $B220^+$ B cells, and $CD11b^+$ macrophages showed fluorescence. Even in $CD8^+$ T cells, TN-XXL expression was marginally above background fluorescence (Figure 3.2.3B). Therefore, none of the hCD2-TN-XXL transgenic founders could be used for further experiments.

3.2.4 Ubiquitous TN-XXL transgenic mice (CAGW-TN-XXL)

Since the hCD2-TN-XXL transgenic mice did not yield the expected pattern of expression, the ubiquitously active CAG promoter was chosen to drive expression of TN-XXL in murine T cells. The CAG promoter is a composite of the human CMV immediate early enhancer element and the chicken β-actin promoter (Niwa *et al.*, 1991). This promoter was used more than a decade ago to generate the well-known GFP transgenic `green mice´ (Okabe *et al.*, 1997), and was also successfully employed in several other studies to drive ubiquitous and robust expression of various fluorescent proteins in almost all cell types (Kawamoto *et al.*, 2000; Long *et al.*, 2005; Riedl *et al.*, 2010). To further ensure proper

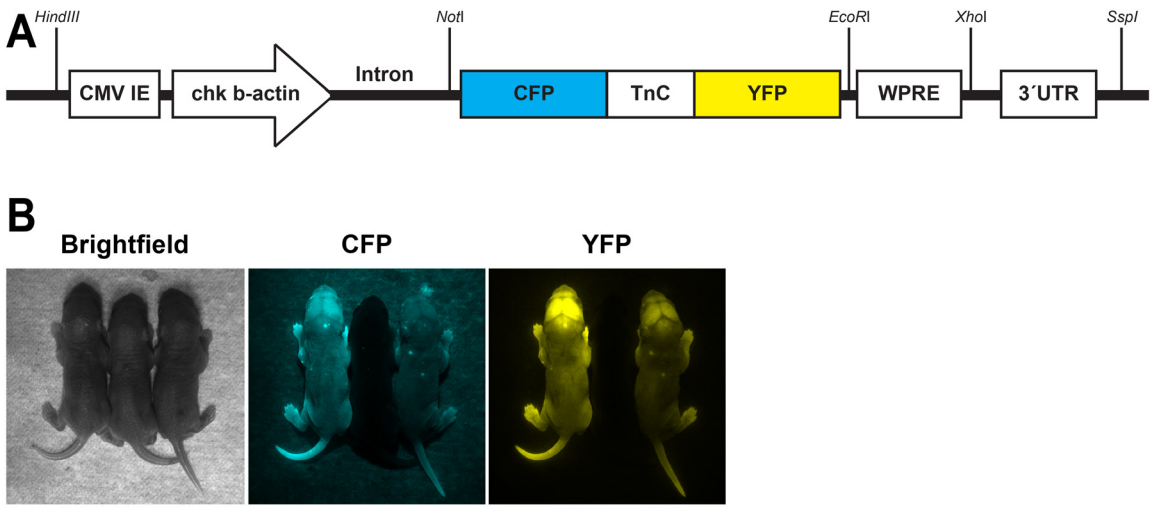

Figure 3.2.4 TN-XXL expressed under control of the CAG promoter and the WPRE. (A) Schematic representation of the transgene construct used for the generation of CAGW-TN-XXL transgenic mice. CMV IE, cytomegalovirus immediate early enhancer; chk, chicken; WPRE, woodchuck post-transcriptional regulatory element; UTR, untranslated region. **(B)** Brightfield and fluorescent images of newborn pups: Homozygous animals showed brighter fluorescence (left) over heterozygous animals (right), while no fluorescence could be seen for WT animals (middle).

expression of TN-XXL, the woodchuck hepatitis virus post-transcriptional regulatory element (WPRE) was included into the transgenic construct, upstream of the chicken β-actin 3´UTR. The WPRE has been shown to boost transgene expression rates (Zufferey *et al.*, 1999), at least partly by enhancing nuclear export of mRNA (Mastroyiannopoulos *et al.*, 2005). TN-XXL was cloned downstream of the CAG promoter, followed by WPRE and 3´UTR (Figure 3.2.4A). After sequence verification, CAGW-TN-XXL was linearized with HindIII and SspI, separated from the bacterial backbone, and microinjected into fertilized C57BL/6 oocytes.

Out of six transgenic founder lines, three transmitted the CAGW-TN-XXL transgene to the next generation. One line showed visible expression of TN-XXL in the skin (Figure

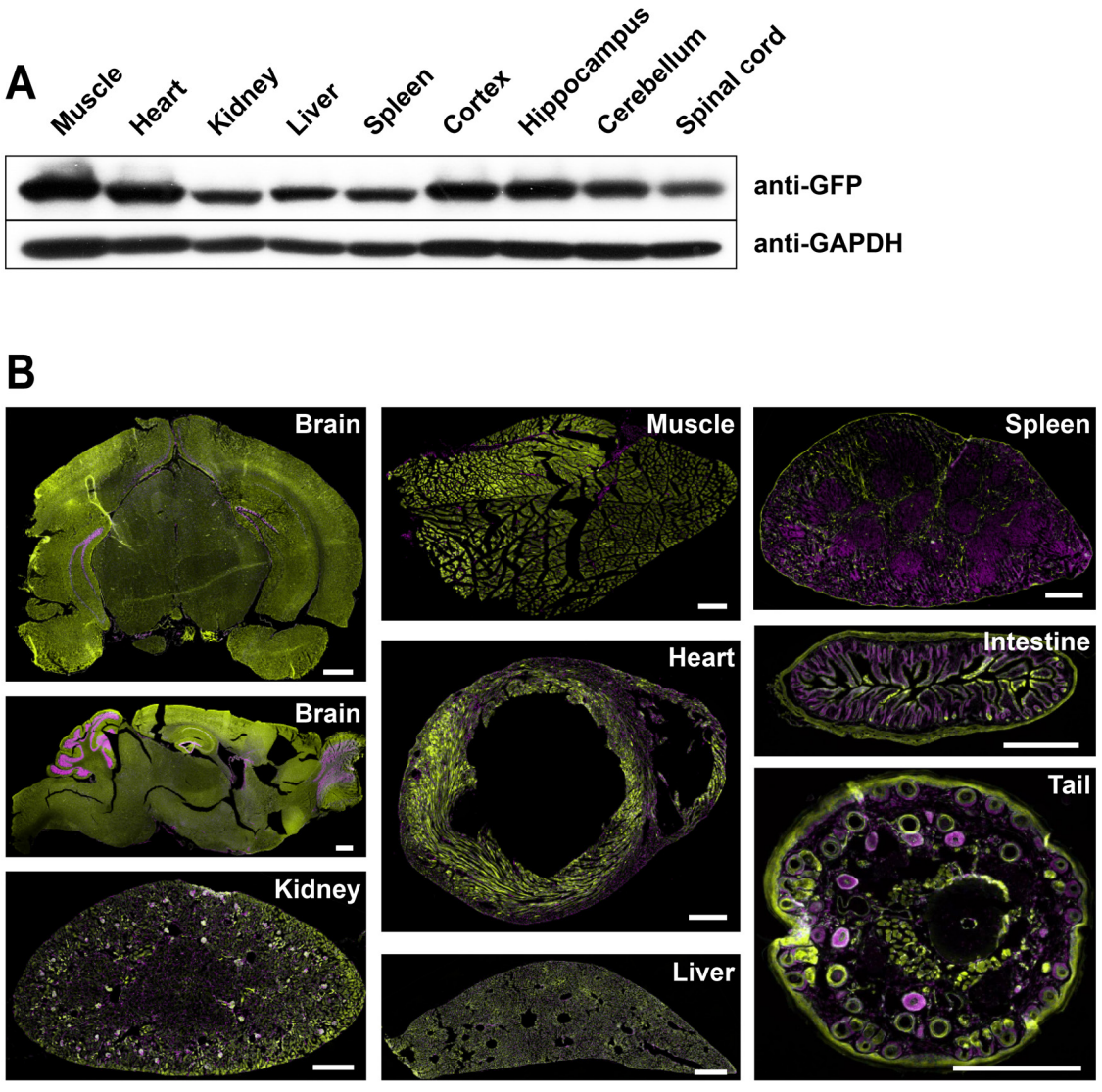

Figure 3.2.5 Expression of TN-XXL in different tissues of CAGW-TN-XXL mice. (A) Western blot analysis of tissue lysates probed with anti-GFP (to estimate TN-XXL expression (69 kDa)) and anti-GAPDH antibodies (loading control (36 kDa)). **(B)** Cryosections (10 µm) of organs from CAGW-TN-XXL mice showing TN-XXL fluorescence (yellow) costained with DAPI for nuclear staining (purple). Scale bars 500 µm.

3.2.4B) and was chosen for further analysis. Anti-GFP western blot analysis (detecting YFP as well) revealed expression of TN-XXL in all organs (Figure 3.2.5A). Microscopic examination of cryosections from different organs further confirmed ubiquitous distribution of TN-XXL: Most cell types analyzed showed strong TN-XXL expression as in CNS tissue, in kidney, liver, and intestine, in muscle tissue, and also in skin and blood vessel endothelium as seen in a tail cross section. In the spleen, however, only limited TN-XXL fluorescence could be detected (Figure 3.2.5B).

3.2.5 Expression of TN-XXL in lymphocytes of CAGW-TN-XXL mice

Next, TN-XXL was analyzed in lymphocyte populations in CAGW-TN-XXL mice. Surprisingly again, TN-XXL was almost not detectable in lymphocytes of CAGW-TN-XXL transgenic animals. TN-XXL fluorescence seen in lymphoid organs was restricted to stromal cells, while lymphocyte areas were devoid of any fluorescence (Figure 3.2.6A). FACS analysis confirmed lack of TN-XXL expression in all cells types of the hematopoietic system, in developing as well as in mature cells (Figure 3.2.6B).

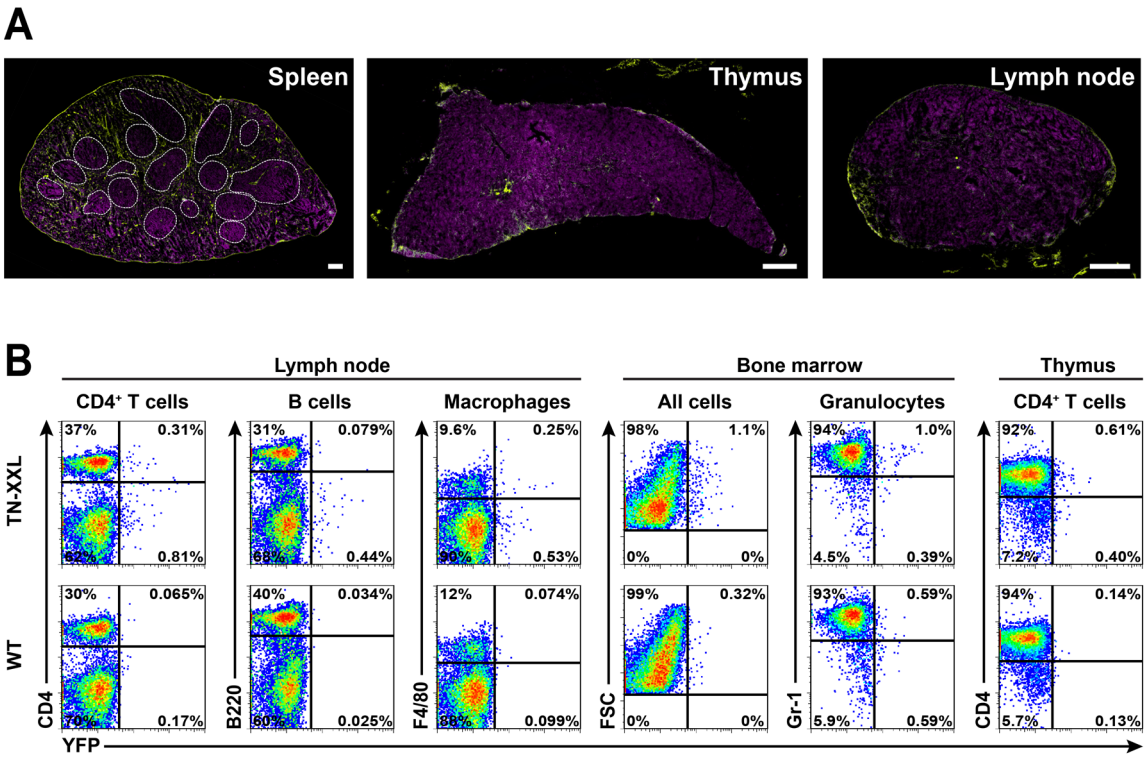

Figure 3.2.6 Lack of TN-XXL expression in lymphoid organs. (A) Cryosections (10 µm) of lymphoid organs from CAGW-TN-XXL mice showing TN-XXL fluorescence (yellow), costained with DAPI for nuclear staining (purple). Lymph follicles in spleen are encircled to highlight lymphocyte areas. Scale bars 200 µm. **(B)** FACS analysis of lymphocytes from various organs from CAGW-TN-XXL mice in comparison to WT.

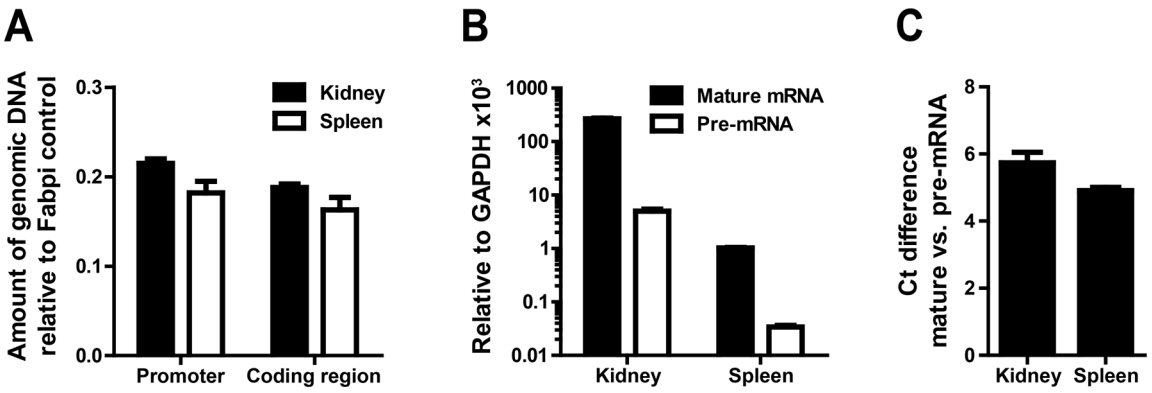

Figure 3.2.7 Downregulation of TN-XXL transcription in lymphoid organs. (A) Comparable amounts of genomic transgene DNA in kidney and spleen, as measured by qPCR at two different positions of the construct (3´end of the chicken β-actin promoter and in the CFP part of the coding region). Fabpi, fatty acid-binding protein. **(B-C)** qRT-PCR analysis of transcript levels showed **(B)** highly reduced mRNA amounts in lymphoid organs, while **(C)** the ratio between mature and pre-mRNA remained similar.

To rule out a selective loss of TN-XXL transgene in lymphocyte populations, genomic DNA was analyzed by quantitative PCR. TN-XXL DNA amplified by transgene-specific primers was present in comparable amounts in kidney cells and splenocytes, ruling out a selective loss of transgene DNA in lymphocyte populations (Figure 3.2.7A). To determine TN-XXL transcript levels, pre-mRNA was quantified by using a forward primer binding in the promoter region, paired with a primer binding in the intron of the transgene. Mature mRNA was quantified using the same forward primer, however, paired with a primer binding in the coding region, thus amplifying only spliced mRNA. In contrast to genomic DNA levels, TN-XXL transcript levels of both, mature and pre-mRNA, were highly reduced in splenocytes compared to kidney cells (Figure 3.2.7B). Nonetheless, the ratio between processed mature and recently transcribed pre-mRNA was comparable between both cell types, suggesting a robust impairment of TN-XXL transcription in splenocytes without any further downstream obstructions in TN-XXL mRNA processing or stability (Figure 3.2.7C).

Transcriptional downregulation in mammalian cells could occur in many ways. CpG methylation of DNA and formation of inactive heterochromatin is one well-known epigenetic mechanism, by which gene expression can be silenced (Suzuki and Bird, 2008; Lal *et al.*, 2009). It was previously shown, that treatment of cells with the demethylating agent 5-aza-2´-deoxycytidine (Aza) (Jones and Taylor, 1980), a cytidine analog, could switch on transcriptionally inactive, methylated promoters. Indeed, stimulation of CAGW-TN-XXL T cells by anti-CD3/CD28 and subsequent culture in the presence of Aza for two days substantially increased the frequency and intensity of TN-XXL expression in a dose-

dependent manner (Figure 3.2.8A and 3.2.8B). Aza, however, was toxic to T cells at higher concentrations necessary to induce substantial TN-XXL expression, precluding its routine use for *in vitro* or *in vivo* studies.

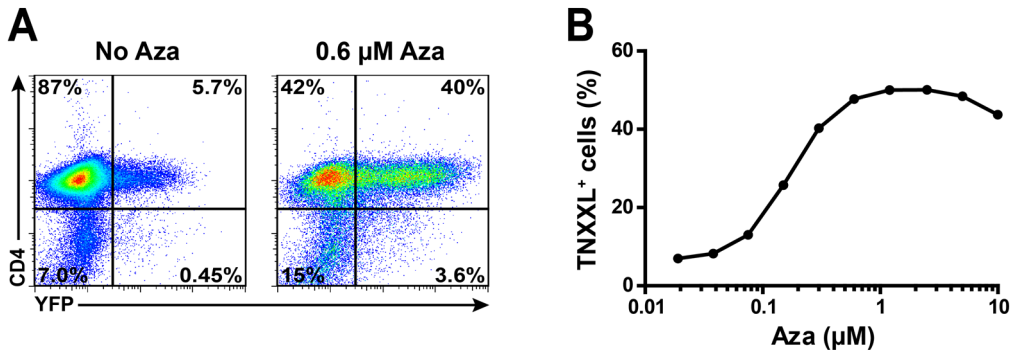

Figure 3.2.8 Induction of TN-XXL expression in lymphocytes after demethylation. (A) FACS analysis of activated T cells from CAG-TN-XXL transgenic mice, cultured in the presence of 0.6 µM Aza for two days, and **(B)** corresponding dose-response curve.

Despite the lack of expression of TN-XXL in lymphoid cells, CAGW-TN-XXL mice are still a valuable tool for calcium imaging in non-lymphoid tissues due to the strong expression of the transgene in many cell types. We chose to study calcium imaging in the heart, since CAGW-TN-XXL mice showed robust expression of the calcium indicator in heart cells (Figure 3.2.5B). To validate this mouse model for calcium imaging in whole organs, hearts from day 8.5 embryos were excised and cultured *in vitro*, where they started spontaneous beating. Calcium waves travelling through the organ with every heart beat could be instantly detected (Figure 3.2.9A and Movie 3). The propagation of the calcium wave over time from the atria to the ventricles was illustrated by a phase plot of one heart beat cycle (Figure 3.2.9B). Successive calcium signals with consistent spike patterns could be readily measured, while the calcium curve progression through different areas selected in the atrial and ventricular region of the heart demonstrated the temporal delay of the conduction of the calcium signal through the organ (Figure 3.2.9C). This experimental setup again demonstrates that, the ratiometric nature of TN-XXL is a prerequisite to facilitate calcium imaging in any migratory cell or an organ preparation that is not immobile.

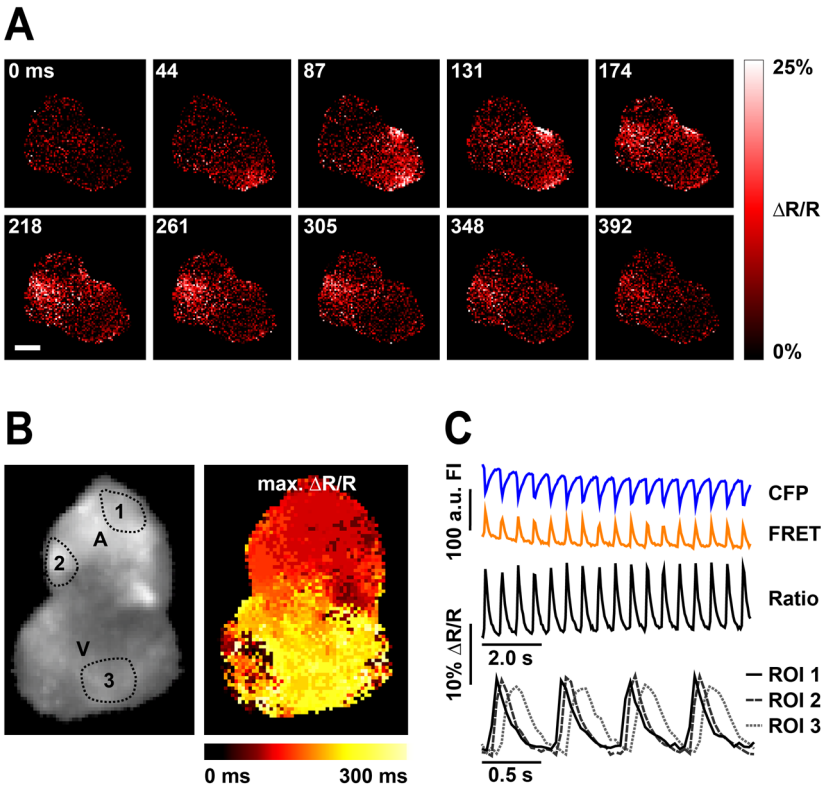

Figure 3.2.9 Calcium waves during spontaneous beating in a day 8.5 embryonic heart. (A) Representative series of microscopic images with calcium levels changing over time for one heartbeat cycle. Scale bar 200 µm. **(B)** Left: Fluorescent image of the embryonic heart with orientation (A, atria; V, ventricles) and regions of interest (ROI 1-3) labeled. Right: Phase plot illustrating the calcium signal over time during one heartbeat cycle. Color code indicates the maximal ΔR/R at a given pixel and time, thus depicting the progression of the calcium wave over the organ. **(C)** Upper graphs: CFP and FRET intensities, and the corresponding ratio change for ROI 1. Lower graph: Detailed view of progressing calcium level changes for all three ROIs indicated.

3.2.6 Ubiquitous TN-XXL transgenic mice without WPRE (CAG-TN-XXL)

One possible reason for lack of TN-XXL expression in lymphocytes of CAGW-TN-XXL mice could be due to an unexpected deleterious effect of the WPRE in lymphocytes. The WPRE was shown to enhance transgene expression in most of the cells tested, however, in some certain cell types a mitigating effect of the WPRE was found (Klein *et al.*, 2006). Hence, while the WPRE was supposed to amplify transgene expression in CAGW-TN-XXL mice, and potentially also did so in most tissues, transgene expression in cells of the hematopoietic system might have been severely attenuated by the WPRE. Therefore, another CAG promoter-based transgene construct was generated for TN-XXL expression, this time driven by the CAG promoter alone without any further influence of the WPRE (Figure 3.2.10A). After sequence verification, CAG-TN-XXL was linearized with HindIII and SspI, separated from the bacterial backbone, and microinjection into fertilized C57BL/6 oocytes.

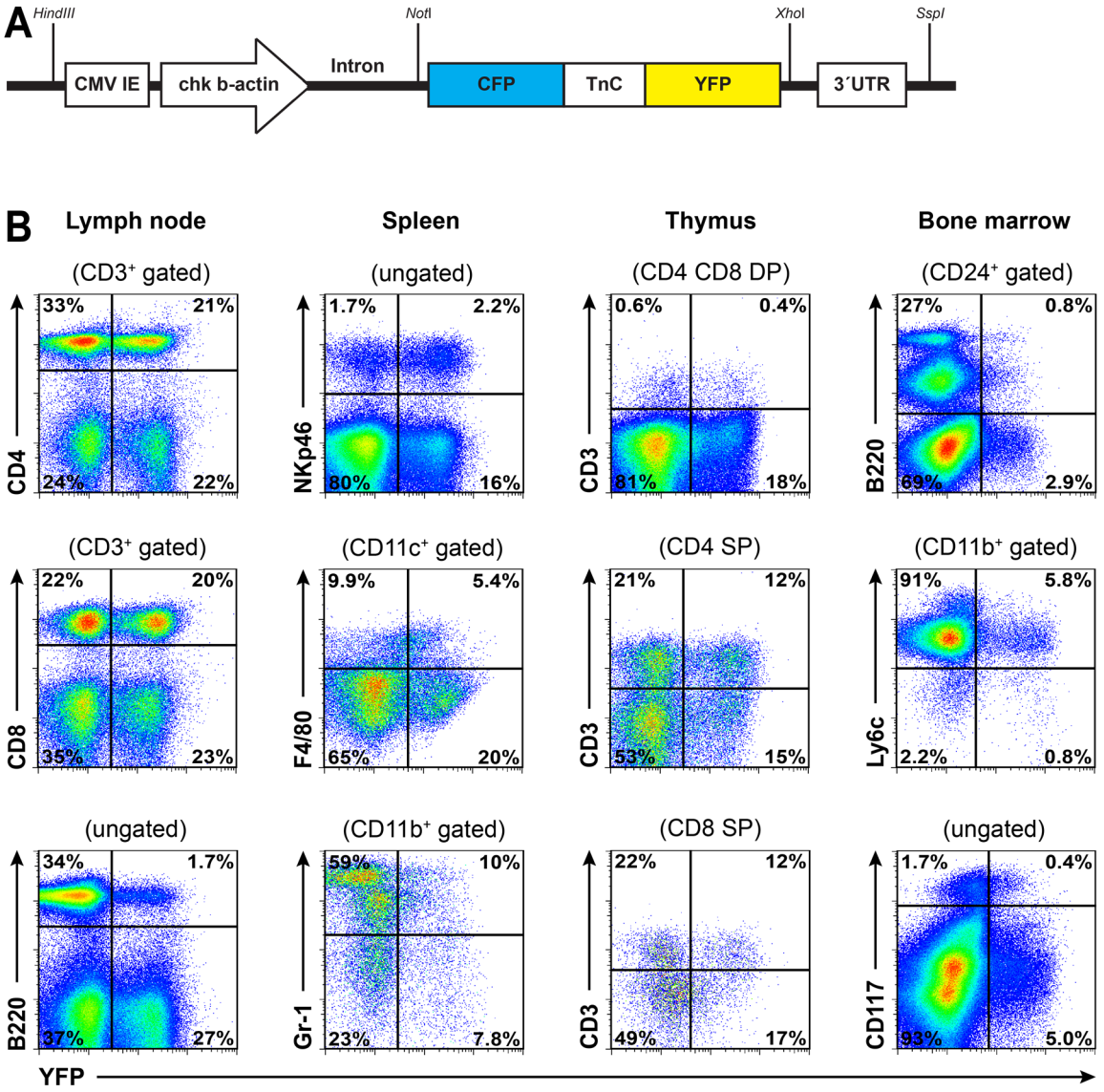

Figure 3.2.10 TN-XXL expression under control of the CAG promoter. (A) Schematic representation of the transgene construct used for the generation of CAG-TN-XXL transgenic mice. CMV IE, cytomegalovirus immediate early enhancer; chk, chicken; UTR, untranslated region. **(B)** FACS analysis of TN-XXL expression in various lymphocyte subpopulations from CAG-TN-XXL lymphoid organs. Lymph node: $CD3^+/CD4^+$, CD4 T cells; $CD3^+/CD8^+$, CD8 T cells; $B220^+$, B cells. Spleen: $NKp46^+$, natural killer cells; $CD11c^+/F4/80^+$, macrophages; $CD11b^+/Gr\text{-}1^+$, granulocytes. Thymus: $CD3^+$, all T cells; DP, double positive; SP, single positive. Bone marrow: $CD24^+/B220^+$, B cells; $CD11b^+/Ly6c^+$, monocytes; $CD117^+$, progenitor cells.

Out of twelve transgenic founder lines, seven transmitted the CAG-TN-XXL transgene, however, only one line showed visible expression of TN-XXL in the skin. When analyzing lymphocytes from all transgenic CAG-TN-XXL F1 offspring by FACS, only the transgenic line with expression in the skin showed fluorescence in lymphocytes as well. Analysis of cells from lymphoid organs from this line revealed a predominant expression of TN-XXL in $CD4^+$ and $CD8^+$ T cells, and natural killer cells, while other cell types as B cells or macrophages mostly lacked TN-XXL fluorescence (Figure 3.2.10B). However, only less than

half of all T cells showed transgene expression, and with a fluorescence intensity of only 20x higher than background levels, rendering these cells barely detectable by fluorescent microscopy.

To analyze any functional influence of TN-XXL expression on T cells, CAG-TN-XXL and WT splenocytes were cultured *in vitro* after stimulation with anti-CD3. As shown by FACS analysis, the expression levels of various surface activation markers on T cells did not differ between transgenic CAG-TN-XXL T cells and control WT cells (Figure 3.2.11A). Also the frequencies of TN-XXL-expressing T cells remained stable over time (Figure 3.2.11B). In addition, no differences between CAG-TN-XXL and WT T cells in cytokine expression profiles on different days after activation were found (Figure 3.2.11C). Thus, the expression of TN-XXL did not seem to negatively influence T cells, however, also the CAG-TN-XXL mice could not be used for *in vivo* microscopy due to insufficient fluorescent intensity.

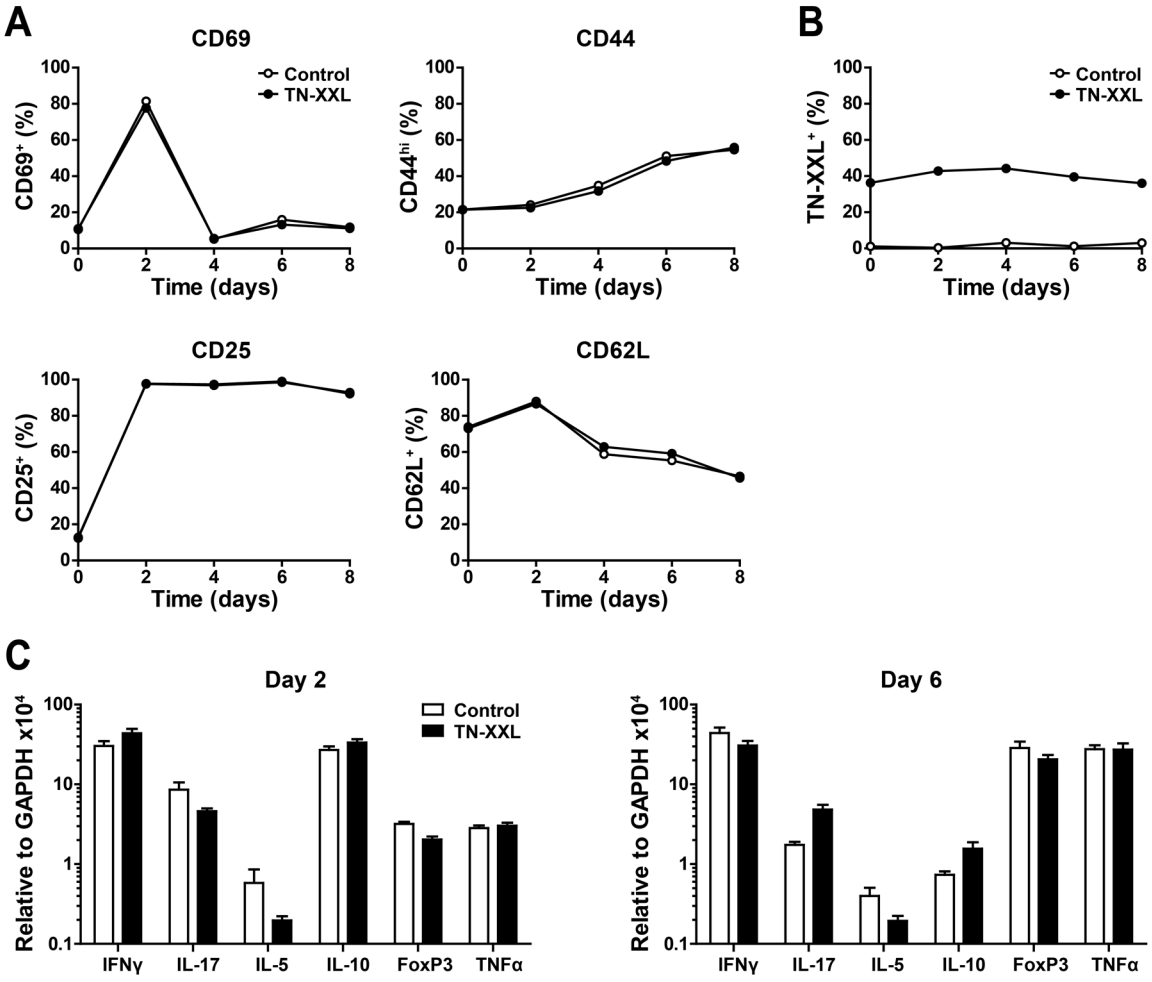

Figure 3.2.11 T cells from CAG-TN-XXL mice do not show an abnormal phenotype. (A) FACS analysis of various surface markers on anti-CD3-stimulated T cells over time. **(B)** TN-XXL fluorescence in transgenic T cells. **(C)** Gene expression analysis of various T cell cytokines. Depicted are mean values ± SEM.

3.3 CALCIUM IMAGING IN T CELLS

3.3.1 Optimization of TN-XXL for expression in primary T lymphocytes

To obtain primary T cells expressing the calcium indicator, TN-XXL should be introduced into T cells by retroviral transduction (Flügel *et al.*, 1999). While TN-XXL was readily expressed in retrovirus producing Phoenix packaging cells, all attempts to express TN-XXL in primary T cells by retroviral transduction were unsuccessful. The expression problems were systematically dissected using series of TN-XXL derivatives. Transduction of T cells with YFP alone (one of the tandem fluorophores used in TN-XXL) produced expected expression levels in T cells (Figure 3.3.1). However, neither the replacement of the calcium sensing domain TnC with an inert linker (neurofilament light aa 130-275), nor the complete removal of TnC improved transduction efficiencies in T cells, suggesting that the combination of CFP-YFP and not the TnC domain caused a problem for expression in T cells (Figure 3.3.1).

Both fluorophores contained in TN-XXL are derived from jellyfish GFP, and sequence comparisons confirmed a very high sequence homology (97%) between CFP and YFP. It was speculated that this high degree of sequence homology might have a deleterious impact

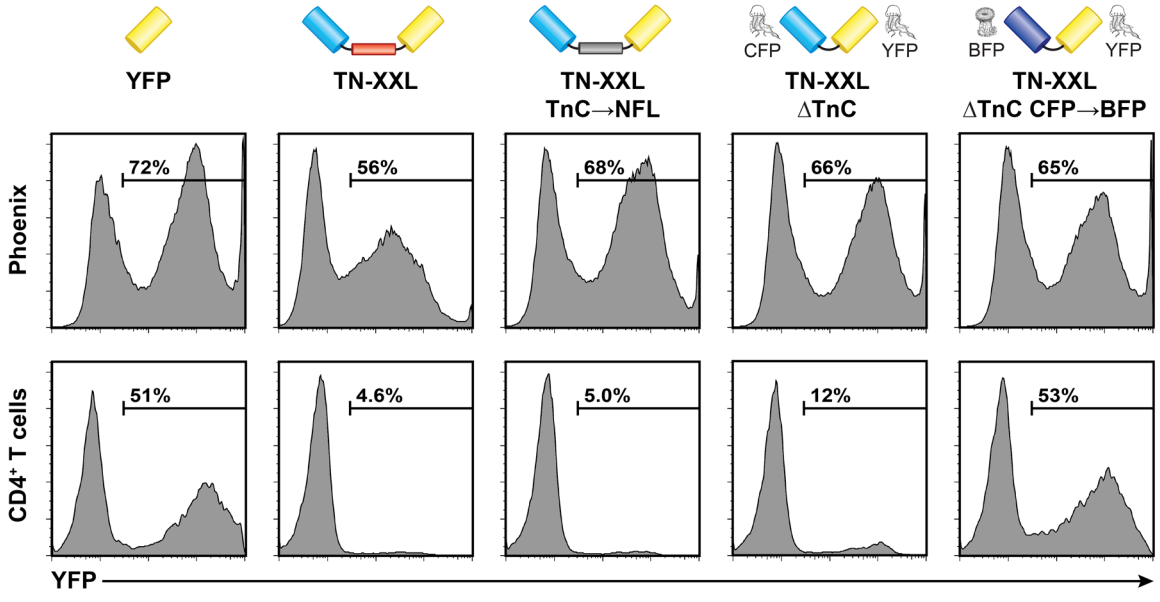

Figure 3.3.1 High sequence homology of CFP and YFP impairs efficient expression in T cells. Schematic representation of TN-XXL and its derivatives featuring various replacements or deletions (top). TN-XXL and all derivatives expressed in Phoenix packaging cells after transfection (middle). T cells efficiently expressed YFP alone and the variant containing a BFP-YFP pair after retroviral transduction with Phoenix cell supernatant, however no other variants containing the highly homologous CFP-YFP pair (bottom).

on the efficient expression of TN-XXL in T cells. As a proof of principle, jellyfish-derived CFP was replaced by coral-derived blue fluorescent protein (BFP), which shares only 62% homology to YFP. Indeed, this exchange led to desired expression levels in primary T cells (Figure 3.3.1). However, the combination of BFP and YFP is not an efficient FRET pair, and thus BFP cannot be used to replace CFP for calcium imaging.

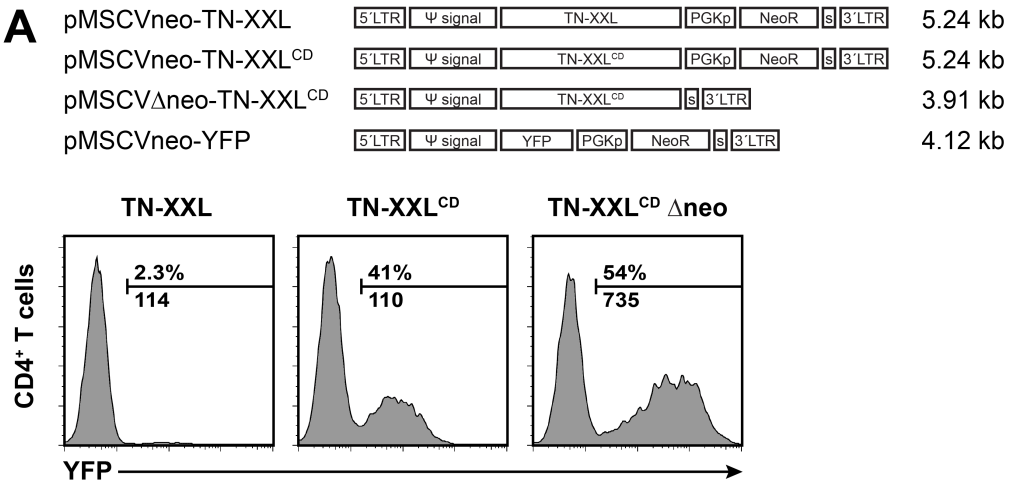

Figure 3.3.2 Optimization of TN-XXL for expression in T cells. (A) Codon diversification of TN-XXL yields higher transduction efficiency in anti-CD3 stimulated WT T cells. Further improvement of the expression intensity was obtained by reducing the size of the retroviral construct. LTR, long terminal repeats; Ψ, packaging; PGKp, phosphoglycerate kinase promoter; NeoR, neomycin resistance cassette; s, spacer. **(B)** Increased transduction efficiencies and fluorescent intensities with RetroNectin in anti-CD3 stimulated WT (left) as well as in rMOG stimulated TCR transgenic T cells (right). Mean fluorescent intensities along with transduction efficiencies are shown.

Based on these findings, the sequence homology between CFP and YFP, and also between the repetitive EF hands of TnC, were reduced by codon diversification while maintaining the amino acid sequence of the original TN-XXL intact (Appendix). Conservative codon diversification resulted in 80% homology between CFP and YFP, and 75% homology between repetitive EF hands of TnC. The modified, codon diversified calcium indicator, TN-XXL^{CD}, showed a 20-fold increased transduction efficiency compared to the original TN-XXL

(Figure 3.3.2A). The fluorescence intensity was further enhanced by reducing the vector size by deleting the neomycin selection cassette, which resulted in a 7-fold increase of fluorescence intensity (Figure 3.3.2A). The use of the transduction enhancing agent RetroNectin additionally increased the fluorescence intensity obtained after retroviral transduction (Figure 3.3.2B).

3.3.2 Functional characterization of TN-XXL^{CD} in T cells

For functional characterization of the calcium indicator TN-XXL^{CD} in T cells, retroviral transduction of MOG-specific TCR transgenic CD4^{+} T cells from C57BL/6 2D2 mice and SJL/J TCR^{1640} mice was performed. Transduction rates were consistently greater than 30% of CD4^{+} T cells (Figure 3.3.3A), and fluorescence intensities remained stable after adoptive transfer of T cells into recipient animals (Figure 3.3.3B).

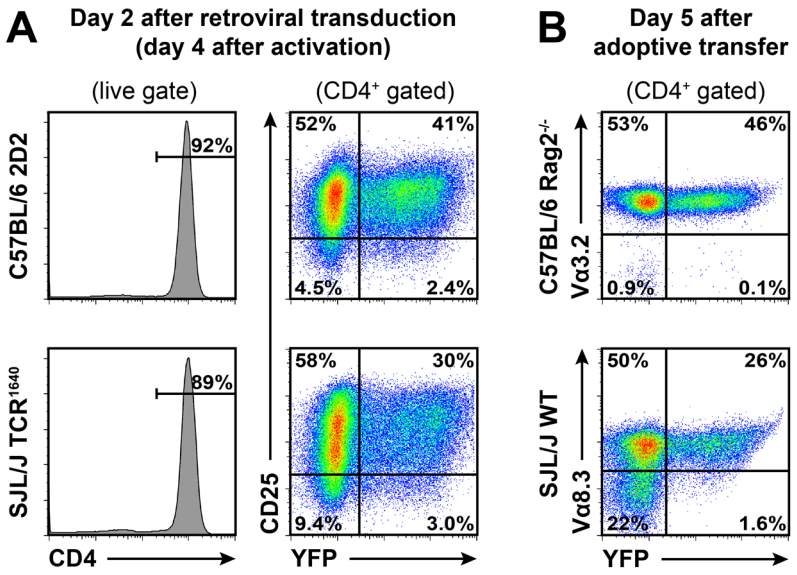

Figure 3.3.3 Stable expression of TN-XXL^{CD} in transduced T cells (A) FACS analysis of TCR transgenic MOG-specific C57BL/6 2D2 and SJL/J TCR^{1640} transgenic T cell cultures. **(B)** Analysis of blood lymphocytes from recipient animals showing stable expression of TN-XXL^{CD} in TCR transgenic T cells five days after adoptive transfer. Vα3.2 as marker for 2D2 T cells, Vα8.3 for TCR^{1640} T cells.

Calcium mobilization measured with TN-XXL^{CD} in T cells after TCR crosslinking was well detectable at the population level (Figure 3.3.4A). Further, to assess the functionality of TN-XXL^{CD} at the single cell level, the activation of individual TN-XXL^{CD}-expressing T cells by anti-CD3/CD28 beads was followed. Cells interacting with beads showed an immediate and swift increase in the ratiometric change, indicating a rapid rise of cytoplasmic calcium levels (Figure 3.3.4B and 3.3.4C, and Movie 4). Similar results were achieved when using rMOG-

pulsed IgH^{MOG} B cells as functional APCs to mimic natural reactivation of TN-XXL^{CD}-expressing 2D2 T cells (Figure 3.3.4D and Movie 5).

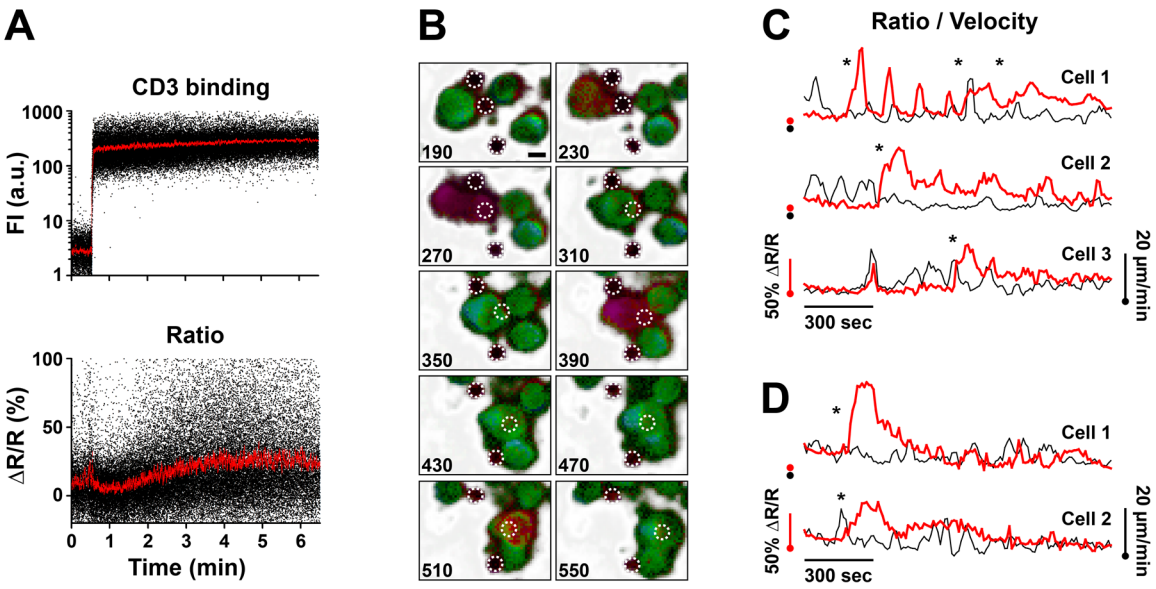

Figure 3.3.4 Functional *in vitro* characterization of TN-XXL^{CD}-expressing TCR transgenic T cells. (A) FACS-based calcium measurements in TN-XXL^{CD}-expressing 2D2 T cells after stimulation with anti-CD3-biotin/streptavidin-APC complexes. FI, fluorescence intensity; a.u., arbitrary units. **(B)** Representative images of a 2D2 T cell interacting with anti-CD3/CD28 beads, taken from Movie 4 (cell #1). White circles show anti-CD3/CD28 beads. Time stamp in seconds, scale bar 10 µm. **(C)** Representative tracks for intracellular calcium levels (red line) and cell velocities (black line) of T cells engaging with anti-CD3/CD28 beads, taken from Movie 4. Asterisks indicate time points of contact initiation, dots depict zero levels for calcium levels and cell velocities. **(D)** Representative tracks for intracellular calcium levels (red line) and cell velocities (black line) of T cells interacting with antigen-pulsed B cells, taken from Movie 5. Asterisks and dots as in (C).

As documented by flow cytometric analysis, various surface activation markers on T cells cultured *in vitro* over time did not differ between transduced and non-transduced 2D2 T cells (Figure 3.3.5A), and frequencies of TN-XXL^{CD}-expressing cells remained stable over time (Figure 3.3.5B). Further, cytokine expression (Figure 3.3.5C) and T cell proliferation in response to rMOG stimulation (Figure 3.3.5D) was unaffected by retroviral transduction. Longitudinal analysis of TN-XXL^{CD} expression in TCR^{1640} T cells over a prolonged time showed that frequencies of TN-XXL^{CD} positive T cells remained stable over a period of more than 30 days, indicating neither any selective advantage nor disadvantage for cells expressing the calcium indicator (Figure 3.3.5E).

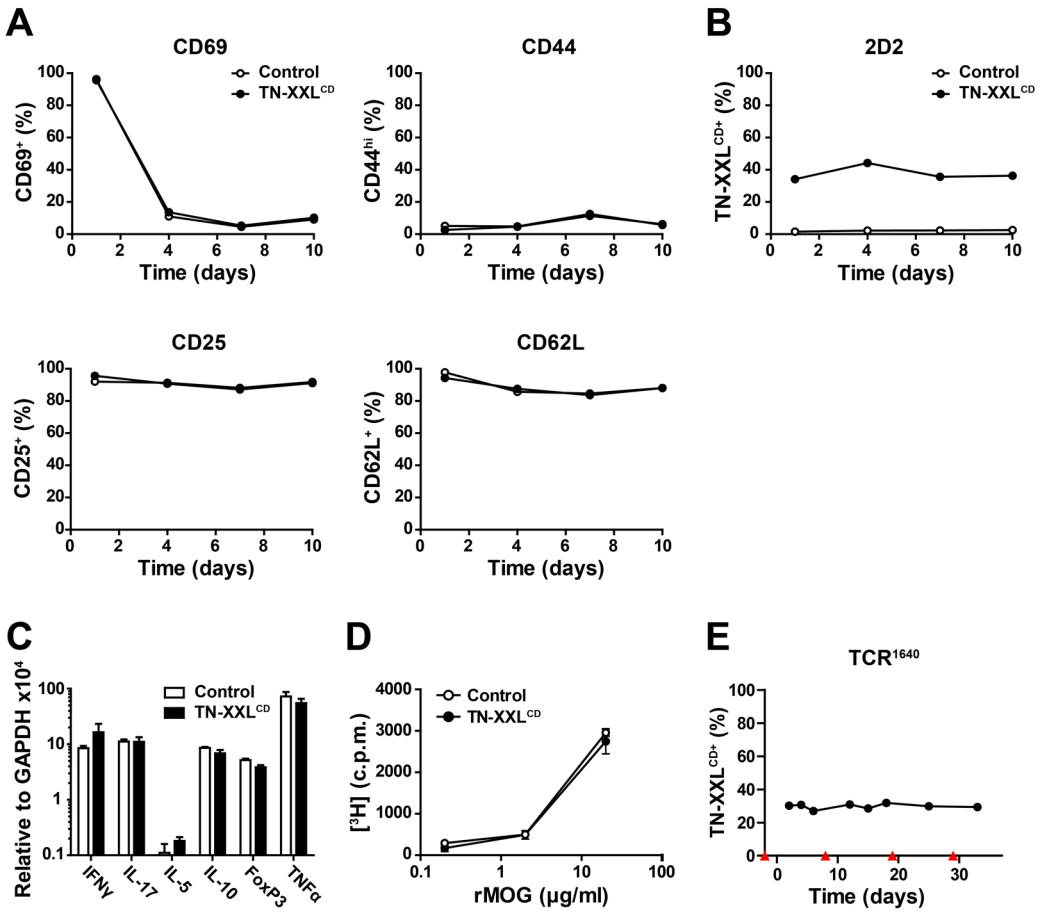

Figure 3.3.5 TN-XXL^{CD}-transduced T cells show no altered phenotype. (A) FACS analysis of surface markers on 2D2 T cells stimulated with rMOG and transduced with TN-XXL^{CD}, in comparison to untransduced control cells. **(B)** TN-XXL^{CD} fluorescence in T cells as determined by FACS analysis. **(C)** Analysis of cytokine expression in 2D2 T cells four days after retroviral transduction. **(D)** Proliferation assay with 2D2 T cells after stimulation with rMOG; c.p.m., counts per minute. **(E)** Long-term expression of TN-XXL^{CD} in TCR^{1640} T cells was stable over time. Red triangles indicate restimulation time points.

Finally, the encephalitogenic potential of TN-XXL^{CD}-expressing, MOG-specific T cells was examined by transferring TN-XXL^{CD}-transduced, sham treated, or untreated control TCR^{1640} T cells into SJL/J recipients. All three cell lines triggered transfer EAE with a similar incidence, severity, and course of the disease (Figure 3.3.6).

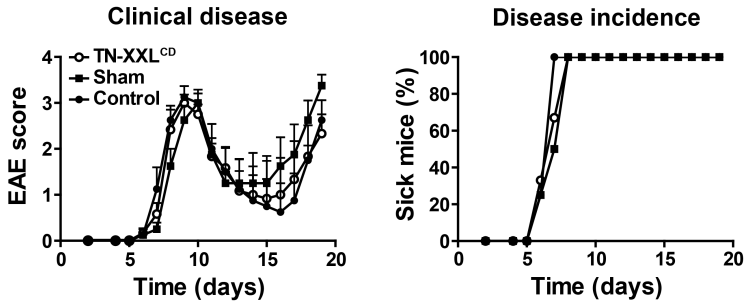

Figure 3.3.6 Adoptive transfer EAE with calcium indicator-expressing T cells. TN-XXL^{CD}-transduced TCR transgenic T cells induced EAE in recipient animals to a similar extent as sham transduced or untreated control T cells.

3.3.3 *In vivo* imaging of calcium dynamics in T cells interacting with DCs

Initial attempts to visualize calcium level changes in T cells *in vivo* by TN-XXL^{CD} unfortunately only gave rise to scarce and faint signals (data not shown). To increase sensitivity, an advanced version of TN-XXL was employed with a higher calcium affinity (Thestrup and Griesbeck, unpublished data), termed TN-3XL. TN-3XL was equally codon diversified to produce TN-3XL^{CD}, again yielding efficient transduction of primary T cells (Figure 3.3.7A). *In situ* calibration of fluorescence changes to intracellular calcium concentrations revealed an approximately 3.5x higher calcium affinity for TN-3XL^{CD}, therefore rendering it more suitable to measure physiologically relevant intracellular calcium changes in T cells (Figure 3.3.7B).

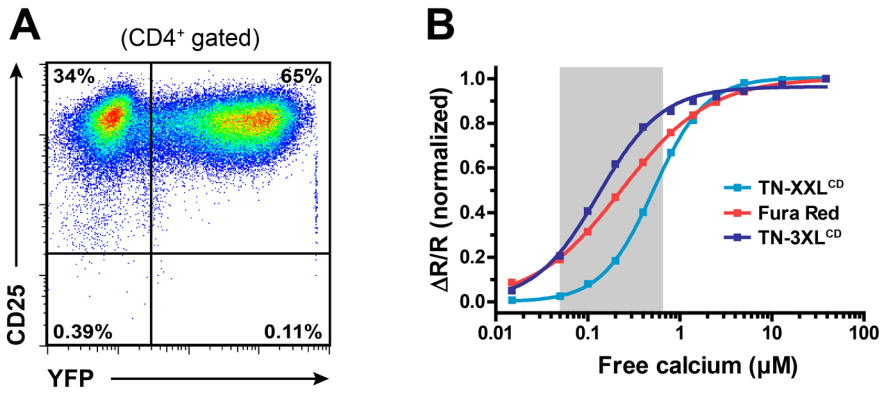

Figure 3.3.7 Expression of TN-3XL^{CD} and dissociation constants of calcium indicators. (A) FACS analysis of 2D2 T cells transduced with TN-3XL^{CD}. **(B)** FACS-based *in situ* calcium calibration: titration curves of TN-XXL^{CD}, TN-3XL^{CD}, and Fura Red in T cells. The resulting dissociation constant Kd (indicating calcium affinity) and the corresponding Hill coefficient h (indicating cooperativity of binding) are Kd ≈ 520 nM and h ≈ 1.5 for TN-XXL^{CD}, Kd ≈ 140 nM and h ≈ 1.3 for TN-3XL^{CD}, and Kd ≈ 230 nM and h ≈ 0.9 for Fura Red, respectively. Grey area highlights range of physiologically relevant calcium levels in T cells.

To functionally evaluate the calcium indicator *in vivo*, the OT-II mouse model system was employed. In these TCR transgenic mice all T cells recognize the ovalbumin peptide $OVA_{323-339}$, which is not endogenously expressed. TN-3XL^{CD}-transduced OT-II T cells (Barnden *et al.*, 1998) were adoptively transferred one week before subcutaneous injection of activated bone marrow-derived dendritic cells (BMDC), labeled with the red fluorescent cell tracer SNARF-1. Next day, cells were imaged in the draining popliteal lymph node by two-photon microscopy, before and after i.v. injection of 100 µg $OVA_{323-339}$ peptide (Movie 6). In the absence of cognate antigen, T cells showed high motility and a large displacement (Figure 3.3.8). After injection of OVA peptide, OT-II T cells immediately engaged with DCs, greatly reduced their motility, and presented a more rounded phenotype (Figure 3.3.8).

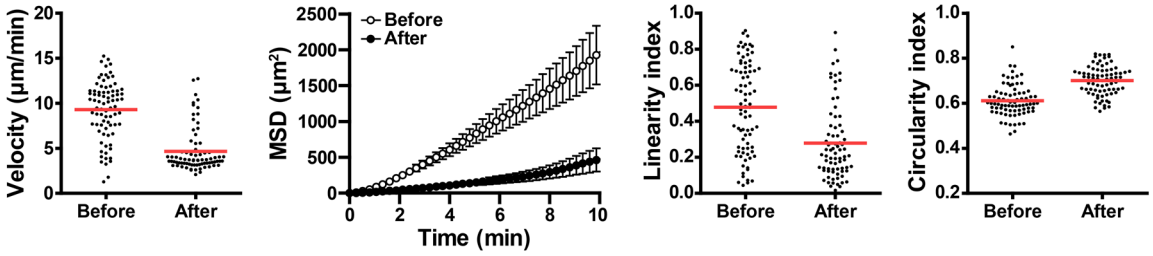

Figure 3.3.8 Tracking of T cells *in vivo* for T cell – DC interactions. Quantification of T cell locomotion within the popliteal lymph node, before and after i.v. injection of 100 µg OVA peptide. Average velocities, mean squared displacement (MSD), movement linearity, and cell circularity are shown.

Before injection of antigen, the calcium signatures in OT-II T cells were generally very low with few and only short-lasting calcium spikes (Figure 3.3.9A and 3.3.9B top). This picture dramatically changed after OVA peptide injection. Calcium levels in T cells rose to high values, and eventually developed into long-lasting calcium oscillations (Figure 3.3.9A and 3.3.9B bottom). As expected, all T cells displaying an elevated calcium signature after antigen application were in sustained contact with DCs (Movie 7). Quantification of calcium levels at each time point showed an inverse correlation with cell motility: T cells with low calcium levels featured a high motility, whereas T cells with elevated calcium levels significantly slowed down (Figure 3.3.9C). Similarly, the overall distribution of average calcium levels estimated for each individual cell skewed markedly towards higher values after injection of OVA peptide (Figure 3.3.9D). Since T cells showed some changes in calcium levels prior to antigen encounter, the duration of elevated calcium levels was analyzed as well. While spontaneous calcium spikes in the absence of antigen were short-lived, T cells displayed long-lasting elevations of intracellular calcium after antigen encounter, persisting over several minutes (Figure 3.3.9E). Plotting the trajectories of T cell movements and highlighting phases of high calcium levels further illustrated the occurrence of spontaneous calcium peaks in freely migrating T cells, while T cells engaged with cognate antigen-presenting DCs stop their migration and undergo sustained calcium signaling (Figure 3.3.9F).

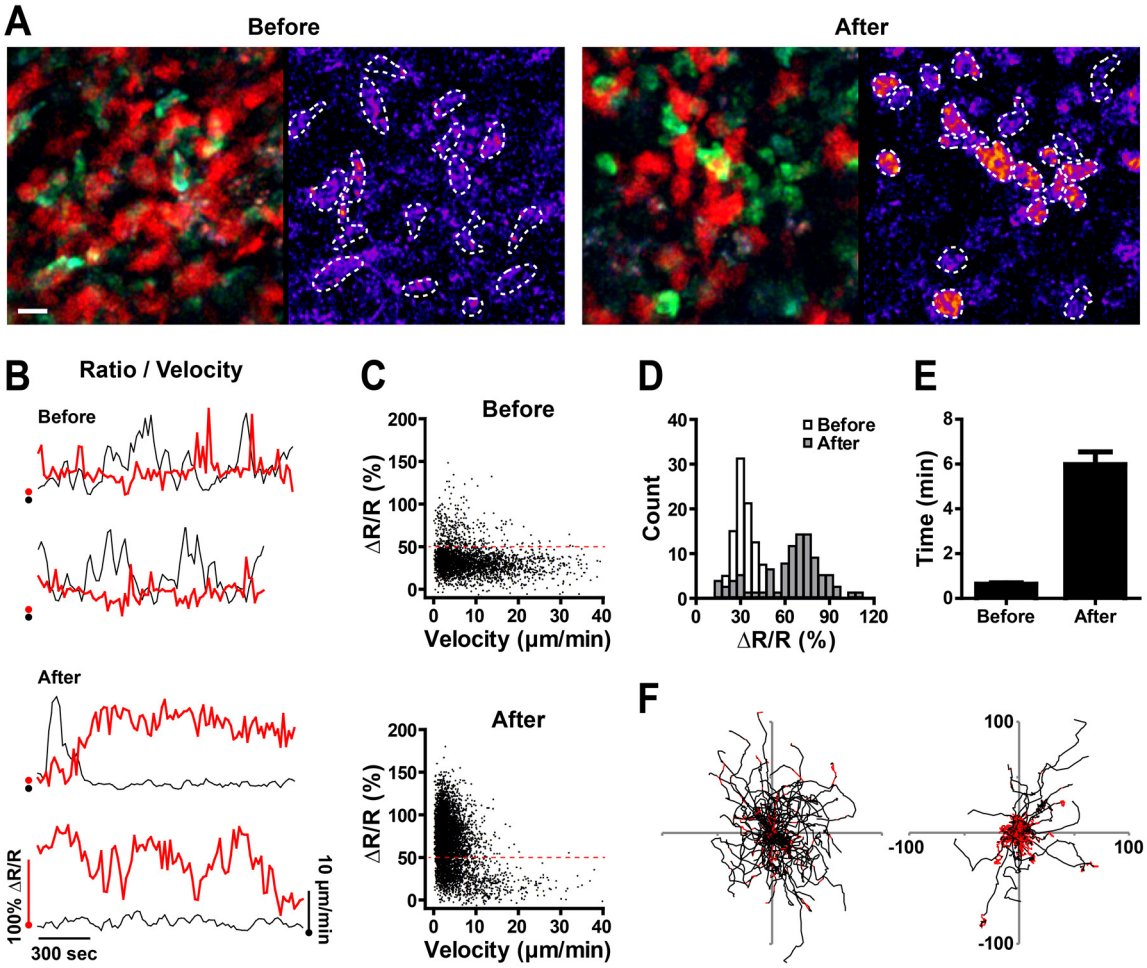

Figure 3.3.9 Calcium imaging in T cells *in vivo* upon encounter with DCs and antigen. (A) Representative images from *in vivo* calcium imaging in the popliteal lymph node, before and after injection of antigen. Depicted are fluorescence overlay of TN-3XL^{CD}-expressing OT-II T cells in green and SNARF-1 labeled DCs in red (left), and pseudocolor ratio image with T cells encircled (right), scale bar 10 µm. **(B)** Two representative tracks each for intracellular calcium levels (red line) and T cell velocities (black line), before and after antigen injection. Dots depict zero levels for calcium levels and cell velocities. **(C)** Scatter plots showing cell velocity vs. intracellular calcium concentration for each individual timepoint analyzed, before and after antigen injection. **(D)** Distribution of average intracellular calcium levels. **(E)** Duration of elevated calcium levels with ΔR/R above 50%. **(F)** Superimposed trajectories of T cell movements, before (left) and after (right) antigen injection. Time points with ΔR/R above 50% are indicated in red.

3.3.4 *In vivo* imaging of calcium dynamics in T cells interacting with B cells

To test the calcium indicator in the context of B cells presenting antigen, TN-3XL^{CD}-expressing 2D2 T cells were adoptively transferred one week before intravenous injection of LPS activated, MOG-pulsed IgH^{MOG} B cells, labeled with the red fluorescent cell tracer SNARF-1. Two-photon imaging of the popliteal lymph node was performed at three different

time points after B cell transfer: early (1 h) (Movie 8), intermediate (8 h) (Movie 9), and late (24 h) (Movie 10). T cells showed a similar motility pattern at all three time points analyzed, with slightly increasing velocity from the early to the late time point. At the intermediated time point, T cells strongly engaged with antigen-presenting B cells, yet forming motile conjugates (Figure 3.3.10A).

While T cells had a reduced velocity, and already some interacting T and B cells could be seen at the early stage, no strong and sustained calcium signals were detectable. In contrast, at the intermediate stage, all cells engaged with B cells showed strong and sustained calcium signaling. Intracellular calcium levels again inversely correlated with T cell velocity as most cells with elevated calcium levels showed a reduced motility. At the late imaging time point strong calcium signals were again absent, while T cells gained a higher velocity, (Figure 3.3.10B). Analysis of the duration of elevated calcium levels revealed sustained calcium signals at the intermediate time point of similar values as obtained before using the OT-II system, while calcium signals during the early and late time point were only of short-lasting nature (Figure 3.3.10C).

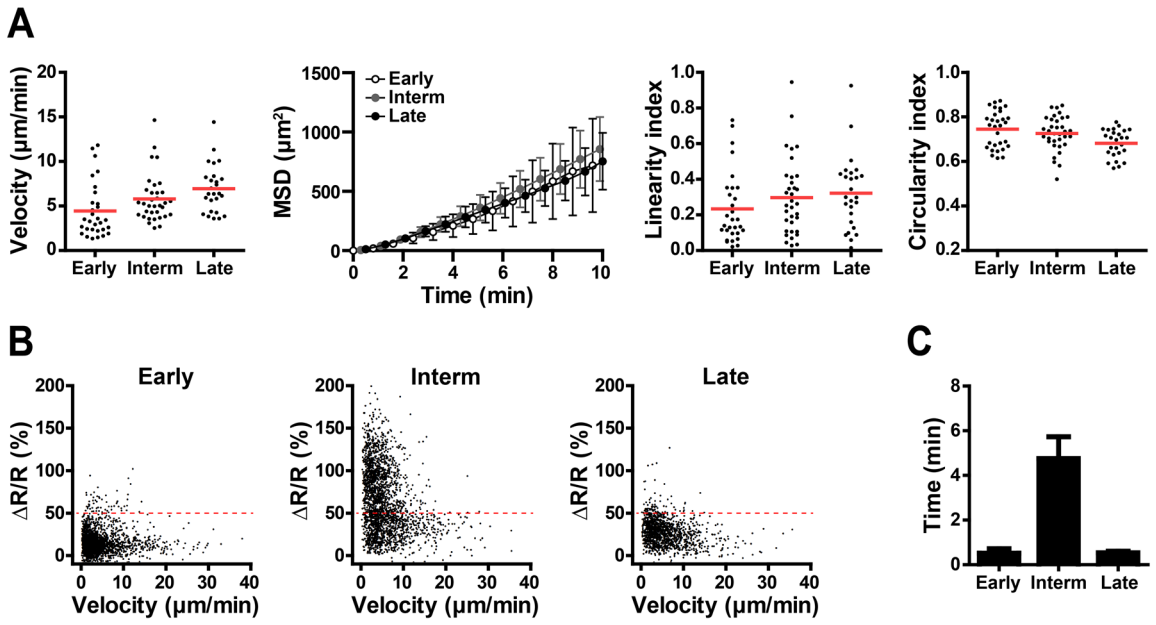

Figure 3.3.10 Calcium imaging in T cells *in vivo* for T cell – B cell interactions. (A) Quantification of T cell locomotion within the popliteal lymph node at early, intermediate, and late time points after B cell transfer. Average velocities, mean squared displacement (MSD), movement linearity, and cell circularity are shown. **(B)** Scatter plots showing cell velocity vs. intracellular calcium concentration for each individual time point. **(C)** Duration of elevated calcium levels with ΔR/R above 50%.

3.3.5 Presentation of antigen to ovalbumin-specific T cells in the inflamed CNS

Presentation of autoantigen by leptomeningeal APCs is a key event in the initiation of EAE (Bartholomäus *et al.*, 2009; Kivisäkk *et al.*, 2009). To directly assess the antigen-presenting potential of leptomeningeal APCs, OT-II T cells were transduced with TN-3XL^{CD} and adoptively transferred into WT recipient animals immunized with MOG for EAE induction. The OT-II T cells, like all non-self-specific T cells, are generally excluded from the brain, but can be piloted into the autoimmune CNS infiltrates by encephalitogenic T cells. As bystanders, they remain there quiescent, but respond promptly to the presentation of infused cognate antigen (Odoardi *et al.*, 2007).

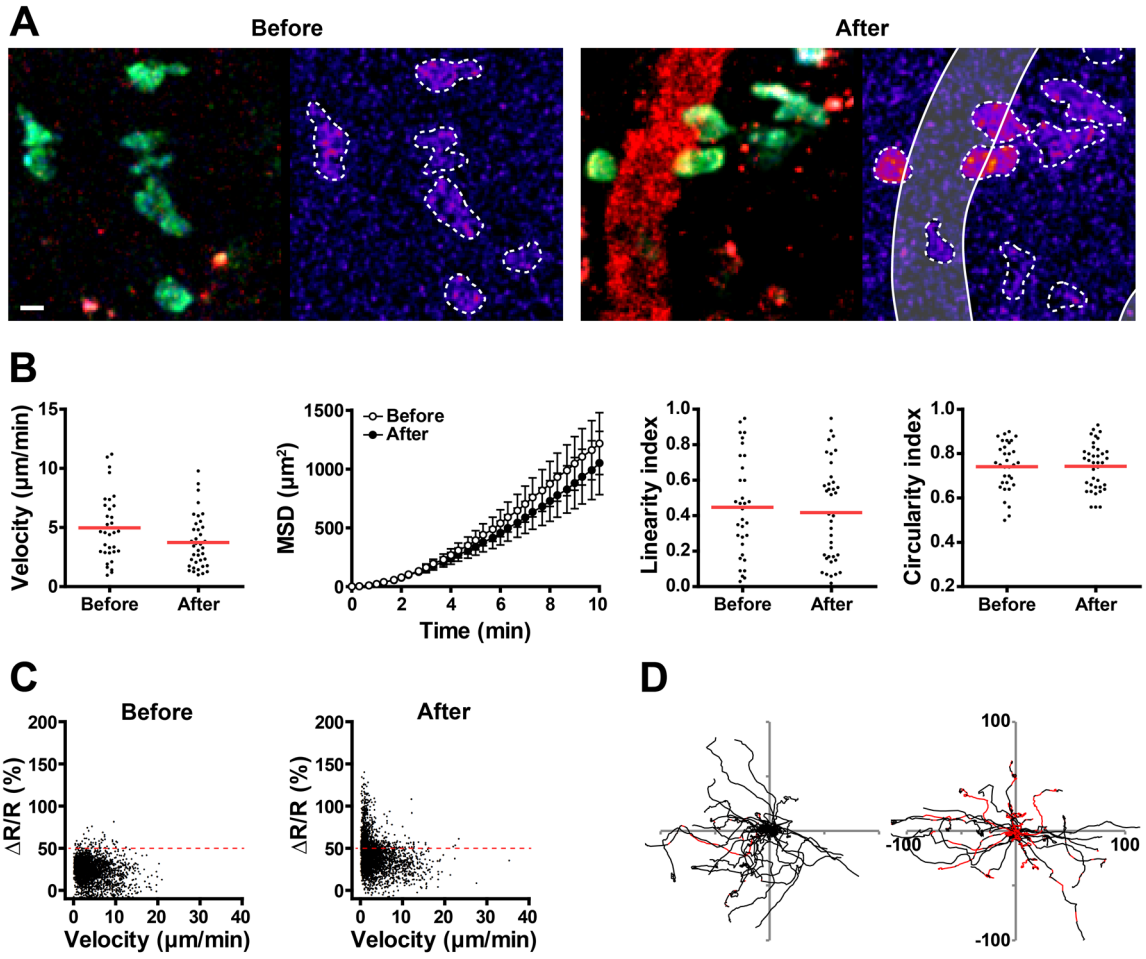

Figure 3.3.11 Calcium imaging in OVA-specific T cells during EAE. (A) Example images from *in vivo* calcium imaging of OT-II T cells in the spinal cord during EAE, before and after injection of antigen and Texas Red dextran. Depicted are fluorescence overlay of TN-3XL^{CD}-expressing OT-II T cells and i.v. infused Texas Red dextran (left), and pseudocolor ratio image with T cells encircled and blood vessel walls retraced (right), scale bar 5 µm. **(B)** Quantification of T cell locomotion in the spinal cord, before and after i.v. antigen injection. Average velocities, mean squared displacement (MSD), movement linearity, and cell circularity are plotted. **(C)** Scatter plots showing cell velocity vs. calcium indicator ratio change for each individual time point analyzed, before and after antigen injection. **(D)** Superimposed trajectories of T cell movements, before (left) and after (right) antigen injection. Time points with ΔR/R above 50% are indicated in red.

Two-photon imaging of extravasated OT-II T cells in the inflamed spinal cord confirmed, that in the absence of cognate antigen T cells migrated randomly through the leptomeningeal space (Figure 3.3.11A and B, and Movie 11), and their calcium signatures were generally very low (Figure 3.3.11C). However, after i.v. injection of OVA peptide (100 µg) along with Texas Red dextran for the visualization of blood vessels, a proportion of the OT-II T cells became arrested, and, like in lymph nodes, most of the immobilized T cells showed elevated calcium levels (Figure 3.3.11C). Plotting the trajectories of T cell movements and highlighting phases of high calcium levels similarly showed the occurrence of elevated calcium levels after application of antigen (Figure 3.3.11D).

3.3.6 *In vivo* imaging of calcium dynamics in encephalitogenic T cells during EAE

For calcium measurements in MOG-specific, encephalitogenic T cells during EAE, 2D2 T cells were retrovirally transduced with TN-3XL^{CD} and adoptively transferred into lymphopenic Rag2$^{-/-}$ mice (Hao *et al.*, 2001). Recipient mice succumbed to EAE at about 11 days after T cell transfer and showed a classical monophasic disease course (Domingues *et al.*, 2010). *In vivo* two-photon imaging revealed intravascular T cells as well as extravasated T cells (Bartholomäus *et al.*, 2009). Interestingly, most T cells rolling on the intravascular lumen showed high intracellular calcium levels (Figure 3.3.12) (Movie 12).

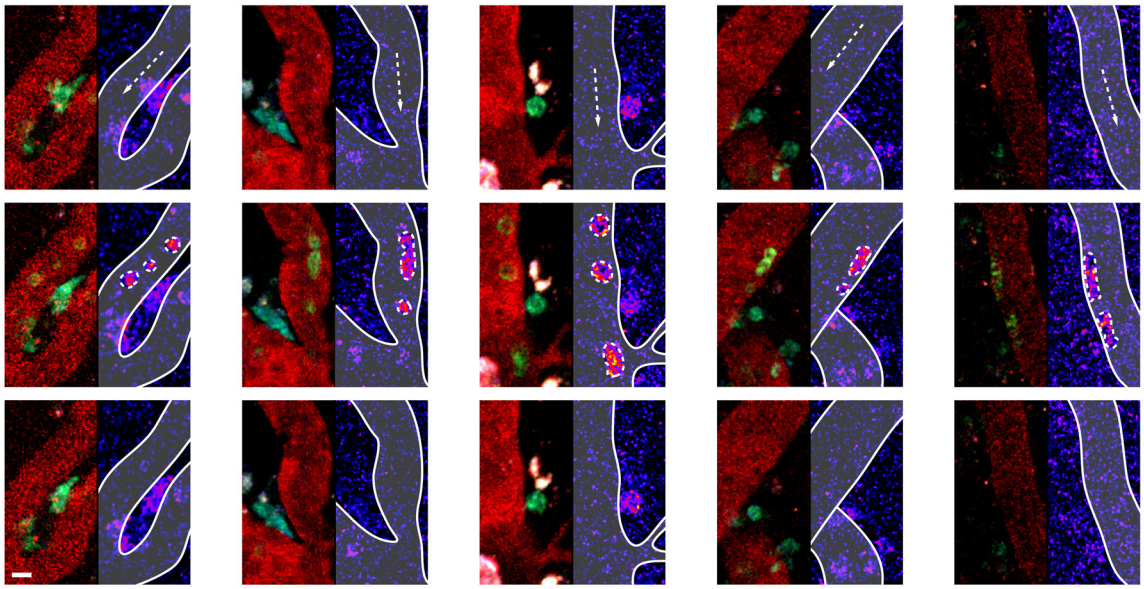

Figure 3.3.12 Rolling T cells show high calcium levels. Five example series from independent in vivo calcium imaging in the spinal cord at early EAE time points. T cells roll at high velocity in the leptomeningeal blood vessel, and thus are seen only for one imaging time frame and appear as successive dots. Depicted are fluorescence overlay of TN-3XL^{CD}-expressing 2D2 T cells and i.v. infused Texas Red dextran (left), and pseudocolor ratio image with T cells encircled and blood vessel walls retraced (right). Arrows indicate direction of blood flow. Imaging frames were taken at 20 seconds time interval, scale bar 10 µm.

In vivo calcium imaging of extravasated T cells during EAE onset (score 0.5) (Movie 12) showed T cells closely associated to blood vessels or freely migrating throughout the leptomeningeal space. T cells moved autonomously throughout the tissue or were found in clusters. Elevated intracellular calcium levels along with ongoing calcium oscillations was seen in T cells localized in such local hot spots (Figure 3.3.13).

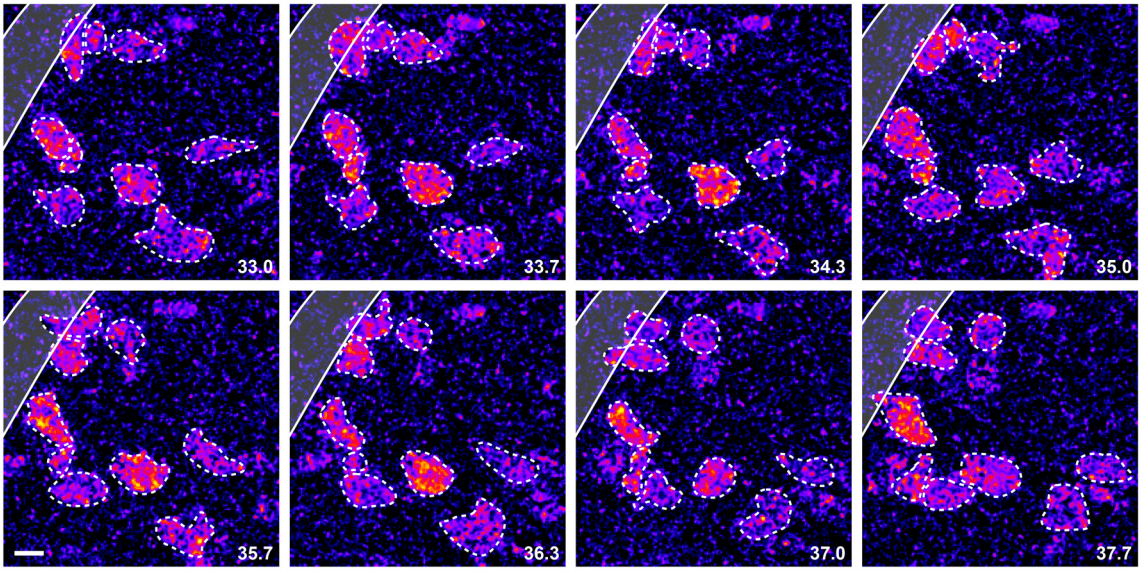

Figure 3.3.13 Calcium signaling in T cell cluster. Series from *in vivo* calcium imaging in the inflamed spinal cord from an early EAE time point (Movie 12). Depicted are pseudocolor ratio images with T cells encircled and blood vessel walls retraced. Time interval in minutes, scale bar 10 µm.

In vivo calcium imaging during peak EAE (score 2) (Movie 13) revealed differential calcium signaling patterns in extravasated T cells. T cells were again found in clusters and showed elevated intracellular calcium levels and calcium oscillations (Figure 3.3.14A). At times T cells stalled their migration to interact with potential antigen-presenting phagocytes (revealed by increased fluorescent Texas Red dextran uptake) and showed sustained intracellular calcium signaling (Figure 3.3.14B). In rare cases presumable intercellular signaling was observed: T cells adjacent to a T cell with persistently elevated calcium levels showed bursts of short-lasting intracellular calcium with high intensity (Figure 3.3.14C). Furthermore, in some T cells subcellular calcium signaling was evident at sites where a T cell remained stationary while stretching out its processes (Figure 3.3.14D).

Quantification of T cell movement and intracellular calcium concentrations during onset and peak EAE revealed comparable values for both disease states. T cells had a velocity of approximately 5 µm/min with predominantly free movement and average migration linearity (Figure 3.3.15A). Interestingly, many T cells showed constantly elevated

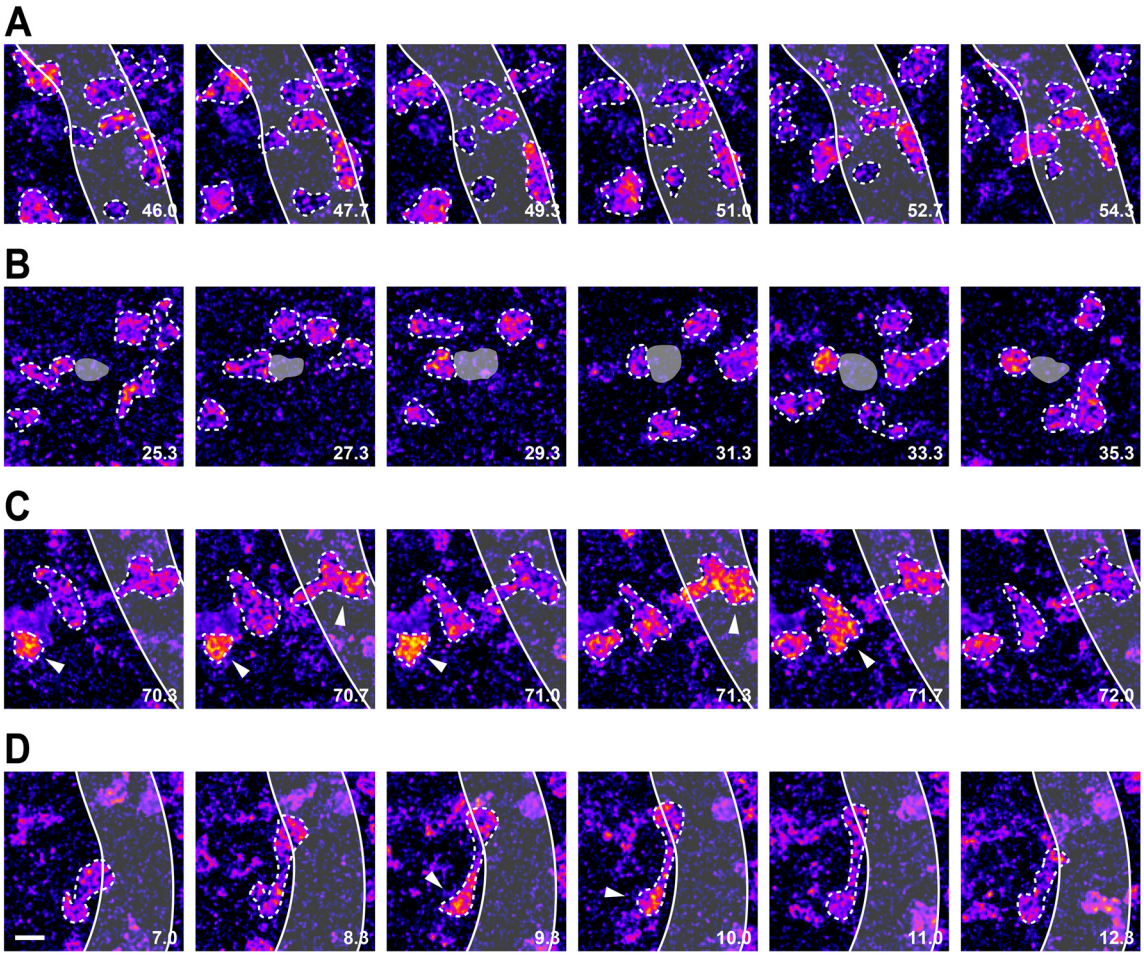

Figure 3.3.14 Differential calcium signaling in T cells during peak EAE. Selected series from *in vivo* calcium imaging in the spinal cord meninges at peak EAE (Movie 13). Depicted are pseudocolor ratio images with T cells encircled and blood vessel walls retraced. Time interval in minutes, scale bar 10 µm. **(A)** Calcium signaling in a T cell cluster. **(B)** T cell arrest and elevated calcium levels after APC (grey) encounter. **(C)** Potential intercellular signaling between a T cell with persistently high intracellular calcium and adjacent T cells. **(D)** Subcellular calcium signaling in a stationary T cells.

calcium levels while migrating through the leptomeningeal space, thus resulting in a less pronounced inverse correlation of T cell motility and intracellular calcium concentrations compared to peripheral immune organs (Figure 3.3.15B). Constantly elevated calcium in T cells, however, was retained at intermediate levels and only transitionally reached peak values accompanied by distinct reductions in cell velocity. In line with these observations, during EAE T cells showed durations of elevated calcium levels well above those base line values of T cells in the popliteal lymph node before antigen encounter (Figure 3.3.15C). Plotting T cell trajectories and highlighting phases of high intracellular calcium similarly revealed the presence of many T cells with constantly elevated calcium levels while maintaining a migratory phenotype, during onset and peak EAE (Figure 3.3.15D).

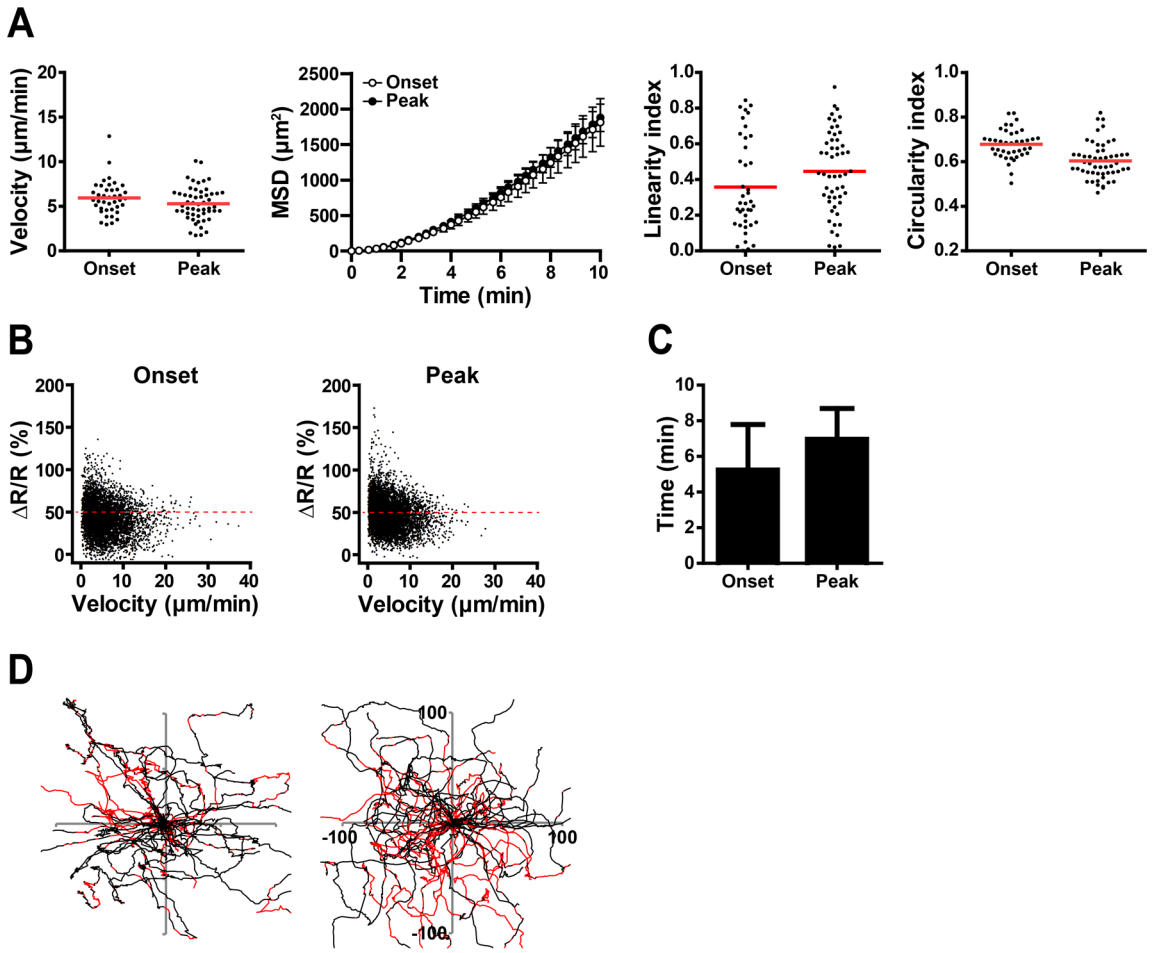

Figure 3.3.15 Analysis of calcium imaging in T cells *in vivo* during EAE. (A) Quantification of T cell locomotion in the spinal cord at onset and peak EAE. Average velocities, mean squared displacement (MSD), movement linearity, and cell circularity are plotted. **(B)** Scatter plots showing cell velocity vs. intracellular calcium concentration. **(C)** Duration of elevated calcium levels with ΔR/R above 50%. **(D)** Superimposed trajectories of T cell movements at onset (left) and peak (right) EAE. Time points with ΔR/R above 50% are indicated in red.

DISCUSSION

4.1 THE R&D MOUSE

The R&D mouse is a promising new model for *in vivo* B cell tracking and depletion. Transgenic expression of RFP and the human DTR under control of the *mb-1* promoter gave rise to bright red fluorescent B cells, that can be depleted by injection of Diphtheria toxin. RFP fluorescence was detectable by all means of standard microscopy, and is resistant to photobleaching over an extended period of time. For effective two-photon imaging *in vivo*, however, a excitation wavelength of over 1000 nm is necessary, which requires a high-end laser source or an optical parametric oscillator (Herz *et al.*, 2010a). Mature peripheral B cells showed a homogeneous fluorescence intensity, whereas variable RFP fluorescence was seen in bone marrow B cells depending on their maturation stage. Along with a progress through development, B cells showed increasing levels of RFP fluorescence, from background levels in pre-pro B cells to full expression of RFP in mature B cells. This stepwise gain in fluorescence intensity most probably reflects the increasing activity of the *mb-1* promoter in successive stages of B cell development (Sakaguchi *et al.*, 1988).

Specific depletion of target cells in mouse models by means of Diphtheria toxin offers several advantages. Since a single molecule of DTx is sufficient to kill a target cell (Yamaizumi *et al.*, 1978), only minute concentrations of the toxin are necessary for depletion *in vivo*. Nonetheless, since rodents are highly insensitive to DTx (Pappenheimer *et al.*, 1982), large amounts of the toxin are tolerated when a very fast and complete depletion of cells needs to be achieved. On the other hand, while DTx itself is rapidly cleared from the systemic circulation, antibodies such as anti-CD20 can persist in circulation for weeks (Vieira and Rajewsky, 1988). Therefore, the use of DTx allows a rather fast ON-OFF system. However, continuous injection of the toxin is necessary, when a sustained depletion is desired. Since the anti-CD20 antibody persists in circulation for extended periods of time and only gradually declines, B cell repopulation kinetics after instantaneous withdrawal of the depleting agent could not be studied so far. Six consecutive injections of DTx removed all circulating B cells in the peripheral blood of R&D mice. Then, only few days after application of the last dose, B cell levels immediately started to recover from depletion, in line with the short half-life of DTx (Yamaizumi *et al.*, 1982). Full recovery, however, was achieved only after about 40 days. Depletion of B cells in the bone marrow already very early in their development, along with a duration of complete B cell maturation in the bone marrow of about two weeks (Arakawa and Takeda, 1996), may account for this long recovery phase.

While antibody-mediated depletion is dependent on helper mechanisms involving other cell types such as macrophages (Uchida *et al.*, 2004), toxin-mediated depletion directly acts on the target cell itself. This effect could be visualized by full depletion of R&D B cells in the peritoneum by DTx, where effectiveness of anti-CD20 treatment is rather limited. Similar results were obtained for B cells of the marginal zone in the spleen which were spared by anti-CD20. Microscopic analysis of B cell depletion in draining lymph nodes from immunized animals revealed, that not all B cells could be depleted by anti-CD20 treatment as already shown before by FACS analysis (Hamel *et al.*, 2008). DTx-mediated depletion, however, eliminated almost all B cell subsets. Another striking observation seen with both depletion methods was the rapid redistribution of T cells throughout the whole lymph node, occupying all former B cell areas within two days. While a certain degree of rearrangement of cells in a lymph node after removal of one population is anticipated, the rate of this process was still surprising and needs further investigation.

In summary, the R&D mouse is a novel tool to analyze B cell function *in vivo*. B cells can be effectively visualized by RFP fluorescence, and are depletable in any organ at any time in a highly controlled fashion. The R&D mouse can be a valuable tool for EAE studies, especially during relapses and remission where B cell functions are not fully understood so far. Furthermore, B cell migration and locomotion inside the CNS could be eventually analyzed using R&D mice.

4.2 TN-XXL TRANSGENIC MICE

Transgenic mice with T cell-specific, strong expression of the genetically encoded calcium indicator TN-XXL would be an excellent source for all kinds of calcium imaging experiments. Unfortunately, however, the TN-XXL transgenic mice generated in this thesis did not meet these expectations. In a first attempt to express TN-XXL in T cells, the hCD2 promoter was used (Zhumabekov *et al.*, 1995). However, this promoter failed to drive strong expression of the transgene in $CD4^+$ T cells, and only $CD8^+$ T cells in one transgenic mouse line showed faint expression of the calcium indicator. Previously, the hCD2 promoter has successfully been used to generate transgenic mice with T cell-specific expression of transgenes such as mCD8α, Cre recombinase (Wilson *et al.*, 2002; De Boer *et al.*, 2003), or human TCRs (Quaratino *et al.*, 2004). In addition, the hCD2 promoter was also shown to efficiently drive expression of GFP, yielding brightly fluorescent T cells. GFP expression in those hCD2-GFP mice, however, was mostly restricted to $CD8^+$ T cells with $CD4^+$ T cells

featuring a fairly reduced fluorescence intensity (Singbartl *et al.*, 2001). This CD8 bias of the hCD2 promoter was also observed in hCD2-TN-XXL mice, nonetheless, the expression strength of TN-XXL in these mice was far too low for efficient microscopic imaging.

In another attempt to obtain transgenic mice with expression of TN-XXL in T cells, the ubiquitously active β-actin promoter was chosen. Quite a number of transgenic mice with all kinds of fluorescent proteins under control of the β-actin promoter has successfully been generated so far, rendering this promoter probably the best candidate for guaranteed, strong expression of any transgene. To further boost expression of TN-XXL, the viral WPRE element, which was shown to enhance expression levels (Zufferey *et al.*, 1999), was included into the transgenic construct CAGW-TN-XXL. One mouse line indeed showed bright TN-XXL fluorescence in most of the organs analyzed. Unfortunately, however, expression of the calcium indicator was absent from all cell types of the hematopoietic system, including T cells. Transgenic DNA amounts in extracts from lymphocytes and non-lymphoid cells were comparable, ruling out a specific deletion of the transgene. RNA levels, in contrast, were highly reduced in lymphocytes. Since the ratio of pre-mRNA to mature RNA was still comparable between fluorescent and non-fluorescent cells, a problem with mRNA stability could be ruled out as well. TN-XXL expression in T cells most likely failed due to transcriptional silencing of the transgene in lymphocytes, since incubation with the demethylating agent Aza (Jones *et al.*, 1980) rendered non-expressing lymphocytes brightly fluorescent. Aza, however, is globally inducing transcriptional activity in the cell, thereby massively interfering with all kinds of cellular mechanisms, and furthermore inducing cell death at the concentrations necessary to obtain fluorescent T cells. Lack of expression in CAGW-TN-XXL lymphocytes could be due to position effects: Integration of the transgene into heterochromatin itself or in close proximity to a heterochromatin domain can lead to transcriptional repression (Wilson *et al.*, 1990). Though the β-actin promoter construct is supposed to yield global and strong expression, the transgenic construct could have integrated at a position in the genome, that is heavily methylated and thereby inactivated specifically in lymphocytes. Nonetheless, it was still very surprising that at all only one transgenic mouse line with strong fluorescence in all organs (except hematopoietic cells) was obtained with the CAGW-TN-XXL construct. In addition to any possible position effects, the WPRE element itself could have had some deleterious effects on the expression of TN-XXL in lymphocytes. While WPRE is supposed to increase expression yields (Zufferey *et al.*, 1999), it was also shown, that in few cell lines the presence of WPRE in a transgene construct could dampen expression levels (Klein *et al.*, 2006). A similar effect was also shown for specific cell lines when combining the CAG promoter with the WPRE (Ramezani *et al.*, 2000). Thus, the integration of the WPRE into the CAGW-TN-XXL transgene might

have boosted expression of the calcium indicator in most cell types, while dampening the expression in cells of the hematopoietic system.

The CAGW-TN-XXL mice, nonetheless, are a useful tool for calcium imaging in a wide variety of non-lymphoid cell types. While cells usually have to be loaded with a calcium sensitive dye prior to calcium measurements, cells from CAGW-TN-XXL mice can be directly used for experiments. In addition, cells could be repeatedly analyzed over an extended period of time. Furthermore, these mice allow calcium imaging in whole organs, which otherwise are very difficult to be homogeneously loaded with a calcium dye. As exemplarily presented in this thesis, calcium waves traveling over explanted, spontaneously beating embryonic hearts could be readily measured without any further pretreatment of the organ.

Since the WPRE might have had negatively influenced the expression of TN-XXL in lymphoid cells, a final attempt using the CAG promoter without the WPRE was initiated to obtain transgenic mice with strong expression of the calcium indicator in T cells. Again, only one line with peripheral fluorescence was obtained with the transgene construct CAG-TN-XXL, this time, however, with expression of TN-XXL also in some cells of the hematopoietic system. When analyzing expression in different immune organs, fluorescence could be found in about 40% of $CD4^+$, $CD8^+$, and natural killer cells, while all other immune cells showed only marginal expression levels. Analysis of the expression patterns of various activation markers or cytokines in T cells after stimulation showed no difference between transgenic and WT T cells, suggesting no negative influence by the persistent expression of the calcium indicator. The fluorescence intensity of TN-XXL in $CD4^+$ T cells, however, was still close to the detection limits of normal widefield microscopy, thus rendering the CAG-TN-XXL line also not suitable for effective two-photon *in vivo* imaging.

Since three attempts to generate transgenic mice with strong TN-XXL expression in T cells failed, and since all attempts produced no more than one line each with at least minor amounts of TN-XXL expression, these problems do not need to be fully attributed to the promoter or the transgene integration site, but could also be intrinsic to the calcium indicator itself. Interference between calcium indicator and host cell has already been reported previously. The FRET-based calcium indicator YC3.12 – similar in design to TN-XXL but featuring calmodulin as calcium sensing moiety – was also inactivated during transgenic expression, while single fluorophore calcium indicators as camgaroo or pericam did at least yield few functional transgenic lines (Hasan *et al.*, 2004). Furthermore, expression of YC3.0 under control of the β-actin promoter in transgenic mice led to sequestered and mosaic expression of the calcium indicator (Tsai *et al.*, 2003). While expression of GECIs for functional characterization in bacteria or in cell lines seems to be practicable, these indicators might feature elements that render generation of transgenic animals problematic.

4.3 CALCIUM IMAGING IN T CELLS

As described in the previous chapter, the calcium indicator TN-XXL could not be expressed in T cells of transgenic mice. To overcome these problems, *ex vivo* stimulated T cells were retrovirally transduced with TN-XXL. Again, while transfection of Phoenix packaging cells was efficient, no TN-XXL fluorescence was seen in $CD4^+$ T cells retrovirally transduced with Phoenix cell supernatant. In contrast, transduction of the single fluorophore YFP yielded brightly fluorescent T cells. A series of experiments with TN-XXL derivatives suggested, that the high sequence homology of CFP and YFP alone was sufficient to impede expression in T cells. Similar observations were made previously, when it was shown that large direct sequence repeats in retroviral vectors were deleted at a high frequency. These deletions occurred during virus replication, and no full-length viruses from plasmids with large direct repeats could be obtained (Rhode *et al.*, 1987). To reduce the sequence homology between the donor and acceptor fluorophore in TN-XXL, YFP was codon diversified by introducing silent mutations without changing the amino acid sequence. This gave rise to $TN\text{-}XXL^{CD}$ which was efficiently expressed in $CD4^+$ T cells after retroviral transduction. The fluorescence intensity was further enhanced by reduction of the retroviral vector. Retroviruses are supposed to tolerate a genome size of up to 8 kb (Coffin *et al.*, 1997). Nonetheless, deletion of the neomycin resistance cassette along with the PGK promoter decreased the size of the retroviral vector by 25% from 5.24 kb to 3.91 kb, and resulted in a 7-fold increase in fluorescence intensity. Removal of the selection cassette was feasible since transduced T cells showed stable fluorescence even in the absence of selecting antibiotics due to stable integration of the retrovirus into the T cell genome.

Calcium measurements in $TN\text{-}XXL^{CD}$-expressing T cells showed a swift rise of intracellular calcium after TCR crosslinking. On a population level only a minor increase was detected, since many cells did not respond to the stimulus. This is most probably due to an anergic state of the T cells after the strong initial stimulation necessary to introduce $TN\text{-}XXL^{CD}$ by retroviral transduction (LaSalle and Hafler, 1994). Nonetheless, cells responding to the trigger showed a high ratio change, reflecting strong intracellular calcium level changes. Similar results were obtained with T cells interacting with anti-CD3/CD28 beads as tracked by microscopy. T cells needed to encounter stimulating beads with their leading edge, where they are more sensitive than at their trailing edge (Wei *et al.*, 1999), and reacted with strong calcium spikes followed by ongoing calcium oscillations. Calcium elevations in $TN\text{-}XXL^{CD}$-expressing 2D2 T cells could also be triggered by co-culture with IgH^{MOG} B cells presenting the cognate antigen. Here, calcium peaks were of comparable intensity as with anti-CD3/CD28 beads, however, seemed to last longer with a reduced

oscillatory frequency. This could resemble the differential response of T cells with respect to varying intracellular calcium signaling after different stimulations (Quintana *et al.*, 2005).

Genetically encoded calcium indicators have been shown to affect host cells. Strong overexpression of fluorescent proteins alone can already induce pathogenic phenotypes: the common actin-GFP transgenic mice, for example, are infertile and smaller in size when bred to homozygosity, and were shown to have already minor defects when heterozygous (Guo *et al.*, 2007). Calcium indicators feature with their calcium-sensing moiety another component that might interfere with the physiology of a cell. When CaM is employed as calcium-sensing domain, overexpression of this ubiquitous signaling molecule could influence other signaling pathways (Hasan *et al.*, 2004). The use of TnC as calcium-binding domain in TN-XXL should overcome this issue; nonetheless, all calcium indicators have a potential calcium buffering capacity that can affect physiological calcium signaling (Ferkey *et al.*, 2007). To rule out a negative influence of TN-XXL^{CD} on T cells, the expression of various surface markers, the transcriptional activity of different cytokines, and the proliferation rate of transduced T cells were compared to control cells. Fortunately, no adverse effect was seen in TN-XXL^{CD}-expressing T cells. Similarly, transduced T cells induced EAE at the same incidence and severity as control cells, a prerequisite for reliable calcium imaging in T cells during EAE.

T cells transduced with TN-XXL^{CD} were readily visible *in vivo* by two-photon microscopy, but showed only modest ratio changes. While it is commonly accepted that T cells feature an intracellular calcium baseline of 50-100 nM, published maximum calcium values vary quite drastically. *In vitro* calcium experiments with naive T cells or T cell lines stimulated by anti-CD3 or calcium release agents reported peak calcium concentrations above 1500 nM (Donnadieu *et al.*, 1992; Murgia *et al.*, 1994). Experiments with naive T cells interacting with APCs *in vitro*, however, reported maximum calcium values lower than 1000 nM (Donnadieu *et al.*, 1994; Negulescu *et al.*, 1994). And the only report somewhat close to *in vivo* settings by using lymph node explants for calcium imaging in T cells interacting with APCs showed intracellular peak calcium levels of only 500 nM (Wei *et al.*, 2007). Therefore, calcium levels measured so far *in vitro* could have been exaggerated, and lower values might actually be present *in vivo*. In T cells, the calcium indicator TN-XXL^{CD} features a dissociation constant K_d of 520 nM, corresponding to an optimal dynamic range of 100-2600 nM intracellular calcium (K_d/5 to K_dx5). This is ranging far beyond a presumable maximum intracellular calcium concentration of 500 nM in T cells *in vivo*, and could explain the lack of strong ratio changes during *in vivo* imaging with TN-XXL^{CD}. To increase sensitivity, an optimized version of the calcium indicator, termed TN-3XL^{CD}, with an increased calcium affinity was used. TN-3XL^{CD} is structurally equivalent to TN-XXL^{CD}, but features a K_d of 140 nM, which corresponds to a dynamic range of 30-700 nM and thus should be optimal to indicate intracellular calcium level changes in T cells *in vivo*. And indeed, initial *in vivo*

calcium imaging experiments with TN-3XL^{CD} promptly revealed spontaneous calcium spikes in migrating T cells, confirming the advantage of this higher sensitivity calcium indicator.

To characterize the functionality of TN-3XL^{CD} in T cells during *in vivo* calcium imaging, the OT-II model system was employed: Ovalbumin-specific T cells were transduced with the calcium indicator and adoptively transferred into WT recipients. One week later, activated dendritic cells were injected subcutaneously, from where they migrated to the draining popliteal lymph node. There they could be imaged *in vivo* together with the OT-II T cells. In the absence of cognate antigen, T cells were highly mobile and randomly migrated through the lymph node tissue, showing sporadic, short-lasting calcium spikes. Such calcium spikes might result from antigen-independent interactions with activated DCs (Montes *et al.*, 1999; Revy *et al.*, 2001), integrin-mediated calcium signaling during migration (Sjaastad and Nelson, 1997), or calcium mobilization in response to chemokine receptor signaling (Ngo *et al.*, 1998; Kershaw *et al.*, 2002). After application of antigen, OT-II T cells stopped and engaged in long-lasting interactions with DCs. Most T cells showed high calcium signaling which correlated with a drastic decrease of cell velocity, similar to thymocytes during positive selection (Bhakta *et al.*, 2005). Many T cells also showed oscillatory calcium signals which lasted far longer than the casual calcium spikes observed in the absence of antigen.

To further test TN-3XL^{CD} in peripheral lymphoid organs in the context of an encephalitogenic antigen, MOG-binding transgenic mouse B cells were used as APCs for MOG-specific 2D2 T cells. Again, TN-3XL^{CD}-transduced 2D2 T cells were adoptively transferred into WT recipients, before MOG-pulsed IgH^{MOG} B cells were injected i.v. one week later. Early *in vivo* calcium imaging in the popliteal lymph node at around 1 hour after adoptive transfer showed, that plenty of B cells already migrated into the lymph node and a fraction of them was interacting with 2D2 T cells. Nonetheless, only sparse calcium signals were detected at this early time point, in freely moving as well as in T cells engaged with MOG presenting IgH^{MOG} B cells. This picture dramatically changed, when T and B cells were imaged at an intermediate time point, at around 8 hours after adoptive transfer. Most 2D2 T cells were interacting with IgH^{MOG} B cells and showed strong and long-lasting, oscillatory calcium signals, comparable to values measured before in OT-II T cells interacting with DCs presenting OVA peptide. 2D2 T cells, however, mostly retained their velocity and formed motile conjugates with MOG-pulsed IgH^{MOG} B cells, as was already described before for HEL-specific T and B cells (Okada *et al.*, 2005). When imaging was performed at a late time point, about 24 hours after adoptive transfer, almost no T and B cell interactions were seen, and likewise strong calcium signals in 2D2 T cells were absent. Furthermore, at this late time point T cells showed the highest velocity of all three stages.

The calcium imaging results obtained with MOG-specific T and B cells fit very well to the model of three different phases of T cell priming (Mempel *et al.*, 2004). While at the early

stage transitional interactions between T and B cells can already be seen, these do not lead to the formation of fully matured immunological synapses, yet, and thus no strong calcium signaling can be observed. T cells seem to integrate small incremental signals over a series of encounters, since only after a sustained period of time T cells fully engage with antigen-presenting B cells and show strong and lasting intracellular calcium signaling. The third phase then is characterized by a return to short-term T and B cell interactions, lacking strong calcium signals. These observations are in contrast to the calcium measurements obtained before from OT-II T cells interacting with antigen-presenting DCs. In this setting, DCs were pulsed with OVA peptide *in vivo*, which lead to a virtually instantaneous arrest of antigen-specific T cells and immediate strong calcium signaling. The rapid T cell activation was most probably due to the strong antigenic stimulation: DCs are known to be much better APCs than B cells (Delon *et al.*, 1998), and a high dose of soluble antigen was injected which forms a very stable complex with the MHC II (Buus *et al.*, 1986). As described previously in a comparable experimental system (Shakhar *et al.*, 2005), the sum of these factors might have exposed T cells to a sufficiently strong level of stimulation to directly induce an immediate arrest of T cells recognizing antigen presented by DCs.

In vivo imaging of ovalbumin-specific T cells introduced into the CNS as bystanders of a developing EAE inflammation (Odoardi *et al.*, 2007) revealed only few calcium signals in these T cells in the absence of antigen, like in lymph nodes. Injection of antigen, however, arrested some of the T cells and induced strong calcium signals. This shows that CNS APCs are capable to efficiently present antigen and to trigger T cell activation. When imaging MOG-specific, encephalitogenic T cells during early EAE time points in the spinal cord, numerous T cells were observed rolling in inflamed vessels with most cells showing high intracellular calcium levels. During rolling, T cells transitionally bind to vascular addressins, which slows down their movement but is too weak to allow extravasation. During rolling, T cells recognize chemokines locally bound in the extracellular matrix, which leads to integrin activation after G protein-coupled receptor (GPCR) signaling and induces firm adhesion of rolling T cells under shear flow (Woolf *et al.*, 2007). GPCR signaling induces calcium fluxes as well and could account for the higher basal calcium levels observed in rolling T cells. Similarly it was reported, that high calcium levels in rolling neutrophils precede firm adhesion (Schaff *et al.*, 2008; Schaff *et al.*, 2010). Prior to T cell extravasation, crawling of T cells inside the blood vessel lumen was described in a rat model system (Bartholomäus *et al.*, 2009). In the mouse model utilized in this thesis, however, only very few crawling T cells were found during EAE. Due to a less predictable course of the disease in the mouse, imaging was done only after animals succumbed to disease. Most T cell crawling, however, takes place before any clinical signs emerge. Thus, no data was collected on calcium levels

in crawling T cells, and the rat model system appears to be much more suitable to study this aspect of T cell infiltration into the brain.

In vivo imaging of TN-3XL^{CD}-expressing T cells, however, revealed first insights into calcium signaling in T cells during EAE. Many extravasated T cells were migrating freely throughout the leptomeningeal space, with elevated calcium levels or located in clusters with ongoing calcium oscillations. This suggests that the majority of T cells features an activated phenotype in the CNS. Since this is the first report of *in vivo* calcium imaging, all data obtained from EAE movies could only be compared to *in vitro* calcium measurements. Yet both, steady calcium elevations and calcium spikes or oscillations have been described, depending on the type and strength of stimulation (Lewis and Cahalan, 1989; Donnadieu *et al.*, 1992; Dolmetsch and Lewis, 1994). Since extravasated T cells were reported to be reactivated by brain resident APCs (Flügel *et al.*, 2001), elevated calcium levels in T cells could be a consequence of *in situ* reactivation. Indeed, during *in vivo* calcium imaging in the spinal cord several instances of T cells interacting with brain resident APCs could be visualized, which resulted in a swift rise of intracellular calcium in those T cells. These interactions were most probably antigen-dependent and led to local reactivation of infiltrating T cells. In addition, during EAE imaging, presumably antigen-independent calcium signals were detected. Freely migrating T cells showed brief calcium spikes, similar to signals seen in T cells during popliteal lymph node imaging in the absence of antigen. As discussed above, such calcium spikes could derive from short-lasting, antigen-independent interactions with APCs, GPCR-mediated calcium mobilization after chemokine receptor triggering, or integrin signaling. Along with concise calcium signals, subcellular changes of intracellular calcium levels could be observed, too, pointing to localized signaling events in T cells interacting with their environment. This was already seen before for neuronal growth cone motility (Dunican and Doherty, 2000) and initiation of cell-cell adhesion between fibroblasts (Ko *et al.*, 2001). Furthermore, T cells showed putative intercellular communication. Wave-like spreading of transient calcium level rises, initiated by an individual cell was observed during EAE imaging. This could result from a release of ATP from an activated cell, triggering a robust change in the concentration of intracellular calcium in neighboring cells (Osipchuk and Cahalan, 1992; Ross *et al.*, 1997; Yegutkin *et al.*, 2006).

Using TN-3XL^{CD} for calcium imaging during EAE, a range of differential calcium signaling patterns was visualized in the inflamed spinal cord, both antigen-dependent and independent. Further in-depth analysis, however, will be necessary to evaluate the origin of all calcium signaling variants observed. Genetic or molecular interference with different signaling pathways in the autoreactive T cell, combined with *in vivo* calcium imaging in the CNS will help to decipher the molecular nature of the disease and shall provide clues for future therapeutic directions.

CONCLUSIONS

Experimental autoimmune encephalomyelitis is an animal model of multiple sclerosis, which provided many insights into the mysteries of this autoimmune disease. Observation of autoreactive immune cells on their way to and also within the target organ helped to gain more knowledge, yet a more detailed analysis of all processes involved in the manifestation of EAE is necessary for a complete understanding. During this thesis, novel tools were established and verified to help visualizing the interplay of various immune cells during the course of the disease.

In chapter 3.1, entitled “THE R&D MOUSE”, a new transgenic mouse model was generated which features fluorescently labeled B cells that can be efficiently depleted. Expression of the transgene under control of the *mb-1* promoter did not show any adverse effects on the composition of the immune system. Interestingly, B cells showed gradually increasing levels of red fluorescence during their development in the bone marrow, which could be used to study B cell development. Since red fluorescence was fully restricted to B cells and highly stable during imaging, this mouse model would be a useful tool for *in vivo* B cell tracking and imaging. B cells can play important roles during disease development, yet so far only limited data is available on the detailed functions of B cells. Well-defined information about the behavior of infiltrating B cells *in vivo* could provide a better understanding of the development of the disease. B cells in the R&D mouse can be depleted at any time by the injection of diphtheria toxin. Depletion occurs rapidly and with a similar or greater efficiency as anti-CD20 antibody-mediated depletion. Since B cells can have various functions during development or manifestation of a disease, timed depletion could help to decipher their particular contribution. Furthermore, since diphtheria toxin exhibits only a very short half-life *in vivo* in contrast to anti-CD20 antibodies, short-term depletion experiments, wiping out the established B cell population to allow repopulation with naive B cells, become feasible. Due to lack of time and the focus of this thesis on calcium imaging in T cells, no additional experiments could be performed to investigate in depth the observations obtained so far, and to further evaluate the full potential of the R&D mouse. Altogether, the R&D mouse is a promising tool for immunological research, for general investigations into B cell development and function, or following the fate of B cells during disease processes.

In chapter 3.2, entitled “TN-XXL TRANSGENIC MICE”, three attempts were made to generate transgenic mice with expression of the calcium indicator TN-XXL in $CD4^+$ T cells. The first attempt, using a T cell-specific promoter, only gave rise to faint expression of TN-XXL in $CD8^+$ T cells. Also the second attempt employing the ubiquitously active CAG promoter along with the WPRE enhancer did not work out for $CD4^+$ T cells. Nonetheless, one mouse line was obtained with otherwise ubiquitous expression of TN-XXL in all cell types of the body, but sparing cells of the hematopoietic lineage. This mouse proved to be a very useful tool for calcium imaging in single cells, as well as in whole-mount organ preparations. The last attempt also used the CAG promoter, however, without the WPRE enhancer. This time the TN-XXL transgene was expressed in $CD4^+$ T cells, albeit only in a small fraction of T cells and with a fluorescence intensity too dim for effective *in vivo* imaging.

In chapter 3.3, entitled “CALCIUM IMAGING IN T CELLS”, retroviral transduction was used to drive expression of the calcium indicator in T cells. Initially, no expression was obtained using the original TN-XXL construct. Only after codon diversification, which reduced the sequence homology between the two fluorophores in the calcium indicator, effective transduction was achieved. The problems encountered were most probably due to homologous recombination of the transgenic construct during virus production. This effect was possibly independent of the problems already encountered during the generation of transgenic mice, and adding another complexity to calcium indicator expression in T cells. Calcium imaging with $TN\text{-}XXL^{CD}$ in T cells after retroviral transduction was feasible *in vitro*. Nonetheless, the higher sensitivity calcium indicator $TN\text{-}3XL^{CD}$ was necessary to efficiently detect intracellular calcium level changes *in vivo*. Strong and sustained calcium signals could be measured in TCR transgenic T cells specific for OVA or MOG antigen, presented by DCs or B cells, respectively. While antigen presentation by DCs induced an immediate T cell arrest accompanied by strong calcium signaling, T cell priming during antigen presentation by B cells followed a multiphase process. Initially, T cells only engaged in short-lasting interactions with B cells in the absence of strong calcium signals. Only after an extended period of time, T cells fully engaged with B cells and showed strong and lasting calcium signals. These differences can be attributed to the differential strength in antigenic signaling between T cells and APCs. Calcium signal characteristics, however, were in the similar range for both types of antigen presentation employed.

When performing calcium imaging in T cells during EAE, various signaling patterns were observed. T cells rolling in inflamed blood vessels in the CNS showed high calcium levels, presumably due to activation of T cells by chemokines deposited on the inner lumen of the vessel. Most extravasated T cells showed a high velocity, yet accompanied by

elevated intracellular calcium. These calcium levels mostly remained in an intermediate level and could be indicative of an activated status of infiltrated T cells. In addition, various other calcium signaling events were detected, such as T cell activation after APC encounter and potential intercellular or subcellular signaling.

Calcium imaging during EAE, diabetes, or rheumatoid arthritis will always necessitate a genetically encoded calcium indicator, since effector T cells are activated and proliferating, which dilutes any synthetic dye. Calcium imaging with TN-3XL^{CD} in T cells presented the highest calcium signals ever measured so far with a ratiometric calcium indicator in an *in vivo* system without direct interference with the cell analyzed. A ratio change of about 15% in pyramidal neurons of mice during visual stimulation was observed using TN-XXL (Mank *et al.*, 2008); up to 60% in cortical astrocytes of mice after electrical forepaw stimulation using YC3.60 (Atkin *et al.*, 2009); and up to 50% in the AWA neuron of C. elegans in response to odor exposure using GEM-GECO1 (Zhao *et al.*, 2011). With TN-3XL^{CD}, however, values of 150% ratio change and greater could be measured in T cells, which facilitates robust signal detection, a fair differentiation from artificial background fluctuations, and yet a highly sensitive graduation of the calcium level changes observed.

A decade after the first dynamic *in vivo* imaging of T cells interacting with antigen-presenting DCs in lymph nodes (Stoll *et al.*, 2002), one essential parameter of T cell functionality can now be visualized by live calcium imaging in T cells *in vivo*. So far, spatial information such as velocity and directionality could be extracted from *in vivo* imaging of T cells in the tissues; however, no functional information could be obtained from these data. A crosstalk of a T cell with an APC can be reckoned from a long-lasting, close contact of two cell types. Whether such an interaction, though, is indeed taking place, and whether such an interaction is of productive nature, can only be visualized by obtaining a functional response from those cells. By establishing calcium imaging in T cells *in vivo*, this additional information can now be obtained which will help to understand basic as well as distinct processes of the immune response.

REFERENCES

Aloisi F (2001) Immune function of microglia. *Glia,* **36,** 165-179.

Arakawa H and Takeda S (1996) Early expression of Ig mu chain from a transgene significantly reduces the duration of the pro-B stage but does not affect the small pre-B stage. *International Immunology,* **8,** 1319-1328.

Atkin SD, Patel S, Kocharyan A, Holtzclaw LA, Weerth SH, Schram V, Pickel J, and Russell JT (2009) Transgenic mice expressing a cameleon fluorescent Ca^{2+} indicator in astrocytes and Schwann cells allow study of glial cell Ca^{2+} signals *in situ* and *in vivo*. *J Neurosci Methods,* **181,** 212-226.

Bailey SL, Carpentier PA, McMahon EJ, Begolka WS, and Miller SD (2006) Innate and adaptive immune responses of the central nervous system. *Crit Rev Immunol,* **26,** 149-188.

Baird GS, Zacharias DA, and Tsien RY (1999) Circular permutation and receptor insertion within green fluorescent proteins. *Proc Natl Acad Sci USA,* **96,** 11241-11246.

Barnden MJ, Allison J, Heath WR, and Carbone FR (1998) Defective TCR expression in transgenic mice constructed using cDNA-based α- and β-chain genes under the control of heterologous regulatory elements. *Immunol Cell Biol,* **76,** 34-40.

Bartholomäus I, Kawakami N, Odoardi F, Schläger C, Miljkovic D, Ellwart JW, Klinkert WEF, Flügel-Koch C, Issekutz TB, Wekerle H, and Flügel A (2009) Effector T cell interactions with meningeal vascular structures in nascent autoimmune CNS lesions. *Nature,* **462,** 94-98.

Baxter AG (2007) The origin and application of experimental autoimmune encephalomyelitis. *Nat Rev Immunol,* **7,** 904-912.

Bekar KW, OWEN T, Dunn R, Ichikawa T, Wang WS, Wang R, Barnard J, Brady S, Nevarez S, Goldman BI, Kehry M, and Anolik JH (2010) Prolonged Effects of Short-Term Anti-CD20 B Cell Depletion Therapy in Murine Systemic Lupus Erythematosus. *Arthritis and Rheumatism,* **62,** 2443-2457.

Ben-Nun A, Wekerle H, and Cohen IR (1981) The rapid isolation of clonable antigen-specific T lymphocyte lines capable of mediating autoimmune encephalomyelitis. *Eur J Immunol,* **11,** 195-199.

Berer K, Mues M, Koutroulos M, Al Rasbi Z, Boziki M, Johner C, Wekerle H, and Krishnamoorthy G (2011a) Commensal microbiota and myelin autoantigen cooperate to trigger autoimmune demyelination. *Nature,* **479,** 538-541.

Berer K, Wekerle H, and Krishnamoorthy G (2011b) B cells in spontaneous autoimmune diseases of the central nervous system. *Mol Immunol,* **48,** 1332-1337.

Bettelli E, Baeten D, Jäger A, Sobel RA, and Kuchroo VK (2006) Myelin oligodendrocyte glycoprotein-specific T and B cells cooperate to induce a Devic-like disease in mice. *J Clin Invest,* **116,** 2393-2402.

Bettelli E, Pagany M, Weiner HL, Linington C, Sobel RA, and Kuchroo VK (2003) Myelin oligodendrocyte glycoprotein-specific T cell receptor transgenic mice develop spontaneous autoimmune optic neuritis. *J Exp Med,* **197,** 1073-1081.

Bhakta NR, Oh DY, and Lewis RS (2005) Calcium oscillations regulate thymocyte motility during positive selection in the three-dimensional thymic environment. *Nat Immunol,* **6,** 143-151.

Buus S, Sette A, Colon SM, Jenis DM, and Grey HM (1986) Isolation and characterization of antigen-Ia complexes involved in T cell recognition. *Cell,* **47,** 1071-1077.

Campbell RE, Tour O, Palmer AE, Steinbach PA, Baird GS, Zacharias DA, and Tsien RY (2002) A monomeric red fluorescent protein. *Proc Natl Acad Sci USA,* **99,** 7877-78882.

Cassan C, Piaggio E, Zappulla JP, Mars LT, Couturier N, Bucciarelli F, Desbois S, Bauer J, Gonzalez-Dunia D, and Liblau RS (2006) Pertussis toxin reduces the number of splenic Foxp3$^+$ regulatory T cells. *J Immunol,* **177,** 1552-1560.

Coffin JM, Hughes SH, and Varmus HE (1997) The Interactions of Retroviruses and their Hosts. *Retroviruses*, Book chapter.

Coles AJ, Cox A, Le PE, Jones J, Trip SA, Deans J, Seaman S, Miller DH, Hale G, Waldmann H, and Compston DA (2006) The window of therapeutic opportunity in multiple sclerosis: evidence from monoclonal antibody therapy. *J Neurol,* **253,** 98-108.

Cordiglieri C, Odoardi F, Zhang B, Nebel M, Kawakami N, Klinkert WEF, Lodygin D, Lühder F, Breunig E, Schild D, Ulaganathan VK, Dornmair K, Dammermann W, Potter BVL, Guse AH, and Flügel A (2010) Nicotinic acid adenine dinucleotide phosphate-mediated calcium signalling in effector T cells regulates autoimmunity of the central nervous system. *Brain,* **133,** 1930-1943.

De Boer J, Williams A, Skavdis G, Harker N, Coles M, Tolaini M, Norton T, Williams K, Roderick K, Potocnik AJ, and Kioussis D (2003) Transgenic mice with hematopoietic and lymphoid specific expression of Cre. *Eur J Immunol,* **33,** 314-325.

Deknuydt F, Bioley G, Valmori D, and Ayyoub M (2009) IL-1β and IL-2 convert human Treg into Th17 cells. *Clinical Immunology,* **131,** 298-307.

Delon J, Bercovici N, Raposo G, Liblau R, and Trautmann A (1998) Antigen-dependent and -independent Ca^{2+} responses triggered in T cells by dendritic cells compared with B cells. *J Exp Med,* **188,** 1473-1484.

Dewitt S, Laffafian I, Morris MR, and Hallett MB (2003) Cytosolic Ca^{2+} measurement and imaging in inflammatory cells. *Methods Mol Biol,* **225,** 47-59.

Dolmetsch RE and Lewis RS (1994) Signaling Between Intracellular Ca^{2+} Stores and Depletion-Activated Ca^{2+} Channels Generates $[Ca^{2+}]_i$ Oscillations in T-Lymphocytes. *J Gen Physiol,* **103,** 365-388.

Domingues HS, Mues M, Lassmann H, Wekerle H, and Krishnamoorthy G (2010) Functional and pathogenic differences of Th1 and Th17 cells in experimental autoimmune encephalomyelitis. *Plos One,* **5,** e15531.

Donnadieu E, Bismuth C, and Trautmann A (1994) Antigen Recognition by Helper T-Cells Elicits A Sequence of Distinct Changes of Their Shape and Intracellular Calcium. *Curr Biol,* **4,** 584-595.

Donnadieu E, Bismuth G, and Trautmann A (1992) Calcium Fluxes in T-Lymphocytes. *JBC,* **267,** 25864-25872.

Drobizhev M, Makarov NS, Tillo SE, Hughes TE, and Rebane A (2011) Two-photon absorption properties of fluorescent proteins. *Nature Methods,* **8,** 393-399.

Dunican DJ and Doherty P (2000) The generation of localized calcium rises mediated by cell adhesion molecules and their role in neuronal growth cone motility. *Mol Cell Biol Res Commun,* **3,** 255-263.

Dustin ML and Depoil D (2011) New insights into the T cell synapse from single molecule techniques. *Nat Rev Immunol,* **11,** 672-684.

Dyment DA, Sadovnick AD, and Ebers GC (1997) Genetics of multiple sclerosis. *Hum Mol Genet,* **6,** 1693-1698.

El-Behi M, Rostami A, and Ciric B (2010) Current Views on the Roles of Th1 and Th17 Cells in Experimental Autoimmune Encephalomyelitis. *J Neuroimmune Pharmacology,* **5,** 189-197.

Engelhardt B and Coisne C (2011) Fluids and barriers of the CNS establish immune privilege by confining immune surveillance to a two-walled castle moat surrounding the CNS castle. *Fluids Barriers CNS,* **8,** 4.

Eyerich S, Eyerisch S, Pennino D, Carbone T, Nasorri F, Pallotta S, Cianfarani F, Odorisio T, Traidl-Hoffmann C, Behrendt H, Durham SR, Schmidt-Weber CB, and Cavani A (2009) Th22 cells represent a distinct human T cell subset involved in epidermal immunity and remodeling. *J Clin Invest,* **119,** 3573-3585.

Fabriek BO, van Haastert ES, Galea I, Polfliet MM, Dopp ED, Van Den Heuvel MM, van den Berg TK, De Groot CJ, van d, V, and Dijkstra CD (2005) CD163-positive perivascular macrophages in the human CNS express molecules for antigen recognition and presentation. *Glia,* **51,** 297-305.

Ferkey DM, Hyde R, Haspel G, Dionne HM, Hess HA, Suzuki H, Schafer WR, Koelle MR, and Hart AC (2007) C-elegans G protein regulator RGS-3 controls sensitivity to sensory stimuli. *Neuron,* **53,** 39-52.

Feske S (2007) Calcium signalling in lymphocyte activation and disease. *Nat Rev Immunol,* **7,** 690-702.

Feske S, Giltnane J, Dolmetsch R, Staudt LM, and Rao A (2001) Gene regulation mediated by calcium signals in T lymphocytes. *Nat Immunol,* **2,** 316-324.

Fillatreau S, Sweenie CH, McGeachy MJ, Gray D, and Anderton SM (2002) B cells regulate autoimmunity by provision of IL-10. *Nat Immunol,* **3,** 944-950.

Flügel A, Berkowicz T, Ritter T, Labeur M, Jenne D, Li Z, Ellwart J, Willem M, Lassmann H, and Wekerle H (2001) Migratory activity and functional changes of green fluorescent effector T cells before and during experimental autoimmune encephalomyelitis. *Immunity,* **14,** 547-560.

Flügel A, Willem M, Berkowicz T, and Wekerle H (1999) Gene transfer into $CD4^+$ T lymphocytes: Green fluorescent protein engineered, encephalitogenic T cells used to illuminate immune responses in the brain. *Nat Med,* **5,** 843-847.

Freund J and McDermott K (1942) Sensitization to horse serum by means of adjuvants. *Proc Soc Exp Biol Med,* **49,** 548.

Friese MA and Fugger L (2005) Autoreactive $CD8^+$ T cells in multiple sclerosis: a new target for therapy? *Brain,* **128,** 1747-1763.

Friese MA, Jakobsen KB, Friis L, Etzensperger R, Craner MJ, McMahon RM, Jensen LT, Huygelen V, Jones EY, Bell JI, and Fugger L (2008) Opposing effects of HLA class I molecules in tuning autoreactive $CD8^+$ T cells in multiple sclerosis. *Nat Med,* **14,** 1227-1235.

Fugger L, Friese MA, and Bell JI (2009) From genes to function: the next challenge to understanding multiple sclerosis. *Nat Rev Immunol,* **9,** 408-417.

Gimenez MA, Sim J, Archambault AS, Klein RS, and Russell JH (2006) A tumor necrosis factor receptor 1-dependent conversation between central nervous system-specific T cells and the central nervous system is required for inflammatory infiltration of the spinal cord. *Am J Pathol,* **168,** 1200-1209.

Gorer PA (1950) Studies in Antibody Response of Mice to Tumour Inoculation. *Br J Cancer,* **4,** 372-379.

Goverman J (2009) Autoimmune T cell responses in the central nervous system. *Nat Rev Immunol,* **9,** 393-407.

Griffioen AW, Rijkers GT, Keij J, and Zegers BJM (1989) Measurement of Cytoplasmic Calcium in Lymphocytes Using Flow-Cytometry - Kinetic-Studies and Single Cell Analysis. *J Immunol Meth,* **120,** 23-27.

Gruver CL, Demayo F, Goldstein MA, and Means AR (1993) Targeted Developmental Overexpression of Calmodulin Induces Proliferative and Hypertrophic Growth of Cardiomyocytes in Transgenic Mice. *Endocrinology,* **133,** 376-388.

Grynkiewicz G, Poenie M, and Tsien RY (1985) A New Generation of Ca^{2+} Indicators with Greatly Improved Fluorescence Properties. *JBC,* **260,** 3440-3450.

Gunter KK and Gunter TE (2001) Measurements of Intracellular Free Calcium Concentration in Biological Systems. *Current Protocols in Toxicology,* 2.5.1-2.5.52.

Guo JK, Cheng EC, Wang L, Swenson ES, Ardito TA, Kashgarian M, Cantley LG, and Krause DS (2007) The commonly used beta-actin-GFP transgenic mouse strain develops a distinct type of glomerulosclerosis. *Transgenic Res,* **16,** 829-834.

Guse AH, Roth E, and Emmrich F (1993) Intracellular Ca^{2+} Pools in Jurkat T-Lymphocytes. *Biochem J,* **291,** 447-451.

Hamaguchi Y, Xiu Y, Komura K, Nimmerjahn F, and Tedder TF (2006) Antibody isotype-specific engagement of Fc receptors regulates B lymphocyte depletion during CD20 immunotherapy. *J Exp Med,* **203,** 743-753.

Hamel K, Doodes P, Cao YX, Wang YM, Martinson J, Dunn R, Kehry MR, Farkas B, and Finnegan A (2008) Suppression of proteoglycan-induced arthritis by anti-CD20 B cell depletion therapy is mediated by reduction in autoantibodies and $CD4^+$ T cell reactivity. *J Immunol,* **180,** 4994-5003.

Handel AE, Lincoln MR, and Ramagopalan SV (2011) Of mice and men: experimental autoimmune encephalitis and multiple sclerosis. *Eur J Clin Invest,* **41,** 1254-1258.

Hao ZY and Rajewsky K (2001) Homeostasis of peripheral B cells in the absence of B cell influx from the bone marrow. *J Exp Med,* **194,** 1151-1163.

Hasan MT, Friedrich RW, Euler T, Larkum ME, Giese G, Both M, Duebel J, Waters J, Bujard H, Griesbeck O, Tsien RY, Nagai T, Miyawaki A, and Denk W (2004) Functional fluorescent Ca^{2+} indicator proteins in transgenic mice under TET control. *PLoS Biology,* **2,** 763-775.

Heim N and Griesbeck O (2004) Genetically encoded indicators of cellular calcium dynamics based on troponin C and green fluorescent protein. *JBC,* **279,** 14280-14286.

Henrickson SE and von Andrian UH (2007) Single-cell dynamics of T-cell priming. *Curr Opin Immunol,* **19,** 249-258.

Herz J, Siffrin V, Hauser AE, Brandt AU, Leuenberger T, Radbruch H, Zipp F, and Niesner RA (2010a) Expanding Two-Photon Intravital Microscopy to the Infrared by Means of Optical Parametric Oscillator. *Biophys J,* **98,** 715-723.

Herz J, Zipp F, and Siffrin V (2010b) Neurodegeneration in autoimmune CNS inflammation. *Exp Neurol,* **225,** 9-17.

Hobeika E, Thiemann S, Storch B, Jumaa H, Nielsen PJ, Pelanda R, and Reth M (2006) Testing gene function early in the B cell lineage in mb1-cre mice. *Proc Natl Acad Sci USA,* **103,** 13789-13794.

Hogan PG, Lewis RS, and Rao A (2010) Molecular Basis of Calcium Signaling in Lymphocytes: STIM and ORAI. *Annual Review of Immunology, Vol 28,* **28,** 491-533.

Homolya L, Hollo Z, Germann UA, Pastan I, Gottesman MM, and Sarkadi B (1993) Fluorescent cellular indicators are extruded by the multidrug-resistance protein. *JBC,* **268,** 21493-21496.

Irvine DJ, Purbhoo MA, Krogsgaard M, and Davis MM (2002) Direct observation of ligand recognition by T cells. *Nature,* **419,** 845-849.

Jones PA and Taylor SM (1980) Cellular-Differentiation, Cytidine Analogs and Dna Methylation. *Cell,* **20,** 85-93.

June CH and Moore JS (2004) Measurement of Intracellular Ions by Flow Cytometry. *Current Protocols in Immunology,* 5.5.1-5.5.20.

Kabat EA, Moore DH, and Landow H (1942) An electrophoretic study of the protein components in cerebrospinal fluid and their relationship to the serum proteins. *J Clin Invest,* **21,** 571-577.

Kawakami N, Lassmann S, Li Z, Odoardi F, Ritter T, Ziemssen T, Klinkert WEF, Ellwart J, Bradl M, Krivacic K, Lassmann H, Ransohoff RM, Volk H-D, Wekerle H, Linington C, and Flügel A (2004) The activation status of neuroantigen-specific T cells in the target organ determines the clinical outcome of autoimmune encephalomyelitis. *J Exp Med,* **199,** 185-197.

Kawamoto S, Niwa H, Tashiro F, Sano S, Kondoh G, Takeda J, Tabayashi K, and Miyazaki J (2000) A novel reporter mouse strain that expresses enhanced green fluorescent protein upon Cre-mediated recombination. *FEBS Lett,* **470,** 263-268.

Kershaw MH, Wang G, Westwood JA, Pachynski RK, Tiffany HL, Marincola FM, Wang E, Young HA, Murphy PM, and Hwu P (2002) Redirecting migration of T cells to chemokine secreted from tumors by genetic modification with CXCR2. *Hum Gene Ther,* **13,** 1971-1980.

Kivisäkk P, Imitola J, Rasmussen S, Elyaman W, Zhu B, Ransohoff RM, and Khoury SJ (2009) Localizing central nervous system immune surveillance: Meningeal antigen-presenting cells activate T cells during experimental autoimmune encephalomyelitis. *Ann Neurol,* **65,** 457-469.

Klein R, Ruttkowski B, Knapp E, Salmons B, Gunzburg WH, and Hohenadl C (2006) WPRE-mediated enhancement of gene expression is promoter and cell line specific. *Gene,* **372,** 153-161.

Ko KS, Arora PD, Bhide V, Chen A, and McCulloch CAG (2001) Cell-cell adhesion in human fibroblasts requires calcium signaling. *J Cell Sci,* **114,** 1155-1167.

Koritschoner R and Schweinburg F (1925) Klinische und experimentelle Beobachtungen über Lähmungen nach Wutschutzimpfung. *Z Immunitätsf,* **42,** 217-283.

Krishnamoorthy G, Lassmann H, Wekerle H, and Holz A (2006) Spontaneous opticospinal encephalomyelitis in a double-transgenic mouse model of autoimmune T cell/B cell cooperation . *J Clin Invest,* **116,** 2385-2392.

Krishnamoorthy G and Wekerle H (2009) EAE: An immunologist's magic eye. *Eur J Immunol,* **39,** 2031-2035.

Kyewski B and Klein L (2006) Central role for central tolerance. *Annu Rev Immunol,* **24,** 571-606.

Lämmli UK (1970) Cleavage of Structural Proteins During Assembly of Head of Bacteriophage-T4. *Nature,* **227,** 680-685.

Lal G, Zhang N, van der Touw W, Ding YZ, Ju WJ, Bottinger EP, Reid SP, Levy DE, and Bromberg JS (2009) Epigenetic Regulation of Foxp3 Expression in Regulatory T Cells by DNA Methylation. *J Immunol,* **182,** 259-273.

LaSalle JM and Hafler DA (1994) T-Cell Anergy. *FASEB Journal,* **8,** 601-608.

Lassmann H, Kitz K, and Wisniewski HM (1981) *In vivo* effect of sera from animals with chronic relapsing experimental allergic encephalomyelitis on central and peripheral myelin. *Acta Neuropathol,* **55,** 297-306.

Ledeist F, Hivroz C, Partiseti M, Thomas C, Buc HA, Oleastro M, Belohradsky B, Choquet D, and Fischer A (1995) A Primary T-Cell Immunodeficiency Associated with Defective Transmembrane Calcium Influx. *Blood,* **85,** 1053-1062.

Lee KY, Turner H, Maynard CL, Olivrt JR, Chen DQ, Elson CO, and Weaver CT (2009) Late developmental plasticity in the T helper 17 lineage. *Immunity,* **30,** 92-107.

Leung S, Liu XB, Fang L, Chen X, Guo T, and Zhang JW (2010) The cytokine milieu in the interplay of pathogenic Th1/Th17 cells and regulatory T cells in autoimmune disease. *Cellular & Molecular Immunology,* **7,** 182-189.

Lewis RS and Cahalan MD (1988) The Plasticity of Ion Channels - Parallels Between the Nervous and Immune-Systems. *Trends in Neurosciences,* **11,** 214-218.

Lewis RS and Cahalan MD (1989) Mitogen-Induced Oscillations of Cytosolic Ca^{2+} and Transmembrane Ca^{2+} Current in Human Leukemic T-Cells. *Cell Regul,* **1,** 99-112.

Li YS, Hayakawa K, and Hardy RR (1993) The regulated expression of B lineage associated genes during B cell differentiation in bone-marrow and fetal liver. *J Exp Med,* **178,** 951-960.

Litzenburger T, Fässler R, Bauer J, Lassmann H, Linington C, Wekerle H, and Iglesias A (1998) B lymphocytes producing demyelinating autoantibodies: Development and function in gene-targeted transgenic mice. *J Exp Med,* **188,** 169-180.

Long JZ, Lackan CS, and Hadjantonakis AK (2005) Genetic and spectrally distinct *in vivo* imaging: embryonic stem cells and mice with widespread expression of a monomeric red fluorescent protein. *BMC Biotechnology,* **5**.

Luche H, Weber O, Rao TN, Blum C, and Fehling HJ (2006) Faithful activation of an extra-bright red fluorescent protein in knock-in Cre-reporter mice ideally suited for lineage tracing studies. *Eur J Immunol,* **37,** 43-53.

Lund FE and Randall TD (2010) Effector and regulatory B cells: modulators of $CD4^+$ T cell immunity. *Nat Rev Immunol,* 236-247.

Lünemann JD, Kamradt T, Martin R, and Munz C (2007) Epstein-barr virus: environmental trigger of multiple sclerosis? *J Virol,* **81,** 6777-6784.

Lyons J-A, San M, Happ MP, and Cross AH (1999) B cells are critical to induction of experimental allergic encephalomyelitis by protein but not by a short encephalitogenic peptide. *Eur J Immunol,* **29,** 3432-3439.

Macian F (2005) NFAT proteins: Key regulators of T-cell development and function. *Nat Rev Immunol,* **5,** 472-484.

Mank M, Santos AF, Direnberger S, Mrsic-Flogel TD, Hofer SB, Stein V, Hendel T, Reiff DF, Levelt C, Borst A, Bonhoeffer T, Hübener M, and Griesbeck O (2008) A genetically encoded calcium indicator for chronic *in vivo* two-photon imaging. *Nature Methods,* **5,** 805-811.

Mann MK, Maresz K, Shriver LP, Tan Y, and Dittel BN (2007) B cell regulation of $CD4^+CD25^+$ T regulatory cells and IL-10 via B7 is essential for recovery from experimental autoimmune encephalomyelitis. *J Immunol,* **178,** 3447-3456.

Mastroyiannopoulos NP, Feldman ML, Uney JB, Mahadevan MS, and Phylactou LA (2005) Woodchuck post-transcriptional element induces nuclear export of myotonic dystrophy 30 untranslated region transcripts. *EMBO Reports,* **6,** 458-463.

Matsushita T, Yanaba K, Bouaziz J-D, Fujimoto M, and Tedder TF (2008) Regulatory B cells inhibit EAE initiation in mice while other B cells promote disease progression. *J Clin Invest,* **118,** 3420-3430.

McCombs JE and Palmer AE (2008) Measuring calcium dynamics in living cells with genetically encodable calcium indicators. *Methods,* **46,** 152-159.

Medana I, Martinic MMA, Wekerle H, and Neumann H (2001) Transection of MHC class I-induced neurites by cytotoxic T lymphocytes. *Am J Pathol,* **159,** 809-815.

Mempel TR, Henrickson SE, and von Andrian UH (2004) T-cell priming by dendritic cells in lymph nodes occurs in three distinct phases. *Nature,* **427,** 154-159.

Messing J (1983) New M13 vectors for cloning. *Methods Enzymol,* **101,** 20-78.

Miyawaki A, Llopis J, Heim R, McCafferty JM, Adams JA, Ikuta M, and Tsien RY (1997) Fluorescent indicators for Ca^{2+} based on green fluorescent proteins and calmodulin. *Nature,* **388,** 882-887.

Montes M, McIlroy D, Hosmalin A, and Trautmann A (1999) Calcium responses elicited in human T cells and DCs by cell-cell interaction and soluble ligands. *International Immunology,* **11,** 561-568.

Murgia M, Mion M, Veronese L, Panozzo M, Coppola V, Rizzuto R, Brini M, Malavasi F, Amadori A, Bianchi LC, and Pozzan T (1994) Cytosolic-Free Calcium-Concentration in the Mitogenic Stimulation of T-Lymphocytes by Anti-Cd3 Monoclonal-Antibodies. *Cell Calcium,* **16,** 167-180.

Nagai T, Sawano A, Park ES, and Miyawaki A (2001) Circularly permuted green fluorescent proteins. *Proc Natl Acad Sci USA,* **98,** 3197-3202.

Nagai T, Yamada S, Tominaga T, Ichikawa M, and Miyawaki A (2004) Expanded dynamic range of fluorescent indicators for Ca^{2+} by circularly permuted yellow fluorescent proteins. *Proc Natl Acad Sci USA,* **101,** 10554-10559.

Nakai J, Ohkura M, and Imoto K (2001) A high signal-to-noise Ca^{2+} probe composed of a single green fluorescent protein. *Nature Biotech,* **19,** 137-141.

Nave K-A (2010) Myelination and the trophic support of long axons. *Nature Rev Neurosci,* **11,** 275-283.

Negulescu PA, Shastri N, and Cahalan MD (1994) Intracellular calcium dependence of gene expression in single T lymphocytes. *Proc Natl Acad Sci USA,* **91,** 2873-2877.

Neyfakh AA (1988) Use of Fluorescent Dyes As Molecular Probes for the Study of Multidrug Resistance. *Exp Cell Res,* **174,** 168-176.

Ngo VN, Tang HL, and Cyster JG (1998) Epstein-Barr virus-induced molecule 1 ligand chemokine is expressed by dendritic cells in lymphoid tissues and strongly attracts naive T cells and activated B cells. *J Exp Med,* **188,** 181-191.

Niwa H, Yamamura K, and Miyazaki J (1991) Efficient selection for high-expression transfectants with a novel eukaryotic vector. *Gene,* **108,** 193-199.

Obermeier B, Mentele R, Malotka J, Kellermann J, Wekerle H, Lottspeich F, Hohlfeld R, and Dornmair K (2008) Matching of oligoclonal Ig transcriptomes and proteomes of cerebrospinal fluid in multiple sclerosis. *Nat Med,* **14,** 688-693.

Odoardi F, Kawakami N, Klinkert WEF, Wekerle H, and Flügel A (2007) Blood-borne soluble protein antigen intensifies T cell activation in autoimmune CNS lesions and exacerbates clinical disease. *Proc Natl Acad Sci USA,* **104,** 18625-18630.

Okabe M, Ikawa M, Kominami K, Nakanishi T, and Nishimune Y (1997) 'Green mice' as a source of ubiquitous green cells. *FEBS Lett,* **407,** 313-319.

Okada T, Miller MJ, Parker I, Krummel MF, Neighbors M, Hartley SB, O'Garra A, Cahalan MD, and Cyster JG (2005) Antigen-engaged B cells undergo chemotaxis toward the T zone and form motile conjugates with helper T cells. *PLoS Biology,* **3,** 1047-1061.

Olitsky PK and Yager RH (1949) Experimental Disseminated Encephalomyelitis in White Mice. *J Exp Med,* **90,** 213-&.

Omilusik K, Priatel JJ, Chen XX, Wang YWT, Xu HJ, Choi KB, Gopaul R, McIntyre-Smith A, Teh H-S, Tan RS, Bech-Hansen T, Waterfield D, Fedida D, Hunt SV, and Jefferies WA (2011) The $Ca_v1.4$ calcium channel is a critical regulator of T cell receptor signaling and naive T cell homeostasis. *Immunity,* **35,** 349-360.

Osipchuk Y and Cahalan M (1992) Cell-To-Cell Spread of Calcium Signals Mediated by Atp Receptors in Mast-Cells. *Nature,* **359,** 241-244.

Palmiter R (2001) Interrogation by toxin. *Nature Biotech,* **19,** 731-732.

Pappenheimer AM, Harper AA, Moynihan M, and Brockes JP (1982) Diphtheria-Toxin and Related Proteins - Effect of Route of Injection on Toxicity and the Determination of Cyto-Toxicity for Various Cultured-Cells. *J Infect Dis,* **145,** 94-102.

Park CY, Hoover PJ, Mullins FM, Bachhawat P, Covington ED, Raunser S, Walz T, Garcia KC, Dolmetsch RE, and Lewis RS (2009) STIM1 Clusters and Activates CRAC Channels via Direct Binding of a Cytosolic Domain to Orai1. *Cell,* **136,** 876-890.

Paterson PY (1960) Transfer of allergic encephalomyelitis in rats by means of lymph node cells. *J Exp Med,* **111,** 119-135.

Pear WS, Nolan GP, Scott ML, and Baltimore D (1993) Production of High-Titer Helper-Free Retroviruses by Transient Transfection. *Proc Natl Acad Sci USA,* **90,** 8392-8396.

Pöllinger B, Krishnamoorthy G, Berer K, Lassmann H, Bösl M, Dunn R, Domingues HS, Holz A, Kurschus FC, and Wekerle H (2009) Spontaneous relapsing-remitting EAE in the SJL/J mouse: MOG-reactive transgenic T cells recruit endogenous MOG-specific B cells. *J Exp Med,* **206,** 1303-1316.

Prechtl S, Roellinghoff M, Scheper R, Cole SPC, Deeley RG, and Lohoff M (2000) The multidrug resistance protein 1: A functionally important activation marker for murine Th1 cells. *J Immunol,* **164,** 754-761.

Quaratino S, Badami E, Pang YY, Bartok I, Dyson J, Kioussis D, Londei M, and Maiuri L (2004) Degenerate self-reactive human T-cell receptor causes spontaneous autoimmune disease in mice. *Nat Med,* **10,** 920-926.

Quintana A, Griesemer D, Schwarz EC, and Hoth M (2005) Calcium-dependent activation of T-lymphocytes. *Pflugers Archiv-European Journal of Physiology,* **450,** 1-12.

Ramezani A, Hawley TS, and Hawley RG (2000) Lentiviral vectors for enhanced gene expression in human hematopoietic cells. *Molecular Therapy,* **2,** 458-469.

Ransohoff RM, Kivisakk P, and Kidd G (2003) Three or more routes for leukocyte migration into the central nervous system. *Nat Rev Immunol,* **3,** 569-581.

Reff ME, Carner K, Chambers KS, Chinn PC, Leonard JE, Raab R, Newman RA, Hanna N, and Anderson DR (1994) Depletion of B-Cells *In Vivo* by A Chimeric Mouse-Human Monoclonal-Antibody to Cd20. *Blood,* **83,** 435-445.

Revy P, Sospedra M, Barbour B, and Trautmann A (2001) Functional antigen-independent synapses formed between T cells and dendritic cells. *Nat Immunol,* **2,** 925-931.

Rhode BW, Emerman M, and Temin HM (1987) Instability of Large Direct Repeats in Retrovirus Vectors. *Journal of Virology,* **61,** 925-927.

Riedl J, Flynn KC, Raducanu A, Gartner F, Beck G, Bosl M, Bradke F, Massberg S, Aszodi A, Sixt M, and Wedlich-Soldner R (2010) Lifeact mice for studying F-actin dynamics. *Nature Methods,* **7,** 168-169.

Rochefort NL, Jia HB, and Konnerth A (2008) Calcium imaging in the living brain: prospects for molecular medicine. *Trends Mol Med,* **14,** 389-399.

Ross PE, Ehring GR, and Cahalan MD (1997) Dynamics of ATP-induced calcium signaling in single mouse thymocytes. *J Cell Biol,* **138,** 987-998.

Saito M, Iwawaki T, Taya C, Yonekawa H, Noda M, Inui Y, Mekada E, Kimata Y, Tsuru A, and Kohno K (2001) Diphtheria toxin receptor-mediated conditional and targeted cell ablation in transgenic mice. *Nature Biotech,* **19,** 746-750.

Sakaguchi N, Nishiwamura S-I, Kimoto M, Thalmann P, and Melchers F (1988) B lymphocyte lineage-restricted expression of *mb-1*, a gene with CD3-like structural properties. *EMBO J,* **7,** 3457-3464.

Sakaguchi N, Takahashi T, Hata H, Nomura T, Tagami T, Yamazaki S, Sakihama T, Matsutani T, Negishi I, Nakatsuru S, and Sakaguchi S (2003) Altered thymic T-cell selection due to a mutation of the ZAP-70 gene causes autoimmune arthritis in mice. *Nature,* **426,** 454-460.

Sambrook J and Russel DW (2001) Molecular Cloning: A Laboratory Manual (3rd ed.). *Cold Spring Harbor Laboratory Press*, Book chapter.

Schaff UY, Dixit N, Procyk E, Yamayoshi I, Tse T, and Simon SI (2010) Orai1 regulates intracellular calcium, arrest, and shape polarization during neutrophil recruitment in shear flow. *Blood,* **115,** 657-666.

Schaff UY, Yamayoshi I, Tse T, Griffin D, Kibathi L, and Simon SI (2008) Calcium flux in neutrophils synchronizes beta(2) integrin adhesive and signaling events that guide inflammatory recruitment. *Ann Biomed Eng,* **36,** 632-646.

Schuhmann MK, Stegner D, Berna-Erro A, Bittner S, Braun A, Kleinschnitz C, Stoll G, Wiendl H, Meuth SG, and Nieswandt B (2010) STIM 1 and 2 are key regulators of autoreactive T cell activation in murine autoimmune central nervous system inflammation. *J Immunol,* **184,** 1536-1542.

Schwarzmann N, Kunerth S, Weber K, Mayr GW, and Guse AH (2002) Knock-down of the type 3 ryanodine receptor impairs sustained Ca^{2+} signaling via the T cell receptor/CD3 complex. *JBC,* **277,** 50636-50642.

Serafini B, Rosicarelli B, Magliozzi R, Stigliano E, and Aloisi F (2004) Detection of ectopic B-cell follicles with germinal centers in the meninges of patients with secondary progressive multiple sclerosis. *Brain Pathol,* **14,** 164-174.

Shakhar G, Lindquist RL, Skokos D, Dudziak D, Huang JH, Nussenzweig MC, and Dustin ML (2005) Stable T cell-dendritic cell interactions precede the development of both tolerance and immunity *in vivo*. *Nat Immunol,* **6,** 707-714.

Shaner NC, Campbell RE, Steinbach PA, Giepmans BNG, Palmer AE, and Tsien RY (2004) Improved monomeric red, orange and yellow fluorescent proteins derived from Discosoma sp red fluorescent protein. *Nature Biotech,* **22,** 1567-1572.

Singbartl K, Thatte J, Smith ML, Wethmar K, Day K, and Ley K (2001) A CD2-green fluorescence protein-transgenic mouse reveals very late antigen-4-dependent $CD8^+$ lymphocyte rolling in inflamed venules. *J Immunol,* **166,** 7520-7526.

Sjaastad MD and Nelson WJ (1997) Integrin-mediated calcium signaling and regulation of cell adhesion by intracellular calcium. *Bioessays,* **19,** 47-55.

Smolders J, Damoiseaux J, Menheere P, and Hupperts R (2008) Vitamin D as an immune modulator in multiple sclerosis, a review. *J Neuroimmunol,* **194,** 7-17.

Sospedra M and Martin R (2005) Immunology of multiple sclerosis. *Annu Rev Immunol,* **23,** 683-747.

Stoll S, Delon J, Brotz TM, and Germain RN (2002) Dynamic imaging of T cell-dendritic cell interactions in lymph nodes. *Science,* **296,** 1873-1876.

Stromnes IM and Goverman JM (2006a) Active induction of experimental allergic encephalomyelitis. *Nature Protocols,* **1,** 1810-1819.

Stromnes IM and Goverman JM (2006b) Passive induction of experimental allergic encephalomyelitis. *Nature Protocols,* **1,** 1952-1960.

Suzuki MM and Bird A (2008) DNA methylation landscapes: provocative insights from epigenomics. *Nature Reviews Genetics,* **9,** 465-476.

Tallini YN, Ohkura M, Choi BR, Ji GJ, Imoto K, Doran R, Lee J, Plan P, Wilson J, Xin HB, Sanbe A, Gulick J, Mathai J, Robbins J, Salama G, Nakai J, and Kotlikoff MI (2006) Imaging cellular signals in the heart *in vivo*: Cardiac expression of the high-signal Ca^{2+} indicator GCaMP2. *Proc Natl Acad Sci USA,* **103,** 4753-4758.

Tsai PS, Friedman B, Ifarraguerri AI, Thompson BD, Lev-Ram V, Schaffer CB, Xiong C, Tsien RY, Squier JA, and Kleinfeld D (2003) All-optical histology using ultrashort laser pulses. *Neuron,* **39,** 27-41.

Tsien RY (1980) New Calcium Indicators and Buffers with High Selectivity Against Magnesium and Protons - Design, Synthesis, and Properties of Prototype Structures. *Biochemistry,* **19,** 2396-2404.

Uchida J, Hamaguchi Y, Oliver JA, Ravetch JV, Poe JC, Haas KM, and Tedder TF (2004) The innate mononuclear phagocyte network depletes B cells by Fc receptor-dependent mechanisms during anti-CD20 antibody immunotherapy. *J Exp Med,* **199,** 1659-1669.

Veldhoen M, Uyttenhove C, Van Snick J, Helmby H, Westendorf A, Buer J, Martin B, Wilhelm C, and Stockinger B (2008) TGF-β 'reprograms' the differentiation of Th2 cells and promotes an IL-9-producing subset. *Nat Immunol,* **9,** 1341-1346.

Vieira P and Rajewsky K (1988) The half-lives of serum immunoglobulins in adult mice. *Eur J Immunol,* **18,** 313-316.

Vig M and Kinet J-P (2009) Calcium signaling in immune cells. *Nat Immunol,* **10,** 21-27.

Vignali DAA, Collison LW, and Workman CJ (2008) How regulatory T cells work. *Nat Rev Immunol,* **8,** 523-532.

Wei SH, Safrina O, Yu Y, Garrod KR, Cahalan MD, and Parker I (2007) Ca^{2+} signals in $CD4^+$ T cells during early contacts with antigen-bearing dendritic cells in lymph node. *J Immunol,* **179,** 1586-1594.

Wei XB, Tromberg BJ, and Cahalan MD (1999) Mapping the sensitivity of T cells with an optical trap: Polarity and minimal number of receptors for Ca^{2+} signaling. *Proc Natl Acad Sci USA,* **96,** 8471-8476.

Wekerle H, Kojima K, Lannes-Vieira J, Lassmann H, and Linington C (1994) Animal models. *Ann Neurol,* **36 Suppl,** S47-S53.

Willenborg DO and Prowse SJ (1983) Immunoglobulin-deficient rats fail to develop experimental allergic encephalomyelitis. *J Neuroimmunol,* **5,** 99-109.

Willenborg DO, Sjollema P, and Danta G (1986) Immunoglobulin deficient rats as donors and recipients of effector cells of allergic encephalomyelitis. *J Neuroimmunol,* **11,** 93-103.

Wilson C, Bellen HJ, and Gehring WJ (1990) Position Effects on Eukaryotic Gene-Expression. *Annu Rev Cell Biol,* **6,** 679-714.

Wilson TJ, Cowdery HE, Xu DK, Kola I, and Hertzog PJ (2002) A human CD2 minigene directs CRE-mediated recombination in T cells *in vivo*. *Genesis,* **33,** 181-184.

Woolf E, Grigorova I, Sagiv A, Grabovsky V, Feigelson SW, Shulman Z, Hartmann T, Sixt M, Cyster JG, and Alon R (2007) Lymph node chemokines promote sustained T lymphocyte motility without triggering stable integrin adhesiveness in the absence of shear forces. *Nat Immunol,* **8,** 1067-1075.

Yamaizumi M, Mekada E, Uchida T, and Okada Y (1978) One molecule of diphtheria toxin fragment A introduced into a cell can kill the cell. *Cell,* **15,** 245-250.

Yamaizumi M, Uchida T, Takamatsu K, and Okada Y (1982) Intracellular Stability of Diphtheria Toxin Fragment-A in the Presence and Absence of Anti Fragment A Antibody. *Proc Natl Acad Sci USA,* **79,** 461-465.

Yednock TA, Cannon C, Fritz LC, Sanchez-Madrid F, Steinman L, and Karin N (1992) Prevention of experimental autoimmune encephalomyelitis by antibodies against alpha 4 beta 1 integrin. *Nature,* **356,** 63-66.

Yegutkin GG, Mikhailov A, Samburski SS, and Jalkanen S (2006) The detection of micromolar pericellular ATP pool on lymphocyte surface by using lymphoid ecto-adenylate kinase as intrinsic ATP sensor. *Mol Biol Cell,* **17,** 3378-3385.

Zhao YX, Araki S, Jiahui WH, Teramoto T, Chang YF, Nakano M, Abdelfattah AS, Fujiwara M, Ishihara T, Nagai T, and Campbell RE (2011) An Expanded Palette of Genetically Encoded Ca^{2+} Indicators. *Science,* **333,** 1888-1891.

Zhumabekov T, Corbella P, Tolaini M, and Kioussis D (1995) Improved Version of A Human CD2 Minigene Based Vector for T-Cell-Specific Expression in Transgenic Mice. *J Immunol Meth,* **185,** 133-140.

Zufferey R, Donello JE, Trono D, and Hope TJ (1999) Woodchuck hepatitis virus posttranscriptional regulatory element enhances expression of transgenes delivered by retroviral vectors. *Journal of Virology,* **73,** 2886-2892.

ABBREVIATIONS

ADP	Adenosine diphosphate
APC	Antigen-presenting cell
ATP	Adenosine triphosphate
a.u.	Arbitrary units
Aza	Aza-2´-deoxycytidine
BBB	Blood brain barrier
BCR	B cell receptor
BFP	Blue fluorescent protein
BMDC	Bone marrow-derived DC
BSA	Bovine serum albumin
cADPR	Cyclic ADP ribose
CAG	CMV early enhancer/chicken beta actin
CaM	Calmodulin
CaMK	Calmodulin-dependent kinase
Ca_V	Voltage-gated calcium
CD	Cluster of differentiation
CFA	Complete Freund´s adjuvant
CFSE	Carboxy-fluorescein diacetate succinimidyl ester
CFP	Cyan fluorescent protein
CMV	Cytomegalovirus
CN	Calcineurin
CNS	Central nervous system
c.p.m.	Counts per minute
CRAC	Calcium release activated calcium
CSF	Cerebrospinal fluid
Ct	Cycle threshold
CTLA4	Cytotoxic T-Lymphocyte Antigen 4
DAG	Diacylglycerol
DC	Dendritic cell
DMEM	Dulbecco´s Modified Eagle´s Medium
DTR	Diphtheria toxin receptor
DTx	Diphtheria toxin
EAE	Experimental autoimmune encephalomyelitis
EF2	Elongation factor 2
EGF	Epidermal growth factor
ER	Endoplasmatic reticulum
ERM	Ezrin, radixin, and moesin
FACS	Fluorescence-activated cell sorting
FI	Fluorescence intensity

FO	Follicular
FP	Fluorescent protein
FRET	Förster resonance energy transfer
FSC	Forward scatter
GAPDH	Glyceraldehyde 3-phosphate dehydrogenase
GECI	Genetically encoded calcium indicator
GFP	Green fluorescent protein
GPCR	G protein-coupled receptor
GWAS	Genome wide association study
HB-EGF	Heparin-binding EGF
hCD2	human CD2
HLA	Human leukocyte antigen
HRP	Horseradish peroxidase
ICAM1	Inter-Cellular Adhesion Molecule 1
IE	Internal enhancer
IFNγ	Interferon gamma
Ig	Immunoglobulin
IL	Interleukin
IP_3	Inositol-1,4,5-trisphosphate
i.p.	Intraperitoneal
IRES	Internal ribosomal entry site
ITK	Inducible T cell kinase
i.v.	Intravenous
KLH	Keyhole limpet hemocyanin
LAT	Linker for activation of T cells
LCK	Lymphocyte-specific protein tyrosine kinase
LCR	Locus control region
LFA1	Lymphocyte function-associated antigen 1
LTR	Long terminal repeat
MBP	Myelin basic protein
MCS	Multiple cloning site
MDR	Multidrug resistance
MHC	Major histocompatibility complex
MOG	Myelin oligodendrocyte glycoprotein
MS	Multiple sclerosis
MSD	Mean squared displacement
MZ	Marginal zone
NAD	Nicotinamide adenine dinucleotide
NeoR	Neomycin resistance cassette
NF-κB	Nuclear factor kappa-light-chain-enhancer of activated B-cells
NFAT	Nuclear factor of activated T-cells
NFL	Neurofilament light
NO	Nitric oxide

OD	Optical density
OSE	Opticospinal EAE
OVA	Ovalbumin
PBMC	Peripheral blood mononuclear cells
PBS	Phosphate buffered saline
PCR	Polymerase chain reaction
PFA	Paraformaldehyde
PGKp	Phosphoglycerate kinase promoter
PLCγ	Phospholipase C gamma
PLP	Proteolipid protein
Ψ signal	Packaging signal
PtdIns(4,5)P_2	Phosphatidylinositol-4,5-bisphosphate
PVDF	Polyvinyliden fluoride
R	Ratio
rcf	Relative centrifugal force
RFP	Red fluorescent protein
rMOG	Recombinant MOG
ROI	Region of interest
ROS	Radical oxygen species
RPMI	Roswell park memorial institute
RR	Relapsing remitting
RT	Room temperature
RYR_3	Ryanodine receptors
SAM	Sterile-a-motif
SLP76	SH2 domain containing leukocyte protein 76
SMAC	Supramolecular activation complex
SNARF-1	Seminaphthorhodafluor 1
SOCE	Store operated calcium entry
SSC	Sideward scatter
STIM	Stromal interaction molecule
TCR	T cell receptor
tdRFP	Tandem dimer red fluorescent protein
TGFβ	Transforming growth factor beta
T_H	T helper
TnC	Troponin C
TNFα	Tumor necrosis factor alpha
T_{reg}	T regulatory
UTR	Untranslated region
WPRE	Woodchuck post-transcriptional element
WT	Wild type
YC	Yellow cameleon
YFP	Yellow fluorescent protein
ZAP70	Zeta-chain-associated protein kinase 70

MOVIE LEGENDS

(Movies are enclosed on the CD at the back of this thesis)

Movie 1 R&D B cells show highly photostable RFP fluorescence. Cluster formation of activated lymphocytes, during coculture of MOG-specific R&D B and 2D2 T cells with 20 µg/ml MOG.

Movie 2 Visualization of calcium influx in EL4 cells by TN-XXL. EL4 lymphoma cells stably expressing TN-XXL were imaged *in vitro*, before and after addition of 4 µM ionomycin.

Movie 3 Whole-organ calcium imaging. Calcium waves travelling through an explanted, spontaneously beating CAGW-TN-XXL embryonic heart.

Movie 4 CD3 binding triggers strong calcium flux in T cells. TN-XXL^{CD}-expressing 2D2 T cells interacting with anti-CD3/CD28 beads were imaged *in vitro*.

Movie 5 APC encounter triggers strong calcium flux in T cells. TN-XXL^{CD}-expressing 2D2 T cells interacting with rMOG-pulsed IgH^{MOG} B cells were imaged *in vitro*.

Movie 6 T cells strongly respond to antigen presented by DCs. TN-3XL^{CD}-expressing OT-II cells were transferred into WT recipient hosts, one week before injection of SNARF-1-labeled BMDCs. One day later, the popliteal lymph node was imaged, before and after i.v. injection of 100 µg OVA peptide.

Movie 7 All T cells displaying strong calcium signals are engaged with DCs. Same experimental settings as Movie 4 after injection of antigen, but highlighting positions of DCs.

Movie 8 Early T – B cell interactions. TN-3XL^{CD}-expressing 2D2 T cells were transferred into WT recipient hosts, and imaged one week later in the popliteal lymph node. SNARF-1-labeled, rMOG-pulsed B cells were injected 1 hour before imaging.

Movie 9 Intermediate T – B cell interactions. Same as Movie 8, but B cells injected 8 hours before.

Movie 10 Late T – B cell interactions. Same as Movie 8, but B cells injected 24 hours before.

Movie 11 CNS resident APCs efficiently present antigen to infiltrating T cells. TN-3XL^{CD}-expressing OT-II cells were adoptively transferred into MOG peptide-immunized WT mice, followed by two-photon microscopy of the spinal cord, before and after i.v. injection of 100 µg OVA peptide.

Movie 12 Extravasated encephalitogenic T cells show calcium oscillations in the CNS. TN-3XL^{CD}-expressing 2D2 cells were adoptively transferred into Rag2$^{-/-}$ recipients, and two-photon microscopy of the spinal cord was performed at the onset of EAE (score 0.5).

Movie 13 Differential calcium signaling in encephalitogenic T cells during peak EAE. Same experimental settings as Movie 12, but with imaging at the peak of EAE (score > 2).

APPENDIX

Comparison of codon diversified TN-XXL sequence with original sequence. Shown is the amino acid sequence of CFP (blue), TnC (red), and YFP (yellow), with codons highlighted when altered.

```
 M   V   S   K   G   E   E   L   F   T   G   V   V   P   I   L   V   E   L   D
ATG GTG AGC AAG GGC GAG GAG CTG TTC ACC GGG GTG GTG CCC ATC CTG GTC GAG CTG GAC
*** *** *** *** *** *** *** *** *** *** *** *** *** *** *** *** *** *** *** ***

 G   D   V   N   G   H   K   F   S   V   R   G   E   G   E   G   D   A   T   N
GGC GAC GTA AAC GGC CAC AAG TTC AGC GTG CGC GGC GAG GGC GAG GGC GAT GCC ACC AAC
*** *** *** *** *** *** *** *** *** *** *** *** *** *** *** *** *** *** *** ***

 G   K   L   T   L   K   F   I   C   T   T   G   K   L   P   V   P   W   P   T
GGC AAG CTG ACC CTG AAG TTC ATC TGC ACC ACC GGC AAG CTG CCC GTG CCC TGG CCC ACC
*** *** *** *** *** *** *** *** *** *** *** *** *** *** *** *** *** *** *** ***

 L   V   T   T   L   T   W   G   V   Q   C   F   S   R   Y   P   D   H   M   K
CTC GTG ACC ACC CTG ACC TGG GGC GTG CAG TGC TTC AGC CGC TAC CCC GAC CAC ATG AAG
*** *** *** *** *** *** *** *** *** *** *** *** *** *** *** *** *** *** *** ***

 Q   H   D   F   F   K   S   A   M   P   E   G   Y   V   Q   E   R   T   I   F
CAG CAC GAC TTC TTC AAG TCC GCC ATG CCC GAA GGC TAC GTC CAG GAG CGT ACC ATC TTC
*** *** *** *** *** *** *** *** *** *** *** *** *** *** *** *** *** *** *** ***

 F   K   D   D   G   N   Y   K   T   R   A   E   V   K   F   E   G   D   T   L
TTC AAG GAC GAC GGC AAC TAC AAG ACC CGC GCC GAG GTG AAG TTC GAG GGC GAC ACC CTG
*** *** *** *** *** *** *** *** *** *** *** *** *** *** *** *** *** *** *** ***

 V   N   R   I   E   L   K   G   I   D   F   K   E   D   G   N   I   L   G   H
GTG AAC CGC ATC GAG CTG AAG GGC ATC GAC TTC AAG GAG GAC GGC AAC ATC CTG GGG CAC
*** *** *** *** *** *** *** *** *** *** *** *** *** *** *** *** *** *** *** ***

 K   L   E   Y   N   Y   I   S   H   N   V   Y   I   T   A   D   K   Q   K   N
AAG CTG GAG TAC AAC TAC ATC AGC CAC AAC GTC TAT ATC ACC GCC GAC AAG CAG AAG AAC
*** *** *** *** *** *** *** *** *** *** *** *** *** *** *** *** *** *** *** ***

 G   I   K   A   H   F   K   I   R   H   N   I   E   D   G   S   V   Q   L   A
GGC ATC AAG GCC CAC TTC AAG ATC CGC CAC AAC ATC GAG GAC GGC AGC GTG CAG CTC GCC
*** *** *** *** *** *** *** *** *** *** *** *** *** *** *** *** *** *** *** ***

 D   H   Y   Q   Q   N   T   P   I   G   D   G   P   V   L   L   P   D   N   H
GAC CAC TAC CAG CAG AAC ACC CCC ATC GGC GAC GGC CCC GTG CTG CTG CCC GAC AAC CAC
*** *** *** *** *** *** *** *** *** *** *** *** *** *** *** *** *** *** *** ***

 Y   L   S   T   Q   S   K   L   S   K   D   P   N   E   K   R   D   H   M   V
TAC CTG AGC ACC CAG TCC AAG CTG AGC AAA GAC CCC AAC GAG AAG CGC GAT CAC ATG GTC
*** *** *** *** *** *** *** *** *** *** *** *** *** *** *** *** *** *** *** ***

 L   L   E   F   V   T   A   A   R   M   L   S   E   E   E   L   A   N   C   F
CTG CTG GAG TTC GTG ACC GCC GCC CGC ATG CTG AGC GAG GAA GAG CTG GCC AAC TGC TTC
*** *** *** *** *** *** *** *** *** *** *** TCT *** GAG *** TTG GCT *** *** ***

 R   I   F   D   K   D   A   N   G   F   I   D   I   E   E   L   G   E   I   L
CGC ATC TTC GAC AAG GAC GCT AAC GGG TTC ATC GAC ATC GAG GAG CTG GGT GAG ATT CTC
*** ATA TTT GAT *** *** GCA *** GGC TTT *** *** ATA *** GAA CTC GGC *** *** CTG
```

```
 R   A   T   G   E   H   V   T   E   E   D   I   E   D   L   M   K   D   S   D
AGG GCC ACT GGG GAG CAC GTC ACC GAG GAG GAC ATA GAA GAC CTC ATG AAG GAT TCA GAC
CGG GCT ACC GGC *** CAT GTA ACG *** *** *** ATC GAG GAT CTG *** *** *** TCC ***

 K   N   N   D   G   R   I   D   F   D   E   F   L   K   M   M   E   G   V   Q
AAG AAC AAT GAC GGC CGC ATT GAC TTC GAT GAG TTC CTG AAG ATG ATG GAG GGC GTG CAG
*** *** AAC GAT *** CGT *** *** *** GAC GAA TTT CTT AAA *** *** *** GGG *** ***

 G   T   S   E   E   E   L   A   N   C   F   R   I   F   D   K   D   A   N   G
GGT ACC AGC GAG GAA GAG CTG GCC AAC TGC TTC CGC ATC TTC GAC AAG GAC GCT AAC GGG
*** *** *** *** *** GAA *** GCT AAT *** TTT AGG *** *** *** *** GAT *** *** GGA

 F   I   D   I   E   E   L   G   E   I   L   R   A   T   G   E   H   V   T   E
TTC ATC GAC ATC GAG GAG CTG GGT GAG ATT CTC AGG GCC ACT GGG GAG CAC GTC ACC GAG
*** ATA *** ATT *** *** CTA GGG *** ATC TTG CGG *** *** GGA *** *** GTG *** ***

 E   D   I   E   D   L   M   K   D   S   D   K   N   N   D   G   R   I   D   F
GAG GAC ATA GAA GAC CTC ATG AAG GAT TCA GAC AAG AAC AAT GAC GGC CGC ATT GAC TTC
*** GAT *** *** GAT CTT *** AAA GAC AGC GAT *** AAT AAC *** *** CGA ATC GAT TTT

 D   E   F   L   K   M   M   E   G   V   Q   E   L   M   G   G   V   Q   L   A
GAT GAG TTC CTG AAG ATG ATG GAG GGC GTG CAG GAG CTC ATG GGC GGC GTG CAG CTC GCC
GAC *** *** TTG *** *** *** GAA *** GTT *** *** *** *** GGT GGG GTC *** CTT GCA

 D   H   Y   Q   Q   N   T   P   I   G   D   G   P   V   L   L   P   D   N   H
GAC CAC TAC CAG CAG AAC ACC CCC ATC GGC GAC GGC CCC GTG CTG CTG CCC GAC AAC CAC
GAT *** *** *** *** AAT ACT CCG *** GGG GAT GGG CCG GTT CTC *** CCT *** *** ***

 Y   L   S   Y   Q   S   K   L   S   K   D   P   N   E   K   R   D   H   M   V
TAC CTG AGC TAC CAG TCC AAG CTG AGC AAA GAC CCC AAC GAG AAG CGC GAT CAC ATG GTC
*** *** TCA *** *** *** *** CTT TCC *** GAT CCT AAT GAA *** CGG *** *** *** ***

 L   L   E   F   V   T   A   A   G   I   T   L   G   M   D   E   L   Y   K   G
CTG CTG GAG TTC GTG ACC GCC GCC GGG ATC ACT CTC GGC ATG GAC GAG CTG TAC AAG GGC
*** *** GAA TTT GTC *** *** *** GGA *** *** *** GGA *** *** *** *** *** AAA GGT

 G   T   G   G   S   M   V   S   K   G   E   E   L   F   T   G   V   V   P   I
GGT ACC GGC GGC AGC ATG GTG AGC AAG GGC GAG GAG CTG TTC ACC GGG GTG GTG CCC ATC
GGG *** GGG GGA TCT *** *** *** *** *** GAA GAA TTG *** ACT GGT GTA GTC CCT ATT

 L   V   E   L   D   G   D   V   N   G   H   K   F   S   V   R   G   E   G   E
CTG GTC GAG CTG GAC GGC GAC GTA AAC GGC CAC AAG TTC AGC GTG CGC GGC GAG GGC GAG
TTG GTG GAA *** GAT GGG GAT GTC *** GGT CAT AAA *** *** *** CGA GGG *** GGT ***

 G   D   A   T   N   G   K   L   T   L   K  F-L  I   C   T   T   G   K   L   P
GGC GAT GCC ACC AAC GGC AAG CTG ACC CTG AAG TTC ATC TGC ACC ACC GGC AAG CTG CCC
GGG GAC GCA ACT AAT *** AAA TTG ACA CTC *** CTC *** *** ACA ACG GGG AAA *** ***

 V   P   W   P   T   L   V   T   T   L   G   Y   G   L   M   C   F   A   R   Y
GTG CCC TGG CCC ACC CTC GTG ACC ACC CTG GGC TAC GGC CTG ATG TGC TTC GCC CGC TAC
*** CCA *** *** ACA *** GTT ACT ACT CTA GGA TAT *** CTT *** TGT *** *** *** ***
```

```
 P   D   H   M   K   Q   H   D   F   F   K   S   A   M   P   E   G   Y   V   Q
CCC GAC CAC ATG AAG CAG CAC GAC TTC TTC AAG TCC GCC ATG CCC GAA GGC TAC GTC CAG
CCA *** CAT *** AAA CAA *** GAT *** TTT AAA TCA *** *** CCA GAG GGG *** *** ***

 E   R   T   I   F   F   K   D   D   G   N   Y   K   T   R   A   E   V   K   F
GAG CGC ACC ATC TTC TTC AAG GAC GAC GGC AAC TAC AAG ACC CGC GCC GAG GTG AAG TTC
*** AGA ACT *** *** *** *** *** GAT GGT AAT *** *** ACT AGG *** *** *** AAA ***

 E   G   D   T   L   V   N   R   I   E   L   K   G   I   D   F   K   E   D   G
GAG GGC GAC ACC CTG GTG AAC CGC ATC GAG CTG AAG GGC ATC GAC TTC AAG GAG GAC GGC
GAA GGG GAT ACA CTT GTC *** CGA *** *** *** *** GGA *** *** TTT *** *** *** GGA

 N   I   L   G   H   K   L   E   Y   N   Y   N   S   H   N   V   Y   I  M-T  A
AAC ATC CTG GGG CAC AAG CTG GAG TAC AAC TAC AAC AGC CAC AAC GTC TAT ATC ATG GCC
*** ATA CTC *** CAT *** TTG GAA *** *** *** *** AGT *** AAT GTT TAC *** ACA ***

 D   K   Q   K   N   G   I   K   A   N   F   K   I   R   H   N   I   E   D   *
GAC AAG CAG AAG AAC GGC ATC AAG GCC AAC TTC AAG ATC CGC CAC AAC ATC GAG GAC TAA
GAT *** CAA *** *** *** ATT *** GCT AAT TTT *** *** CGT *** *** ATT *** GAT TGA
```

RESOURCES

Microscopic imaging and data analysis of calcium signals in the spontaneously beating CAGW-TN-XXL embryonic heart was performed by Stephan Direnberger.

Mouse surgery and two-photon *in vivo* imaging, along with comprehensive support in microscopic data analysis, was provided by Ingo Bartholomäus.